NOTICE

The quality of this microfiche is heavily dependent upon the quality of the original thesis submitted for microfilming. Every effort has been made to ensure the highest quality of reproduction possible.

If pages are missing, contact the university which granted the degree.

Some pages may have indistinct print especially if the original pages were typed with a poor typewriter ribbon or if the university sent us a poor photocopy.

Previously copyrighted materials (journal articles, published tests, etc.) are not filmed.

Reproduction in full or in part of this film is governed by the Canadian Copyright Act, R.S.C. 1970, c. C-30. Please read the authorization forms which accompany this thesis.

THIS DISSERTATION
HAS BEEN MICROFILMED
EXACTLY AS RECEIVED

AVIS

La qualité de cette microfiche dépend grandement de la qualité de la thèse soumise au microfilmage. Nous avons tout fait pour assurer une qualité supérieure de reproduction.

S'il manque des pages, veuillez communiquer avec l'université qui a conféré le grade.

La qualité d'impression de certaines pages peut laisser à désirer, surtout si les pages originales ont été dactylographiées à l'aide d'un ruban usé ou si l'université nous a fait parvenir une photocopie de mauvaise qualité.

Les documents qui font déjà l'objet d'un droit d'auteur (articles de revue, examens publiés, etc.) ne sont pas microfilmés.

La reproduction, même partielle, de ce microfilm est soumise à la Loi canadienne sur le droit d'auteur, SRC 1970, c. C-30. Veuillez prendre connaissance des formules d'autorisation qui accompagnent cette thèse.

LA THÈSE A ÉTÉ
MICROFILMÉE TELLE QUE
NOUS L'AVONS REÇUE

INFRARED CHEMILUMINESCENCE FROM THE REACTIONS OF ATOMIC HYDROGEN, OXYGEN AND ACTIVE NITROGEN WITH FLUOROETHYLENES.

by

GREGORY H. MATINOPOULOS

A Thesis

submitted in partial fulfillment of the requirements for

the Degree of Doctor of Philosophy

at Dalhousie University

CANADA

April, 1976

Approved by

INFRARED CHEMILUMINESCENCE FROM THE REACTIONS OF ATOMIC HYDROGEN, OXYGEN AND ACTIVE NITROGEN WITH FLUOROETHYLENES.

by

GREGORY H. MATINOPOULOS

A Thesis

submitted in partial fulfillment of the requirements for

the Degree of Doctor of Philosophy

at Dalhousie University

CANADA

April, 1976

Approved by

Table of Contents

List of Tables

Page

List of Figures

Abstract

The population distributions of vibrationally excited hydrogen fluoride from the reactions of atomic hydrogen, oxygen and, nitrogen with fluoroethylenes were found using IR chemiluminescence technique. These populations were corrected for radiative and collisional relaxation and the results are discussed. Furthermore, Berry's Model was applied to the reaction of atomic hydrogen with vinyl fluoride for calculation of the energy distribution, followed by "Surprisal" analysis.

A preliminary study of the visible chemiluminescence from the reactions of atomic oxygen and nitrogen with the fluoroethylenes was also carried out.

Acknowledgments

The author wishes to express his sincere thanks to Dr. W.E.Jones for his help throughout the course of this study. He is indebted to Dr. J.Wasson for his generous participation in discussions and valuable suggestions during the writing of the thesis.

Special thanks to Dr. K.Subbaram and R.Vasudev for their helpful assistance with the visible spectroscopy experiments.

Thanks are also due to Mr. J.Muller for his help in setting up the glass apparatus.

The financial assistance from the Graduate Studies Faculty of Dalhousie University is gratefully acknowledged.

1. INTRODUCTION

1.1 General.

The basic step in chemical kinetics was the use by Hood (1) of the empirical equation

$$\log k = B - A' T \qquad [1]$$

to explain the increase of the rate of a chemical reaction by increasing the temperature. This relationship was later expressed by Van't Hoff and Arrhenius in the form

$$k = Ae^{-E_{exp}/RT} \qquad [2]$$

The idea was extended by Arrhenius (2) and was successfully applied by him to the data relative to a large number of reactions and thus, the equation is generally referred to as the Arrhenius law. The preexponential or frequency factor A and the activation energy E are practically independent of temperature.

Trautz and Lewis (3) identified A with a collision number which they calculated by using a simple collision theory where the molecules were treated as structureless spheres. Eyring (4) and Evans with Polanyi (5) treated the collisions in a more satisfactory way by taking into account the structures of the reacting molecules and the manner in which the reacting molecules come together on collision.

These theories assume an activated complex intermediate, which is in the process of passing over the top of the potential-energy barrier. It is assumed that the concentrations of these activated complexes can be calculated on the basis of equilibrium theory. A plot of energy as a function of the various interatomic distances in the activated complex gives the so called potential energy surfaces on which the reactions take place.

The experimental activation energy is calculated from the change of the rate constant with temperature. Theoretically the activation energy can be calculated from the potential energy surfaces or other classical and semi-classical treatments. The pure quantum-mechanical methods are slowly becoming sufficiently refined so that a reliable activation energy can be calculated for the very simplest of reactions, but the calculations are not encouraging for more complex reactions.

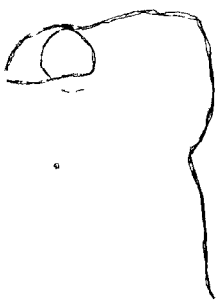

The equilibrium hypothesis is valid for reactions having substantial activation energies and which are therefore slow. However, it is useless for very fast reactions. Therefore, nonequilibrium theories have also been developed. A second reason for developing such theories was that, during recent years, there has been increasing interest in the so called "fine structure" or "detailed rates"

of chemical reactions. These theories have provided valuable information on the precise way in which reactive collisions occur, and about the way in which the energy released in a reaction is distributed among the products. An experimental study of energy distributions combined with a dynamical treatment for a variety of hypothetical potential-energy surfaces can lead to valuable conclusions about the actual shapes of potential-energy surfaces.

Special techniques providing information about the details of reaction processes are necessary in order to draw conclusions about the general form of the potential-energy surfaces. The most important of these are chemiluminescence studies and molecular-beam investigations. The flash photolysis technique has also been employed to measure the rates of formation of specific vibrational quantum states (6,7).

When the non-equilibrium theories are explicitly related to potential-energy surfaces, the subject is conveniently referred to as molecular dynamics.

1.2 Disequilibrium in the Products of a Chemical Reaction.

In disequilibrium there is non-Boltzmann energy distribution in several degrees of freedom. Under these circumstances, it ceases to be possible to describe the energy distribution over electronic, vibrational or rotational states by using characteristic temperatures. The only method of characterising the energy distribution is by giving the vibrational populations in the various vibrational levels of each electronic state, as well as the rotational populations of each vibrational level. The large majority of elementary chemical reactions proceed by the lowest potential surface, which connects the electronic ground states of the reactants with the electronic ground states of the products. In such cases, a significant proportion of the energy released in the reaction appears as vibrational-rotational excitation of the newly formed bond, giving rise to infrared-chemiluminescence. If the reaction releases sufficient energy to produce products in electronically excited states, it becomes necessary to consider the forces that are present as the system proceeds across more than one potential-energy hypersurface. Electronically excited states will not be discussed since the main interest of this work was IR chemiluminescence.

However, electronically excited species were observed in the reactions of atomic oxygen and active nitrogen with fluoroethylenes.

1.3 Classical Dynamics.

1.3.1 Dynamical Models.

A purely quantum-mechanical treatment of dynamical calculations is too complicated. Thus, most calculations have been made largely on the basis of classical mechanics by imposing quantum conditions for the initial state. Since the pure classical treatment neglects quantization, it does not account for the existence of the zero-point energy level and quantum-mechanical tunneling through the barrier. Recently, Karplus and coworkers (8,9) have made classical and quantum-mechanical calculations for the same potential-energy surface of the $H+H_2$ system. Their results, indicate a small but significant tunneling effect but on the whole it appears that quantum-mechanical tunneling is not of great importance except perhaps for light atoms at low temperatures. More recently, Schatz, Bowmann and Kuppermann (10) presented exact quantum, quasi-classical and semiclassical reaction probabilities for

the collinear reaction [3] and they compared the results obtained from these methods.

$$F + D_2 \longrightarrow FD + D' \qquad [3]$$

In a dynamical study, the first step is the calculation of the potential-energy surface. Usually, the potential-energy hypersurface used in connection with IR chemiluminescence experiments is the extended LEPS (London, Eyring, Polanyi and Sato) equation [4] (11).

$$U(r_1, r_2, r_3) = \frac{Q_1}{1+a} + \frac{Q_2}{1+b} + \frac{Q_3}{1+c} - \left[\frac{J_1^2}{(1+a)^2} + \frac{J_2^2}{(1+b)^2} + \frac{J_3^2}{(1+c)^2} - \frac{J_1 J_2}{(1+a)(1+b)} - \frac{J_2 J_3}{(1+b)(1+c)} - \frac{J_3 J_1}{(1+c)(1+a)} \right] \qquad [4]$$

The coordinates r_1, r_2 and r_3 refer to AB, BC and AC internuclear separation of the reaction [5] respectively.

$$A + BC \longrightarrow A\cdots B\cdot C \longrightarrow AB + C \qquad [5]$$

Q and J are the Coulombic and exchange integrals which were obtained from the Morse function for the pair of atoms, and from the repulsive analogue of the Morse function proposed by Sato (11). The constants a, b and c are adjustable parameters. The parameters in the function are adjusted

to give a reasonable classical barrier height when compared with the activation energy E_a.

The second step in a dynamical study is to formulate the classical Hamiltonian for the system. The classical Hamiltonian for the three-particle system is

$$H = T(p_1, \ldots, p_i) + U(q_1, \ldots, q_i) \qquad [6]$$

where T and U are kinetic and potential energies, p_i and q_i are momenta and positions. For the three atoms moving in three dimensions, $i=9$. If the motion of the center-of-mass is eliminated, $i=6$. There are consequently twelve equations of motion

$$\partial H/\partial p_i = \dot{q}_i \quad , \quad \partial H/\partial q_i = -\dot{p}_i \qquad [7]$$

Integration of the Hamilton's equations subject to a complete set of initial conditions, leads to the collision trajectories, i.e., to a description of the motion of the system over the surface. In order for the results of the calculations to have statistical significance, it is necessary to choose a representative group of initial dynamical variables and initial orientation parameters of the collision partners by the use of an averaging procedure. The one most commonly used is the Monte Carlo procedure (12,13). Two techniques employed to transform

the random numbers generated in the computer to random variables with the desired distribution are: the "inversion" method, and the "rejection" method (12). Details of how the Monte Carlo weighting procedure is applied are given by Blais and Bunker (14). A comprehensive description of the method is also given by Laidler (15).

A number of useful dynamical models are employed in trajectory calculations (16).

a) The impulsive model (IMP) assumes an instantaneous release of force in B·C [5], and derives the outcome from conservation of momentum.

b) The constant force model (CONST.F) assumes a release of force from B·C of finite duration, forcing A····B [5], which can be initially under tension, into oscillation.

c) The simple harmonic force model (SHF) resembles CONST.F but with a linearly decaying force in B·C.

d) The direct interaction with product repulsion (DIPR) assumes that a generalized force produces a known total impulse between atoms A and C.

e) The FOTO model describes the reactive event as forced oscillation in a tightening oscillator taking into account the fact that in the second half of a chemical reaction, the B·C repulsion is forcing oscillation into

an oscillator, thus, increasing its characteristic frequency and decreasing its equilibrium separation.

1.3.2 Vibrational-Rotational Excitation - Methods of Determining Population Distribution.

1.3.2.1 IR Chemiluminescence.

A. IR Chemiluminescence Technique.

The earliest evidence of vibrational disequilibrium among the products of exothermic reactions comes from sodium flame experiments of Polanyi (17)

$$X + Na_2 \longrightarrow NaX^{\dagger} + Na \qquad [8]$$

$$Na + XM \longrightarrow NaX^{\dagger} + M \qquad [9]$$

The method used to determine the vibrational energy in the product molecule was the indirect method (18) i.e., by observation of emission from atoms which had been excited by collision with newly formed products.

$$NaX^{\dagger} + Na \longrightarrow NaX + Na^{*} \qquad [10]$$

$$Na^{*} \longrightarrow Na + h\nu \qquad [11]$$

The interest in this observation was revived later

by the discovery that highly vibrating hydroxyl radicals were formed in the reaction of $H + O_3$ (19).

In following years the investigation of the products of the reactions $O + O_3$, $Cl + O_3$, $Br + O_3$, $O + NO_2$, $O + ClO_2$ by kinetic absorption spectroscopy revealed a high initial concentration of vibrationally excited product molecules (20,21).

Cashion and Polanyi (22) directly observed for the first time the infrared emission of the vibrationally excited product $HCl^{\dagger}$ formed in the room-temperature gas-phase reaction

$$H + Cl_2 \longrightarrow HCl^{\dagger} + Cl \qquad [12]$$

At that time, they realized the potential of the method in elucidating details of reaction dynamics.

The next year (23), they managed to calculate the vibrational distribution of $HCl^{\dagger}$ in the same reaction and produced the first publication on the energy distribution among the products of atomic reactions (18).

After that, they formulated the theory of IR chemiluminescence (24). In parallel, a study of the energy distribution among the products was initiated. A simple valence bond resonance description of the activated complex in exothermic reactions of the type [5]

$$A + BC \longrightarrow AB + C \qquad [5]$$

coupled with experimental and theoretical evidence concerning the efficiency of transfer of vibrational energy during a collision, led to the incorrect prediction that almost all of the heat of reaction should be contained in vibration of the bond being formed from the reaction [12]. The error was due to the fact that this was true only for the reaction with alkali metals and to the poor experimental techniques available at that time.

Better results were obtained by improving the experimental method known as stationary-state "flow method" (25). This method was used for seven years for infrared chemiluminescence experiments in conjunction with calculations of the extent of relaxation (24,26). It employs a reaction cell of large volume and a large pumping speed. The light is collected by a multireflection mirror system (Fig. 1a). For reactions with low chemical yields, the "single-window flow method" is used. In this method (27) the observation is along the line-of-flow with the consequence that the emission is stronger. However, it gives a mean distribution which is approximately equal to the initial population since the flow is rapid (Fig. 1b).

The study gained more interest, when, from preliminary results for the reaction

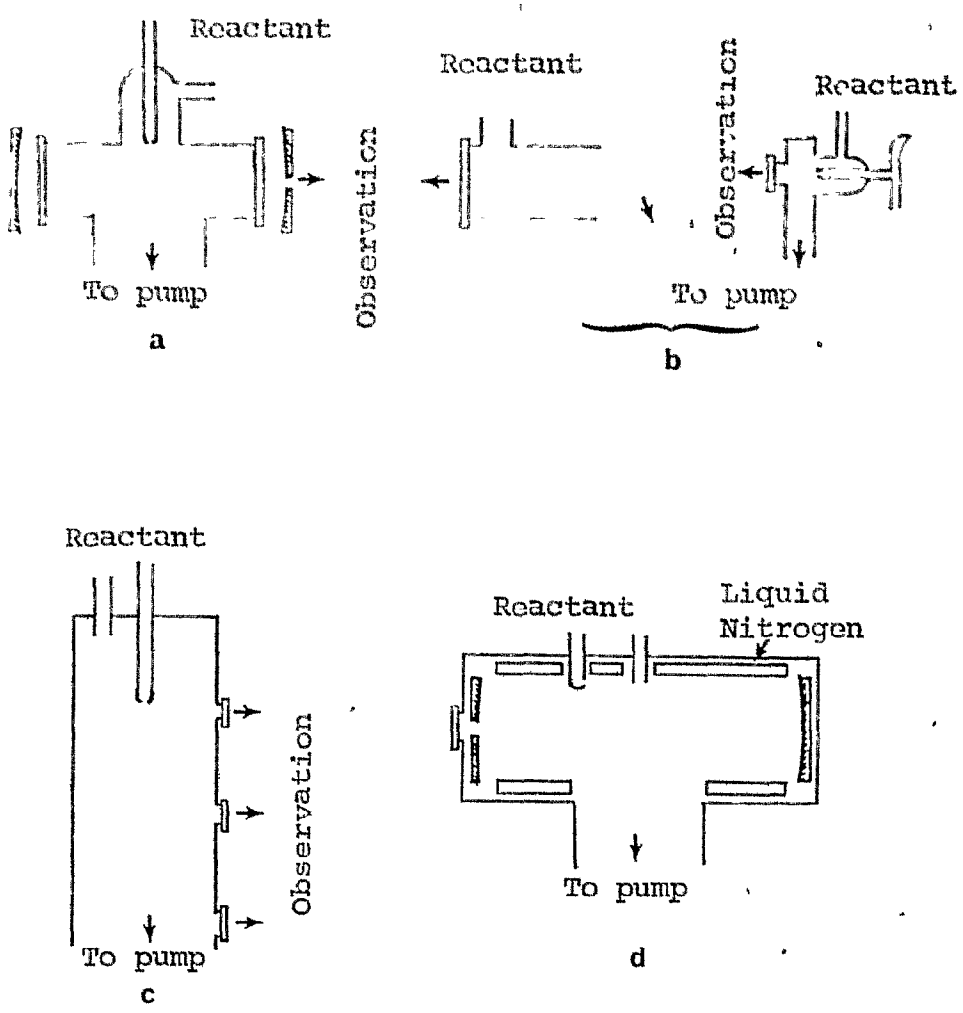

Flg. 1. IR chemiluminescence reaction cells.

(a) Flow method

(b) Single window flow method

(c) Measured relaxation method

(d) Arrested relaxation method

$$K + BrH \longrightarrow KBr + H \qquad [13]$$

in crossed Maxwellian molecular beams (28), it was shown that it would be possible to calculate the recoil energy of the KBr product from its angular distribution. By subtracting the recoil energy from the total energy available, a value could be obtained for the total internal energy, rotational and vibrational, of KBr (29). This discovery made the crossed beam method complementary to the IR chemiluminescence method since it was possible, in principle, to obtain the detailed rates for formation of rotational-vibrational states from IR chemiluminescence.

By using the flow method, it was found (30) that the exothermic reaction [12] proceeds with greatest probability to form excited HCl' in lower vibrational states.

$$H + Cl_2 \longrightarrow HCl' + Cl \qquad [12]$$

This result ran counter to the general expectation that reactions $A + BC$ would proceed most rapidly into the highest accessible vibrational states of AB' [5]. For the same reaction [12] in 1-2 Torr pressure range, Findlay and Polanyi (31) found approximately the same stationary-state vibrational distribution as at reduced pressure of 10^{-2} Torr but they found a higher rotational

temperature of 1300±100 °K. The same stationary-state vibrational population would suggest that collision deactivation was not of major importance. In order to account for the high translational-rotational temperature in the absence of substantial vibrational deactivation, it was necessary to suppose that the greater part of the energy liberated by the reaction [12] went directly into translational and rotational motion of the products (31). They were also able to determine the population of the v=0 vibrational level by self absorption measurements (32).

In connection with the experiments in IR chemiluminescence, trajectory calculations were performed for the determination of the energy distribution in the products. Two kinds of surfaces were recognized in the beginning: the attractive one (Fig. 2a) on which the energy of the reaction is released as A approaches B [5] and the repulsive surface (Fig. 2b) when the energy is released as the products separate. For a given mass combination, the efficiency of conversion of the reaction exothermicity into vibration in the newly formed bond, increases as the surface becomes increasingly attractive (11, 14, 33). The reaction [14] is a reaction of this type and 90% of its exothermicity is released as internal energy of the products (34).

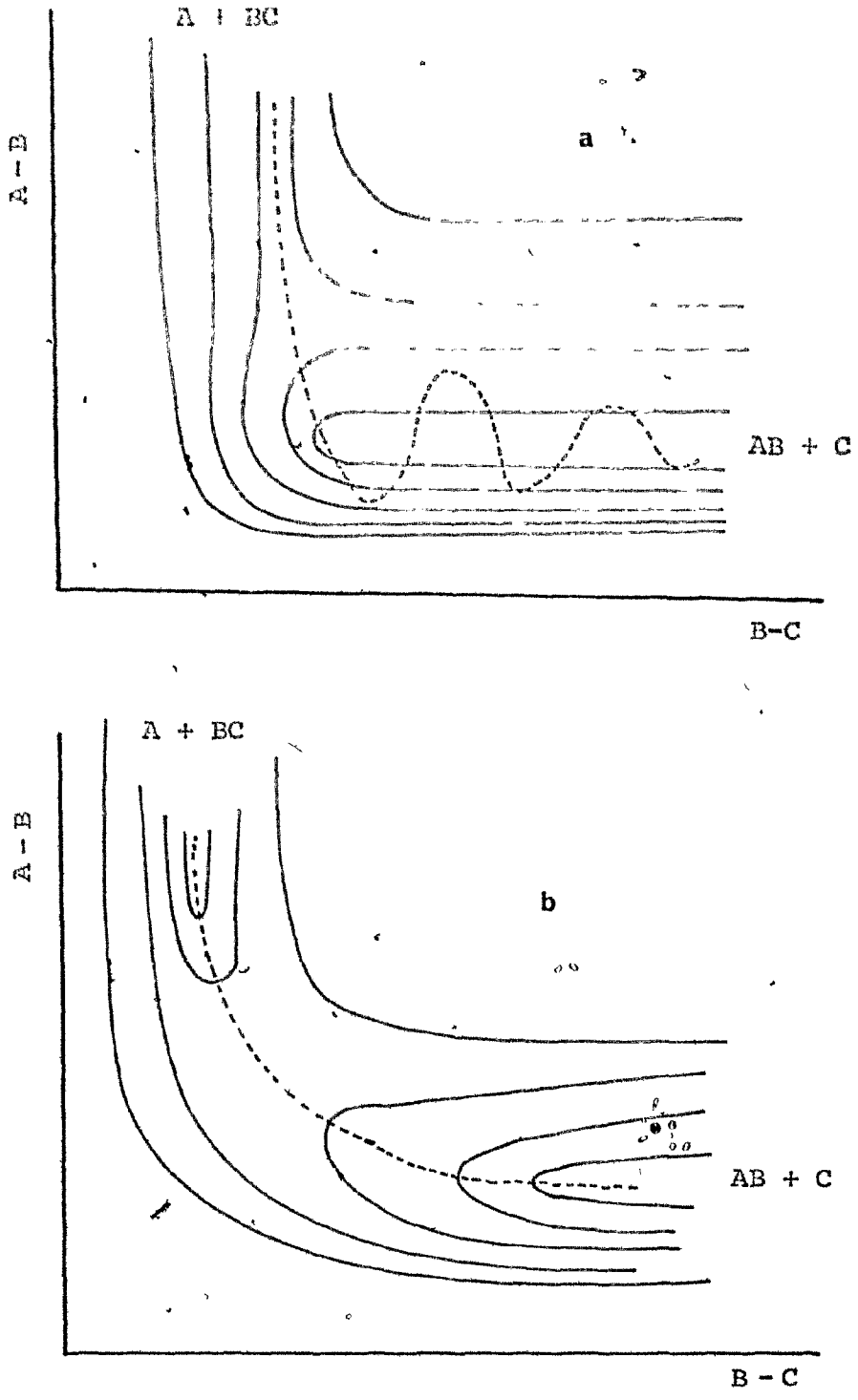

Fig. 2. Potential energy surface; (a) Attractive

(b) Repulsive

$$K + ICH_3 \longrightarrow KI + CH_3 \qquad [14]$$

On a repulsive surface, the energy is released as the products recoil. Therefore, only a part of the energy is released as vibrational energy (11, 33, 35). In addition to the attractive and the repulsive types of energy release, a third type of energy release, called mixed energy release, has been distinguished (11, 33, 35). The term mixed energy release indicates that a portion of the energy of reaction is released while the products are separating but the reagents are still attracting one another. This category of energy release was introduced to take cognizance of the fact that AB-C repulsion, evidenced by the tendency of the products to separate, is more effectively converted into vibration of AB if the A—B bond is under tension, since there is less tendency for A to

$$A + BC \longrightarrow AB + C \qquad [5]$$

recoil along with B, yielding translation of AB as a whole. The mixed energy release has two components, the "late-attractive" and the "early-repulsive" energy release (33). The combination of masses involved in the reactive encounter has a profound effect on the energy release. On a repulsive hypersurface, when the attaching atom is

light then, the energy released as vibration is very small and this is called "light-atom anomaly" (11, 33). The simplest explanation is that the light atom approaches faster, and allows correspondingly less time for the BC bond to extend.

In 1967 Polanyi and coworkers developed two new experimental methods for IR chemiluminescence measurements. These are the "measured relaxation" method and the "arrested relaxation" method.

The measured relaxation (MR) is capable of finding detailed rates of formation in various vibrational levels, k_v , accurately (36,37). Several observation windows are placed at known intervals along the line of flow. Provided that the observation windows are situated at distances corresponding to times during which relaxation is moderate, a graphical extrapolation back to zero time will yield fairly good values for the relative initial values of k_v. The same method was also used by Jonathan and coworkers (38,39). A very detailed numerical analysis has been made by Pacey and Polanyi (37) of the reaction [12] taking into account the combined effects of reaction, diffusion, flow, radiation and, collisional deactivation.

$$H + Cl_2 \longrightarrow HCl + Cl \qquad [12]$$

The method of arrested relaxation (AR) (36) makes use of molecular flow rather than streaming flow. Two uncollimated molecular beams of reagents meet in the center of a vessel which has a background pressure of 10^{-4}-10^{-5} Torr. A multiple-reflection Welsh cell increases the collection efficiency of IR radiation (Fig. 1d). The IR emission from the vibrationally excited product is monitored by either conventional grating spectroscopy or by Fourier transform spectroscopy (40). Reaction occurs in the dense crossing region of the two beams. The products are scattered out of this region after no more than a few collisions and are trapped by the cold wall (20-40 ^{o}K) which surrounds the reaction zone or through the orifice to a large diffusion pump. The combination of molecular flow plus rapid "pumping" reduces relaxation to an insignificant amount. Therefore, not only vibrational but also the rotational distribution is largely unrelaxed. The steady-state distribution then yields $k(v,J)$ and consequently $k(v,J,T)$. This method was also employed by Setser and coworkers (41, 42). Both methods give excellent results and have stimulated many classical trajectory studies.

There are two distinguishable lines along which classical trajectory studies are developing. One line has to do

with studies of model potential energy surfaces to ascertain the effect of systematic variations in their major features. The other line of development has been concerned with obtaining potential energy surfaces that are to a greater or lesser degree, successful in reproducing the reaction dynamics of systems studied experimentally.

A parameter of interest in terms of the molecular mechanics of IR chemiluminescence was found to be the angular distribution of the newly formed reaction products. The scattering is termed "forward" if the molecular product is ejected along the continuation of the direction of approach of the attacking atom. It turns out that the "attractive" and "repulsive" criteria correlate quite strongly with scattering angles; attractive interaction favors forward scattering, repulsive interaction favors backward scattering (43, 44). As for product energy distributions, the angular distribution on a repulsive surface is affected by the mass combination; the light-atom anomaly gives rise to more backward scattering than does mixed energy release (43).

A special feature of the attractive surface is a tendency for "indirect" (or,"complex") encounters to take place. A trajectory is called indirect if the separation

between the products, once it has started to increase, subsequently decreases (43, 45). This frequently has the consequence that the force between the products, having begun to diminish in absolute magnitude, exhibits a secondary peak. This is termed a "secondary encounter" (43). Secondary encounters can be either "clouting" (if the secondary peak in the force is positive) or, "clutching". The effect of secondary encounters is to reduce vibrational excitation. Such encounters are rare on repulsive surfaces. The exceptions are reactions with a high degree of mixed energy release, since they tend to channel the repulsion quite efficiently into internal excitation of the products.

In related families of exchange reactions, there is evidence of a strong correlation between height and location of the barrier. The barrier moves to successively later positions along the reaction coordinate with increasing barrier height (18, 46, 47, 48). In general, the slope of the downhill region of the potential energy surface is not as important a characteristic as its location.

The effect of reagents having energy in excess of that needed to cross the barrier was also examined. In thermoneutral reactions, translational energy in the

reagent is vastly more effective than vibrational energy in promoting a reaction with an early barrier. If, however, the crest of the barrier is displaced into the exit valley, then vibration in the bond under attack is vastly more effective than is reagent translation energy in producing reaction (46). Enhanced collision energy gives rise to a small decrease in the computed mean product vibrational excitation, a small increase in mean product rotational excitation and a large increase in product translational excitation on a highly repulsive hypersurface (49, 50). Additional reagent vibrational energy is channelled principally into additional product vibration (50).

The role of rotation in reaction dynamics is less understood than that of translation and vibration. There are two sources of rotational excitation in product AB of reaction [5] :

$$A + BC \longrightarrow AB + C \qquad [5]$$

i) reagent orbital angular momentum L and

ii) repulsion between the products.

The first of these factors will be prominent when A and B are heavy atoms while C is a light atom. The reagent orbital angular momentum of A with respect to BC is then almost entirely momentum of A about B. The second factor

will be significant if three requirements are fulfilled: substantial repulsive energy release, reaction through a bent intermediate and significant mass for the ejected atom C (51).

The reactions studied by IR chemiluminescence can be categorized in the following five classifications.

i) Three Center Exchange Reactions.

$$A + BC \longrightarrow AB + C \qquad [5]$$

Since this reaction is the simplest one, it has received the most attention. The efficiency of conversion of the available energy into vibration tends to be lower for repulsive surfaces and even lower for reactions involving hydrogen as the attacking atom, due to the so-called "light atom anomaly" on a repulsive surface (11, 33).

The $H+Br_2$ reaction is more efficient in converting the available energy into vibration than is $H+Cl_2$ (36) since the energy barrier is lower for $H+Br_2$ (early barrier). The reaction $H+F_2$ occupies a special place in the $H+X_2$ (X is Halogen) family in that the repulsive energy release is restricted to the period when the fluorine atoms are at close range (52).

ii) Four-Center Exchange Reactions.

$$A + BCD \longrightarrow AB^{\dagger} + CD \qquad [15]$$

The reaction $H+O_3$ (40) is extremely efficient in converting available energy into vibration in the new bond, and shows no evidence of the light-atom anomaly. The surface is therefore likely to be an attractive one. For a reaction of this type, it seems that the available energy efficiently enters in the new bond without perturbing the old one (40, 53). The four-center exchange reaction of the type

$$AB + CD \longrightarrow AC^{\dagger} + BD \qquad [16]$$

has been studied theoretically on potential energy hypersurfaces which favor collinear reaction (54) or coplanar rectangular reaction (55).

iii) Dissociation of Polyatomic Molecules.

$$\text{Polyatomic} \longrightarrow AB^{\dagger} + \cdots \qquad [17]$$

In the case of CH_3CF_3 dissociation (27), the "excess" energy of the RRKM (Ramsperger, Rice, Kassel and Marcus) theory could not account for the vibrational excitation in the $HF^{\dagger}$ (v=4) level, but the specific chan-

nelling of the energy, E([illegible]) $= E_c - \Delta H_{react}$, released was required. E_c is the critical energy for elimination of HF. The same was found for photoelimination of HCl from chloroethylenes acting as chemical lasers (56). Furthermore, Bogan and Setser (57) found that only part of the localized energy is available for internal excitation when the reaction yields resonance stabilized radicals.

iv) Atom + Polyatomic Molecule.

The common reaction of this type is

$$F + RH \longrightarrow HF^{\dagger} + R \qquad [18]$$

The most interesting question here is what fraction of the available energy becomes internal excitation in the polyatomic fragment R. The observations for these reactions are (a) the constancy of the fraction of energy released as vibrational energy of $HF^{\dagger}$ ($\langle f_v \rangle$), for a series of primary hydrocarbons (41, 42, 58) with the same D^o(H-C), but with significantly different numbers of internal degrees of freedom, (b) the similarity of $\langle f_v \rangle$ for the CH_4, SiH_4 and GeH_4 series (59), (c) the similarity of the $HF^{\dagger}$ vibrational energy distribution from reactions with CH_4, SiH_4 and GeH_4 to that from the HCl, HBr and HF reactions,

respectively (58).

v) More Complex Systems.

The study of reactions with vibrationally excited triatomic products are particularly difficult since the excited triatomic molecule is rapidly relaxed (60). In addition, it was found that for the reactions

$$NO + O_3 \longrightarrow NO_2 + O_2 \qquad [19]$$

$$NO + O \longrightarrow NO_2 \qquad [20]$$

a significant fraction of the triatomic product is formed in an electronically excited state (61).

Studies have been made of IR chemiluminescence from more complicated systems for which the elementary step cannot be so easily identified. These reactions are the reactions of atomic oxygen with acetylene (62), carbon suboxide and cyanoacetylene (61) in which cases, the vibrationally excited diatomic product is $CO^{\dagger}$.

B. Techniques Employing Chemical Lasers.

Chemical lasers are chemiluminescent processes which take place in a laser cavity. When the population of the vibrationally excited species reaches a threshold, stimulated emission is obtained mainly in the laser cavity.

Chemical lasing was predicted by Polanyi (63) in 1961 and was achieved experimentally for the first time by Kasper and Pimentel in 1964 (64). Since then, a large number of chemical laser systems have been found and examined but the main interests have been the threshold concentration and the power of the laser. We are interested only in the methods which can give information on population distributions and consequently the energy distributions in products of chemical reactions. The methods employed in this specialized chemiluminescence technique to obtain vibrational population distributions are described in the following paragraphs.

i) Simple Laser Method.

This method (65, 66) makes use of the gain equation for a chemical laser given by Patel (67). The relative gain $\alpha_v(J)$ of the $P_v(J)$ transition $v \rightarrow (v-1)$, $(J-1) \rightarrow J$

is given by equation [21]

$$\alpha(J) = (\text{const}) \cdot J \cdot N_{v-1} / kT_t \cdot T_R \cdot \left[\frac{N_v}{N_{v-1}} B_v \exp \frac{-B_v J(J-1)}{kT_R} - B_{v-1} \exp \frac{-B_{v-1} J(J+1)}{kT_R} \right] \quad [21]$$

in which N_v is the population of the vth vibrational state, B_v is the inertia constant of the vth vibrational state, T_t is the translational temperature, T_R is the rotational temperature and k is Boltzmann's constant. Experimentally, it is assumed that (a) the rotational temperature is a Boltzmann temperature, T_R, which is well defined and equal to the thermal temperature when a sufficient excess of inert gas is present and (b) neither laser emission nor collisional deactivation contributes to the change of the gain. Therefore, the gain depends only on the rotational temperature. These observations and the time needed to transfer maximum gain from one transition to the next provide estimates of the fine rate-constant ratios k_v/k_{v-1}. The method estimates only the ratio of the two vibrational levels with the highest gain. The problem is to estimate reliably the rotational temperature, T_R, from the heat release and the question is to what extent the laser emission is itself responsible for a change in the gain with time. Lin and Green (67, 68,

69,70) use a similar approach to estimate limits for the initial vibrational population.

ii) Equal Gain Temperature Technique.

This method (71) represents an improvement in accuracy over the previous one. The rotational temperature is always assumed to be equal to the translational temperature. By external heating, which is always under control, the rotational temperature of the gas mixture is increased until conditions are obtained for which two vibrational-rotational transitions initiate laser pulses simultaneously with the same gain. Under these conditions, the two transitions $P_V(J)$ and $P_V(J+1)$ have equal gain. Thus, since the rotational temperature is known, equation [21] can be used to equate $\alpha(J)$ and $\alpha(J+1)$ and to give an expression for the ratio N_V/N_{V-1} for the first transition to reach laser threshold.

$$\frac{N_V}{N_{V-1}} = \frac{B_{V-1}}{B_V} \frac{J \exp[-B_{V-1} J(J+1)/kT_R] - (J+1)\exp[-B_{V-1}(J+1)(J+2)/kT_R]}{J \exp[-B_V J(J-1)/kT_R] - (J+1)\exp[-B_V J(J+1)/kT_R]} \qquad [22]$$

By using different pressures for the gas mixture, a plot of N_V/N_{V-1} versus pressure is obtained and the extrapolated ratios N_V/N_{V-1} include corrections for collisional vibrational deactivation, so they can be equated to the

detailed rate constant ratios k_v/k_{v-1}. Reproducibility is a problem near equal gain temperature, T_{eq}, where slight variations in physical conditions may have a large effect. Therefore, an improvement of the method (72) introduces the relative intensity difference $d(J,J+1)$. This is defined by

$$d(J,J+1) = (I_J - I_{J+1})/(I_J + I_{J-1}) \qquad [23]$$

where, I_J is the peak intensity of $P_v(J)$ at first laser emission. For $T = T_{eq}$, d is equal to 0; for $T < T_{eq}$, $d > 0$ with $\lim_{T \ll T_{eq}} d = +1$ and, for $T > T_{eq}$, $d < 0$ with $\lim_{T \gg T_{eq}} d = -1$. Thus, the plot of $d(J,J+1)$ versus T, which is a straight line, gives accurately T_{eq} for $d = 0$. This method also improves the equation [22] by including vibrational-rotational interaction and frequency factors that were ignored earlier. The equal-gain temperature technique permits direct measurement of the fine rate constant ratio k_v/k_{v-1} for the $v \rightarrow v-1$ transition that displays highest gain. In order to extend the technique to other fine rate constant ratios, two versions of this method were developed: the tandem equal gain laser and the grating equal gain methods.

iii) Tandem Equal-Gain Method.

The possible use of two pumping reactions in the same optical cavity, a "tandem" laser, was proposed by Tablas and Pimentel (73). One reaction, the "driver", must have enough gain in the $v \rightarrow v-1$ transition to cause it to reach threshold first even though the other reaction the "slave", would reach threshold first in some other transition or, perhaps, would not reach threshold at all (Fig. 3b). Two independent tandem equal-gain temperature measurements are required to fix the slave rate constant ratio. This can be achieved by adjusting the pressure of the gas mixtures. When the transitions $P_v(J)$ and $P_v(J+1)$ have equal gain, we can write

$$\alpha_D(J) + \alpha_S(J) = \alpha_D(J+1) + \alpha_S(J+1) \qquad [24]$$

The subscript D refers to the driver, S to the slave. By further pressure adjustment, we can achieve equal-gain for $P_v(J+1)$ and $P_v(J+2)$. Then,

$$\alpha_D(J+1) + \alpha_S(J+1) = \alpha_D(J+2) + \alpha_S(J+2) \qquad [25]$$

From these two relations, (N_v/N_{v-1}) can be determined when the ratio (N_v/N_{v-1}) is known by using the simple equal-gain technique.

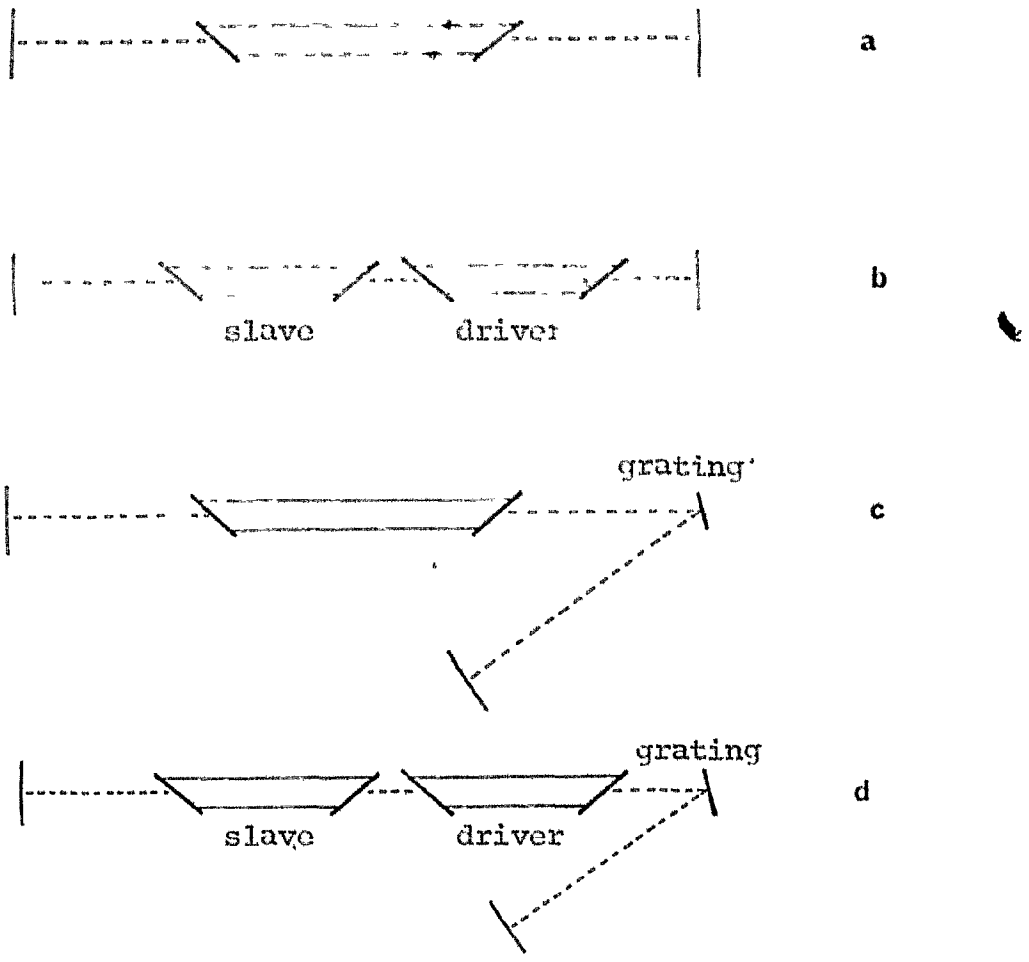

Fig. 3. Cavities of chemical lasers employed for vibrational population distributions

(a) Chemical laser
Equal-gain temperature method

(b) Tandem equal-gain temperature method

(c) Grating equal-gain temperature method
Grating-selected laser emission method

(d) Zero-gain temperature method (Grating-Tandem arrangment)

Another version of the "tandem" laser (74) uses the "driver" laser at its equal-gain temperature and changes the temperature of the slave reaction until the equal-gain condition is restored. So, in that case we require only a single tandem equal-gain temperature measurement and mitigate the uncertainty. For improvement, equation [22] is elaborated to include explicitly the J dependence of the pressure broadening effect. Thus, finally the equal-gain expression becomes

$$\frac{N_v}{N_{v-1}} = \frac{B_{v-1}}{B_v} \frac{\phi x \Pi \exp F_{v-1}(J)/kT_{eq} - \exp F_{v-1}(J+1)/kT_{eq}}{\phi x \Pi \exp F_v(J-1)/kT_{eq} - \exp F_v(J)/kT_{eq}} \quad [26]$$

where, $x = J/(J+1)$

ϕ = the ratio of the Herman-Wallis factors due to vibration - rotation interaction and,

$F_v(J)$ is the rotational energy of the Jth state.

The pressure dependence is embodied in Π, which is equal to $H(J)/H(J+1)$. The quantity $H(J)$ is a factor which, if multiplied by the gain of a Doppler-broadened line, gives the gain resulting from the combined pressure and Doppler-broadening effect.

iv) Grating Equal-Gain Method.

This method (75) replaces one end mirror by a curved reflectance grating (Fig. 3c). Thus, there is a wavelength for which the losses are smallest and this varies with the orientation of the grating. By using a second mirror at the focal point of the grating with focal length the same as that of the grating, there is a range of wavelengths for which the cavity is equally well aligned. An iris aperture completes the system. By changing the orientation of the grating any two adjacent transitions can be observed simultaneously. They also have equal losses so that one can search for conditions which give equal-gains.

v) Zero-Gain Temperature Method.

The grating equal-gain method is more flexible than the tandem method but the optical cavity losses tend to be large because of the use of the bracketing technique. So, only those ratios can be measured for which some relatively high gain transitions reach laser threshold. The tandem technique, on the other hand, is limited by the availability of a suitable driver but it has much less loss. The "zero-gain temperature" method combines the other two methods. If the ratio N_v/N_{v-1} is below unity, the gain

for P-branch transitions is a maximum for some value of the rotational quantum number J and it decreases as J decreases, becoming negative if J is sufficiently low. For ratios N_v/N_{v-1} above unity, we have the opposite for some R-branch transition. The temperature at which the gain of the transition passes from positive to negative, the "zero-gain temperature" (T_z), results in the "zero-gain" equation.

$$\frac{N_v}{N_{v-1}} = \frac{B_{v-1}}{B_v} \exp\left\{\frac{hc}{kT_z}\left[B_v J(J\mp 1) - B_{v-1} J(J\pm 1)\right]\right\} \qquad [27]$$

where the upper signs apply to a $P_{v\to v-1}[(J-1)\to J]$ transition and the lower signs to an $R_{v\to v-1}[J\to(J-1)]$

Experimentally, this zero-gain temperature can be determined (75) with a grating-tandem arrangement (Fig. 3d). If the "slave" furnishes positive gain for the transition under study, the time to threshold is reduced relative to that of the driver alone. If the "slave" reaction has negative gain, the opposite situation occurs. By varying the "slave" reaction temperature, the zero-gain temperature can be determined. The accuracy of the zero-gain technique is only limited by the reproducibility of the time to reach threshold for the "drive" reaction. This method is very useful for the determination of low

population inversion reactions which are not able to achieve laser threshold alone in a laser cavity (76).

vi) Grating-Selected Laser Emission.

The optical configuration of the laser cavity is the autocollimation (Littrow configuration (77)) (Fig. 3c), where a plane diffraction grating is used as one element of the optical cavity. The diffraction grating restricts oscillation to a single vibrational-rotational transition, thereby allowing all transitions with net positive gain to lase by tunning (56), which does not happen in a free running laser.

1.3.2.2 Molecular Beam Spectroscopy.

This is a method complementary to chemiluminescence (16). It has been used to determine the angular distribution and translational energy distribution. To a limited extent, and for a limited range of reactions, final-state selection of angles (including polarization of the molecular angular momentum with respect to the velocity of the attacking atom) and energies (translational, vibrational and rotational) have been achieved.

Attempts have also been made to determine the effect on reaction cross-section and product energy distribution

of variation in reagent translation, vibration and rotation. The recent extension of the molecular beam method to reactions other than those of alkali metal atoms represents a major advance (78). State-to-state reaction rates were reported by Zare and coworkers (79) for the reaction [28].

$$Ba + HF(v=0,1) \longrightarrow BaF\ (v=0\text{-}12) + H \qquad [28]$$

A combined method of laser-induced fluorescence (section 1.3.2.4) and molecular beam spectroscopy under single-collision conditions was used.

1.3.2.3 Time Resolved Gain Spectroscopy.

This method uses a laser acting on rotational-vibrational transition of molecules formed in the chemical reaction (80). By passing the laser beam through the reaction cell, the evolution of amplification coefficients for radiation corresponding to the center of transitions between two levels from initiation of the reaction can be studied. The amplification coefficient α is defined by

$$\alpha = (1/\ell)\ln(I_t/I_o) \qquad [29]$$

where, I_t and I_o are transmitted and incident intensities

respectively, and ℓ is the path length.

For a transition between levels v" and v', α is related to the $N_{v"}$ and $N_{v'}$ populations by the complicated equation

$$\alpha^{v,J}_{P_{Branch}} = \frac{8\pi^3 c}{3kT}\left(\frac{M}{2\pi RT}\right)^{\frac{1}{2}} |R_V^{V+1}|^2 \, F_V^{V+1}(J)$$

$$J\left\{N_{V+1} \; B'_{V+1} \exp\left[-\frac{hcB_{V+1}}{kT}J(J+1)\right]\right. \qquad [30]$$

$$\left. -N_V B_V \exp\left[-\frac{hcB_V}{kT}J(J+1)\right]\right\}$$

From the evolution of amplification coefficients, relaxation rates can also be studied.

1.3.2.4 Laser-Induced Fluorescence Method.

The laser-induced fluorescence method is a recent and powerful addition to the tools available for measuring product energy distribution and is based on electronic fluorescence spectroscopy (81). In this method, the wavelength of a tunable narrow-band light source (laser) is changed until it coincides with a molecular absorption line. The molecule makes a transition to an excited electronic state which is detected by observing the subsequent light emission of the molecule. The principal deter-

minations from the fluorescence spectra are the values of vibrational band intensities, $I_{v''}^{v'}$, which are related to the vibrational populations $N_{v'}$. While individual rotational lines are not observed, it is still possible to estimate the rotational distribution of some vibrational levels from the envelope of the vibrational band.

1.4 Berry Model: Golden Rule Calculations.

While the dynamical models described above are extremely useful for simple molecules, it is impossible to apply them to polyatomic systems because the number of parameters increases quite rapidly. Therefore, some simpler models for dissociation processes of polyatomic molecules have been developed. All these semiclassical (82) and quantum mechanical models of dissociation of polyatomic molecules (83, 84) make a series of assumptions known collectively as the quasidiatomic assumption. The final state reaction coordinate (i.e., dissociation) is assumed in these models to be a normal mode of vibration in the initial electronic state of the polyatomic molecule. Furthermore, this normal mode is taken to be a pure bond vibration, and the remaining vibrations are

assumed to be unchanged. Interactions due to the recoil of the fragments is the only mechanism taken to lead to changes in the distribution of the latter. For example, in the case of the photodissociation of a linear triatomic molecule, the dissociation is regarded as due to photon absorption into the localized bond that breaks. The remaining diatomic fragment is assumed to have the same structure as in the initial state of the triatomic molecule. If the triatomic molecule is initially in its ground vibrational state, then, upon absorption of the photon, the diatomic fragment would be only in its ground vibrational state. The only means of vibrationally exciting the fragment is via the interactions that occur between the fragments due to their recoil.

Some theories incorporate an incoherent distribution of diatomic vibrational states after photon absorption but, the basic quasidiatomic model is still retained (85, 86, 87). In most molecules, the reaction coordinate, a bond vibration, is not a normal coordinate of the initial electronic state of the molecule (88); it is a linear combination of normal modes. In addition, for most cases, the remaining diatomic vibration does not have the same structure as in the initial polyatomic molecule. Furthermore, the stipulation that the final fragment,

i.e., the remaining bond, is identical before and after the recoil seems a severe restriction.

The Berry Model (56, 89, 90) is similar to the models used to calculate the vibrational probabilities for photoionization of a diatomic molecule (88). It is discussed here in more detail since it has been used in the present work.

Berry has developed a very simplified model to calculate the vibrational probability of a diatomic product of a chemical reaction (89).

$$\begin{array}{l} A + BC \rightarrow ABC^{\neq} \rightarrow AB + C \\ \qquad\qquad\quad \searrow \quad \nearrow v' \\ \qquad\qquad\quad AB^{\neq} + C \\ \qquad\qquad\quad v''=0 \end{array} \qquad [31]$$

In this model, the diatomic species is suddenly stripped of the rest of the molecule at the transition state. One is left with an undressed diatomic oscillator in $v''=0$ vibrational state. The bond length of this oscillator is determined by the nature of the potential surface and the dynamics of the reaction. Berry treats this bond length, $r_e^{\neq}$, as a parameter to be used to fit the observed vibrational populations. The transition probabilities from the undressed diatomic oscillator in its lowest vibrational level to the final vibrational levels of the ob-

served spectroscopic state of the product diatomic molecule may be calculated by using Fermi's Golden Rule for resonant decay

$$P_{v'} \propto \left| \int \psi_{v'} \psi_{v''=0} dr \right|^2 \rho_{v'} \qquad [32]$$

The probability of vibrational level v' is proportional to the Franck-Condon factor between this level and the v"=0 level of the undressed oscillator, multiplied by the density of rotational and translational states of the two-body system treating C [31] as an atom.

Since the model is a localized one, in a localized picture, only a portion of $E(^{Localized}_{Available})$ is partitioned into evolving degrees-of-freedom which couple efficiently to the final AB vibrational coordinate. Localized energies available to products may be calculated from the relation

$$E(^{Localized}_{Available}) = E_a - \Delta H_{react} + 3RT \qquad [33]$$

for polyatomic systems(57). In the above equation, E_a is the activation energy for molecular elimination of AB , ΔH_{react} the heat of reaction and the 3RT factor corresponds to the relative translational energy plus the rotational energy of the polyatomic reagent as being available to AB.

The Berry model concludes that an initial highly

displaced dressed product oscillator favors high population inversion due to large Franck-Condon factors for overlap of the initial state with high v' states of the undressed undisplaced oscillator. The non-classical region overlap dominates in this high displacement limit. An initial weakly-displaced oscillator favors low v' final states due to large integrand cancellation in overlap integrals for high v' states in the classical region. In both limits or in intermediate cases, the amount of product structural change which occurs as energy is released, determines product vibronic state distributions. The model approach identifies vibronic reaction surprisals(section 1.6) as the logarithms of Franck-Condon factors for initial and final oscillator states.

If C in equation [34] is polyatomic, a complication arises. Since any polyatomic system has a large density of states, we must assume that partial relaxation of AB occurs. Berry simulates this situation numerically by solving the master equation with rate constants

$$k_{v_1 \rightarrow v_2} = \exp\left(-\alpha \Delta E_{v_1, v_2}\right) \qquad [34]$$

where α is an empirical coupling constant, the so-called "intercontinuum coupling constant" (56) between the discrete set of vibrational levels of AB and the dense levels

of the C fragment in Berry's model for intercontinuum coupling (56). This part of the model shows how the available energy becomes distributed over the internal degrees of freedom on account of coupling of the vibrations of AB to modes of the polyatomic fragment. The rate constant of Berry's model is a special case of the energy gap "law" (10).

$$k_{v_1 \rightarrow v_2} = A(T)\ k^{(ap)}_{v_1 \rightarrow v_2}\ \exp\ (-\ \alpha \Delta E_{v_1, v_2}) \qquad [35]$$

The first factor is a pre-exponential factor and will be ignored because the time scale is arbitrary; the time for relaxation is measured in half-lives of the highest highly populated level. Berry uses the third factor as his model for intercontinuum coupling (56). On the basis of a surprisal synthesis, α for AB is expected to be independent of temperature up to 6000 ^{o}K (10). Above this temperature, α is proportional to T^{-1} (10) (Surprisals are discussed in the Section 1.6). The second factor is the a priori rate constant, which would be obtained if the rate was determined by the density of states of the final vibrational state of the product. This factor has been derived by Rubinson and Steinfeld and by Proccacia and Levine (91); its value increases with temperature (91). In Berry's Model, the temperature dependence of

the *a priori* rate constant must be simulated by changing α. It has already been observed that the value of α for deactivation of carbon monoxide by inert gases is a function of the inert gas (91).

Berry has established that this model successfully fits experimental vibrational populations in simple (90) and polyatomic systems (56). In the particular case of

$$F + H_2 \longrightarrow HF + H \qquad [36]$$

the bond length of HF predicted by the Berry Model, 1.61 Å (89), is in good agreement with the saddle-point value on an LEPS surface, 1.71 Å (92), or an ab initio surface, 1.53 Å (93). The bond length predicted by the BEBO method, 1.60 Å (94), is in good agreement with the Berry Model but the value calculated by the method of Gavitsas, 1.2 (95), is shorter than all these. Elsewere, Berry has shown that reasonable values for bond lengths may be derived from this model (90). Some theoretical support for the model may be adduced (73).

1.5 Random Statistical Model.

A very simplified statistical model assuming complete randomination of energy amongst all internal modes of the intermediate is frequently used with the dynamical models. In this type of model, the localised energy is randomly distributed amongst internal modes of the intermediate. The total energy level sum, $\Sigma P(E)$, of a molecule with s vibrational modes and r active internal rotations at energy E can be evaluated according to the approximation of Whitten and Rabinovitch (96)

$$\Sigma P(E) = C \frac{\Gamma(1+r/2)\,(E+aE_z)^{s+r/2}}{\Gamma(1+r/2+s)\prod_{i=1}^{s} h\nu_i} \qquad [37]$$

Although the "Random Statistical Model" succeeds in explaining the mechanism of extrusion of carbon monoxide from oxygen adducts of allene by using a loose dynamical model and of methylacetylene by using a tight model (97), it fails to predict the vibrational probabilities of hydrogen fluoride formed by elimination from chemically excited CH_3CF_3 (27).

1.6 The Information Theoretic Approach.

Bernstein and Levine (98) have pioneered the application of an information-theoretic approach to the understanding of detailed data regarding the dynamics of molecular encounters. They characterise the energy disposal by the statement that elementary exoergic reactions are usually highly specific in their mode of energy release (99, 100) and they have provided expressions for the extent of specificity of a process in terms of its deviation from the statistical expectation. The key to the approach is the concept of the "surprisal", the deviation from the statistical expectation. Having decided upon the a priori distribution $P^o(v)$, we can evaluate the surprisal of the observed population from the relation

$$I(f_v) = -\ln [P'(f_v)/P^o(f_v)] \qquad [38]$$

where f_v is the fraction of available energy partitioned into the vibrational level v of the products and $P(f_v)$ the experimental probability. A plot of the vibrational surprisal vs. f_v can reveal the trends in the "deviation from expectation" as a function of the degree of vibra-

tional excitation of the product. While $P(f_v)$ has an entirely different character from $P^o(f_v)$, the surprisals of many reactions show linear dependence on f_v (99, 100). In these cases, the probability may be expressed as

$$P(f_v) = P^o(f_v)\exp(-\lambda_v f_v)/\exp(\lambda_o) \qquad [39]$$

where $\exp(\lambda_o)$ plays the role of a partition function and λ_v^{-1} the role of a temperature-like parameter. Population inversion corresponds to a negative value of λ_v. In a linear case, a given value of λ_v is sufficient to characterize the entire f_v dependence of $P(f_v)$ and the gain in chemical lasers. Formerly, an ill-defined "vibrational temperature", T_{vib} had been used for this purpose. The drawback here was that different T_{vib} were needed for each v state. Bogan and Setser (57) have taken advantage of the linear nature of the surprisal plots to estimate the relative population of HF (v=0) for the abstraction of hydrogen from polyatomic molecules by F atoms.

Although linear surprisals are found for many reactions, this is not a completely general finding. In nonlinear cases, it is assumed that the surprisal can be represented by a series of f_v

$$I(f_v) = \lambda_0 + \sum_{j=1} \lambda_j f_v^j \qquad [40]$$

The coefficients λ_j can be determined by fitting the equation [40] to the experimental distribution.

The surprisal is a measure of the deviation of a particular population from the a priori one. The negative of the value of the surprisal is known as the entropy of the distribution (91, 93, 101, 102). In the thermodynamic approach, the key is the "entropy deficiency" (98, 99, 103). This is defined as the non-negative quantity

$$\Delta S^{(vib)} = S^{o}(vib) - S^{(vib)} = R\sum_v P(f_v) \ln[P(f_v)/P^{o}(f_v)] \qquad [41]$$

Here, $S^{o}(vib)$ is the value when $P=P^{o}$.

Bernstein and Levine proposed as a test of the theory that the branching ratio $\Gamma_{HF/DF}$ for the reaction F + HD would be linked to the surprisals. Polanyi and coworkers found an excellent agreement with the experimentally measured branching ratio (104).

Recently, the information-theoretic approach was applied to the analysis of state-to-state rotational energy transfer cross-sections. Linear surprisals plots were found which facilitated the interpretation of the results (105).

2. RESULTS AND DISCUSSION

2.1

REACTIONS OF ATOMIC HYDROGEN WITH VINYL FLUORIDE, 1,1-DIFLUOROETHYLENE, TRIFLUOROETHYLENE AND, TETRAFLUOROETHYLENE.

2.1.1 General.

The reactions of atomic hydrogen with fluorocarbons have received only summary attention. Chadwell and Titani (106), using the discharge tube method at room temperature, found no reaction of hydrogen atoms with methyl fluoride. Later, Dacey and Hodgins (107) investigated the mercury photosensitized reactions of mixtures of tetrafluoromethane and hydrogen molecules but again no evidence was found for the occurrence of a reaction. Clark and Tedder (108, 109, 110), studied a series of free radical substitutions in aliphatic compounds. They found that the first step in the reactions of hydrogen atoms with bromotrichloromethane and fluorotrichloromethane was the abstraction of a halogen atom. The resulting trihalomethyl radical added H to form a vibrationally excited molecule, which either stabilized or, decomposed by elimination of HX. If fluorocarbons were the reactant species, the elimination of HF always occurred in preference to stabilization.

Scott and Jennings (111), studied the products formed by the addition of hydrogen atoms to C_2H_3F, 1,1-$C_2H_2F_2$ and, C_2HF_3 using the mercury photosensitization method. Hydrogen atoms have been shown to add largely or,

exclusively to the less fluorinated carbon of these fluoroethylenes. In an early investigation, Allen, Melville and Robb (112) obtained a collision efficiency of $.3 \times 10^{-4}$ for the reaction of atomic hydrogen with tetrafluoroethylene.

More recently, Penzhorn and Sandoval (113), studied the addition and abstraction reactions of thermal hydrogen atoms with fluorinated ethylenes using hot hydrogen atoms produced from the photolysis of HBr. They found that the relative rates of addition for C_2H_4:C_2H_3F:1,1-$C_2H_2F_2$:C_2HF_3:C_2F_4 are 1:0.785:1.451:1.649:1.69 . According to these ratios, the reaction of tetrafluoroethylene with hydrogen atoms is 1.69 times faster than the reaction of ethylene with hydrogen atoms. However, Robb et. al. (112) found that the reaction of hydrogen atoms with tetrafluoroethylene was about 25 times slower than the reaction with ethylene. They used heterogeneous removal of atomic hydrogen on molybdenum oxide to provide competition with the fast gas-phase removal of atomic hydrogen by unsaturated compounds (112).

Jones and coworkers (114) studied the products formed in the reaction of atomic hydrogen with tetrafluoroethylene and later investigated the kinetics of the same reaction (115). They also studied the products formed in the react-

ions of atomic hydrogen with C_2H_3F and 1,1-$C_2H_2F_2$ using the Wood's discharge method of producing hydrogen atoms (116, 117). The determination of the reaction mechanism was complicated by the large number of products formed. The calculation of the rate constants and testing of the mechanisms was accomplished by numerical integration of the simultaneous differential equations for each species involved in the reactions.

They give (116, 117), at 1.2 torr, the rate constant values (cm^3 $molecule^{-1}$ s^{-1})

C_2H_3F: k

$$H\cdot + C_2H_3F \rightarrow C_2H_4F^{*}\cdot \xrightarrow{M} C_2H_4F\cdot \qquad 4.5 \times 10^{-14} \quad [42]$$

$$H\cdot + C_2H_4F\cdot \rightarrow C_2H_5F^{**} \rightarrow C_2H_4 + HF^{\dagger} \qquad <3.92\times 10^{-11} \quad [43]$$

1,1-$C_2H_2F_2$:

$$H\cdot + 1,1\text{-}C_2H_2F_2 \rightarrow 1,1\text{-}C_2H_3F_2^{*}\cdot \xrightarrow{M} 1,1\text{-}C_2H_3F_2\cdot \qquad 1.3 \times 10^{-14} \quad [44]$$

$$H\cdot + 1,1\text{-}C_2H_3F_2\cdot \rightarrow 1,1\text{-}C_2H_4F_2^{**} \rightarrow C_2H_3F + HF^{\dagger} \qquad 3.98\times 10^{-11} \quad [45]$$

$$H\cdot + C_2H_3F \rightarrow C_2H_4F^{*}\cdot \xrightarrow{M} C_2H_4F\cdot \qquad [42']$$

$$H\cdot + C_2H_4F\cdot \rightarrow C_2H_5F^{**} \rightarrow C_2H_4 + HF^{\dagger} \qquad [43']$$

Excited $HF^{\dagger}$ is predicted from reactions [43], [45] and [43']. The available energy from the exothermicity

of these reactions is at least 58 kcal/mol (117) which is enough to excite the hydrogen fluoride to the eighth vibrational level.

The IR chemiluminescence from the reaction of atomic hydrogen with fluorine has been studied quite extensively (39, 52, 118, 119). The reaction has also been studied by chemical laser techniques (120). The reactions of atomic hydrogen with more complicated inorganic compounds have also been studied such as $H+OF_2$ by chemiluminescence (121) and H+ClF and $H+ClF_3$ by chemical lasers (122). However, there is no such work for reactions of fluorocarbons with atomic hydrogen.

An attempt to study the reactions of atomic hydrogen with organic fluoro-compounds by chemiluminescence is presented in the present work. In particular, the reactions of atomic hydrogen with vinyl fluoride, 1,1-difluoroethylene, trifluoroethylene and tetrafluoroethylene have been examined by IR chemiluminescence using the "single window flow method". The method is discussed in the introduction and more details are given in the experimental Chapter.

2.1.2 Preliminary Study of the Reactions.

The reaction of atomic hydrogen with tetrafluoroethyl-

one was examined initially. The experimental conditions were varied until an emission corresponding to HF P(3) v'=1 v"=0 was observed. The region from 2 to 3 μm of the vibrational-rotational spectrum of HF was scanned and the emission was positively identified as due to vibrationally excited HF .

After the first spectrum had been obtained, some tests were made to ascertain whether the emission was really the result of the reaction of atomic hydrogen with the fluoroethylene using vinyl fluoride as the reactant. Thus, one run was performed without the reactant, C_2H_3F, and no emission was observed. A run using hydrogen fluoride instead of the reactant also gave no emission which assured us that we did not have emission from energy transfer processes. A run in which the reactant C_2H_3F was present, with the microwave discharge operating only on pure inert gas (no hydrogen), showed no emission, indicating that no reactant was flowing upstream into the discharge. During a regular run, the position of the discharge was moved some distance (approximately 60 cm) from the reaction zone. The emission, in this case remained strong which proved that it resulted from the reaction of atomic hydrogen with the fluoroethylene and not from reaction of excited molecular or atomic hydrogen. Metastable electronic levels of hydrogen atoms or molecular hydrogen cannot survive

long transit times from the discharge to the reaction cell. This also applies to vibrationally excited molecular hydrogen which is rapidly deactivated in the presence of H atoms (123).

2.1.3 Experimental Data.

In Figures 4-7 the sample emission spectra of the reactions of atomic hydrogen with the fluoroethylenes are presented. In each case the spectrum represents emission from the bands 1-0, 2-1 and 3-2, at a pressure of 1.07 mmHg and flow rates of molecular hydrogen 16 μmol/s, Argon 258 μmol/s and fluoroethylene (FE) 207 μmol/s.

After obtaining similar spectra for each compound and set of conditions, the data analysis began by assigning the vibrational-rotational lines to each spectrum. The lines were easily identified by comparison with the published vibrational-rotational frequency values (124, 125). The area of the peaks representing each line were obtained by two methods. The heights of the non-overlapped peaks were converted to peak area by multiplication by the half-width of the peaks. For partially overlapped peaks, equivalent triangles were used for the estimation of the area. The errors on measured areas were less than 2% for

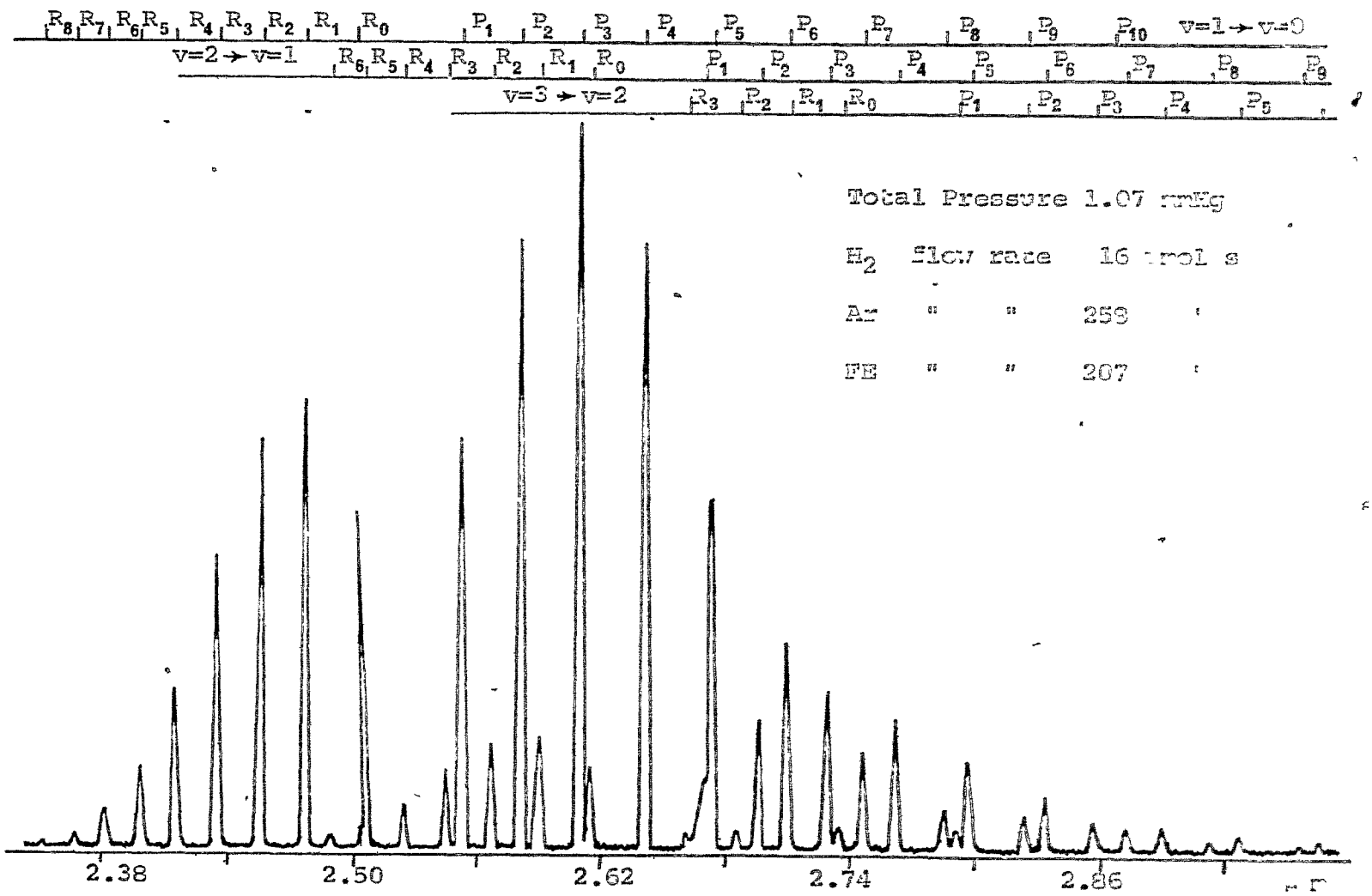

Fig. 4. The $HF^{\dagger}(\Delta v=1)$ emission spectrum from the reaction of H atoms with C_2H_3F.

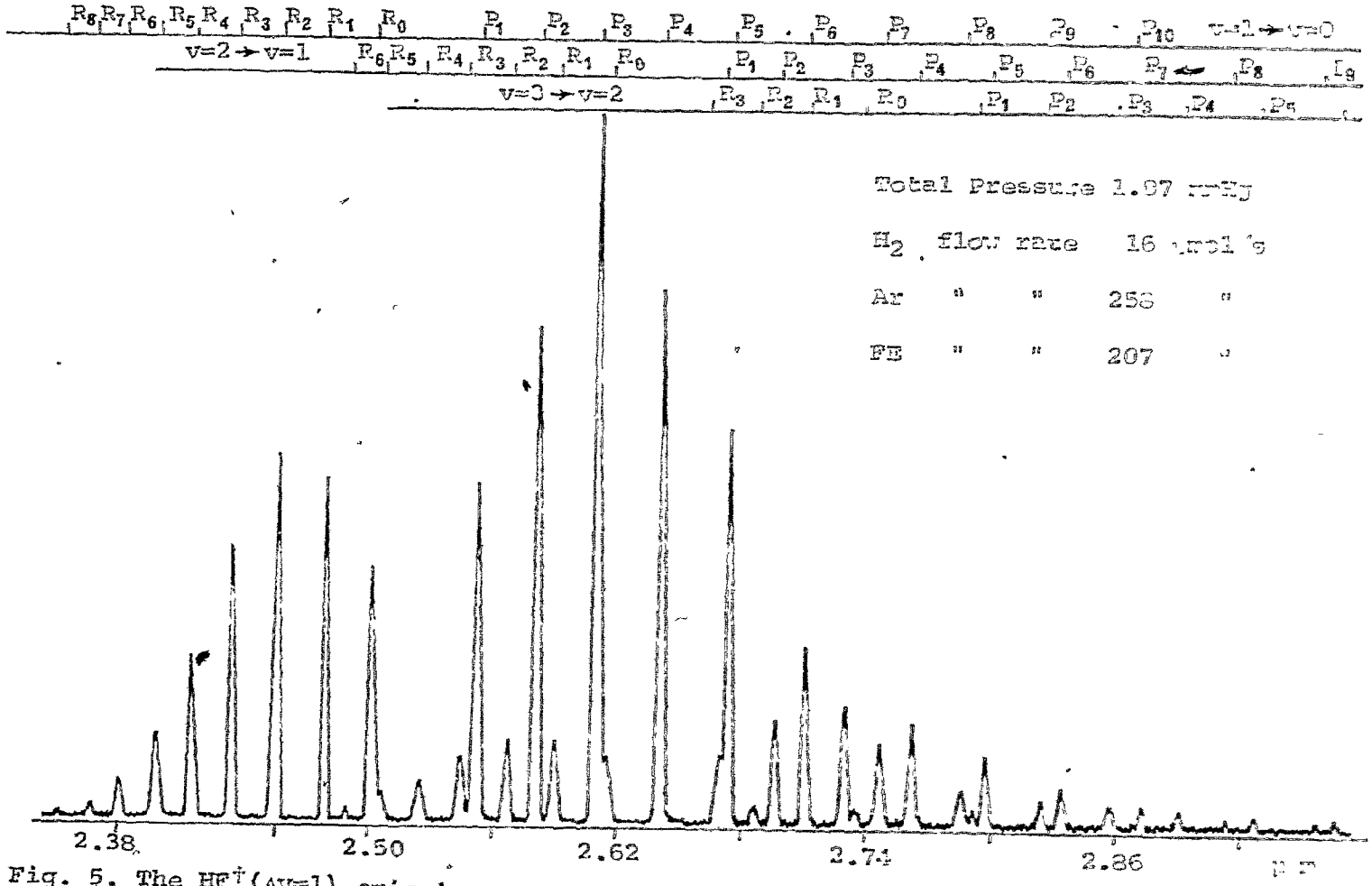

Fig. 5. The $HF^{\dagger}(\Delta v=1)$ emission spectrum from the reaction of H atoms with 1,1-$C_2H_2F_2$.

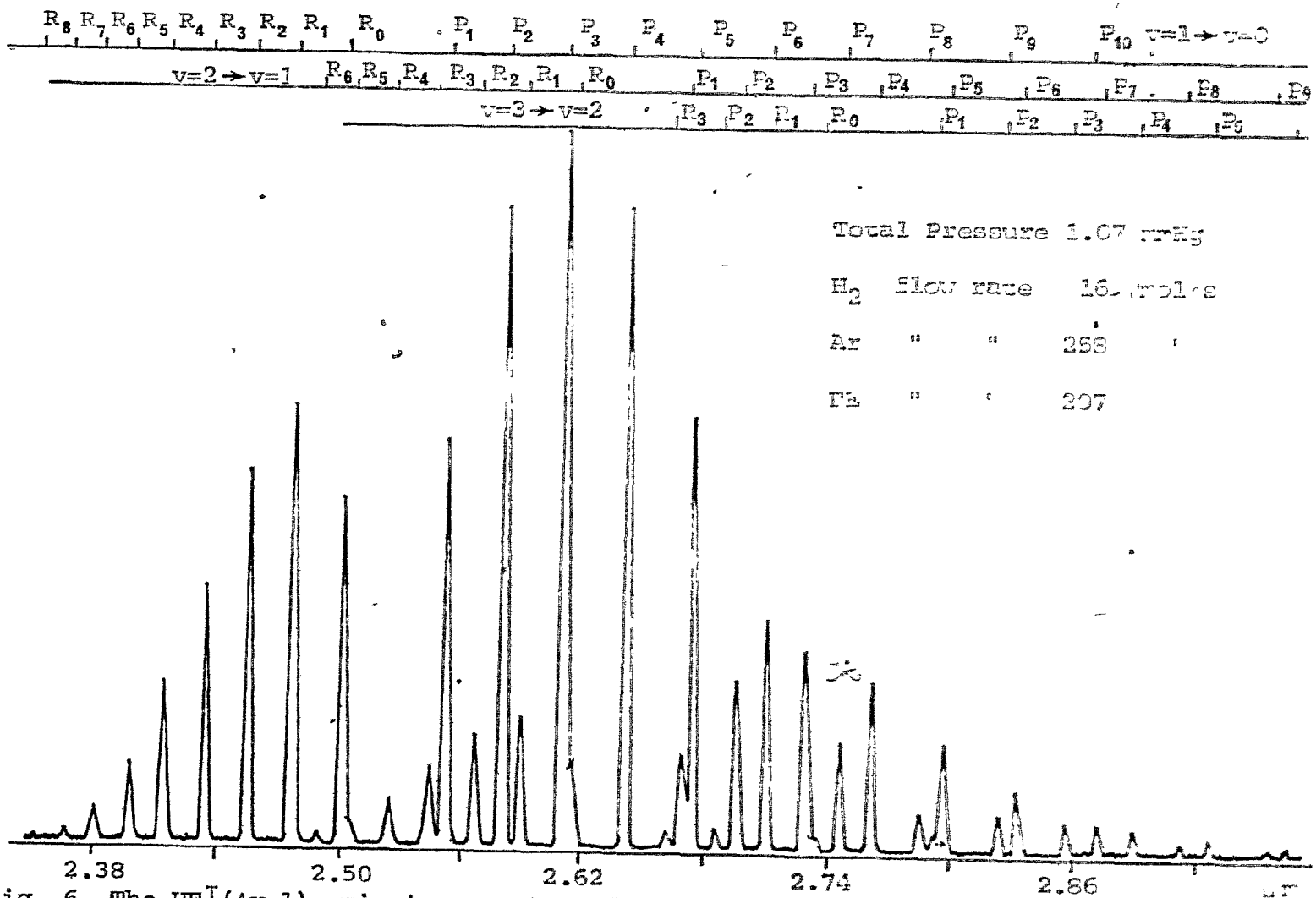

Fig. 6. The $HF^{T}(\Delta v=1)$ emission spectrum from the reaction of H atoms with C_2HF_3.

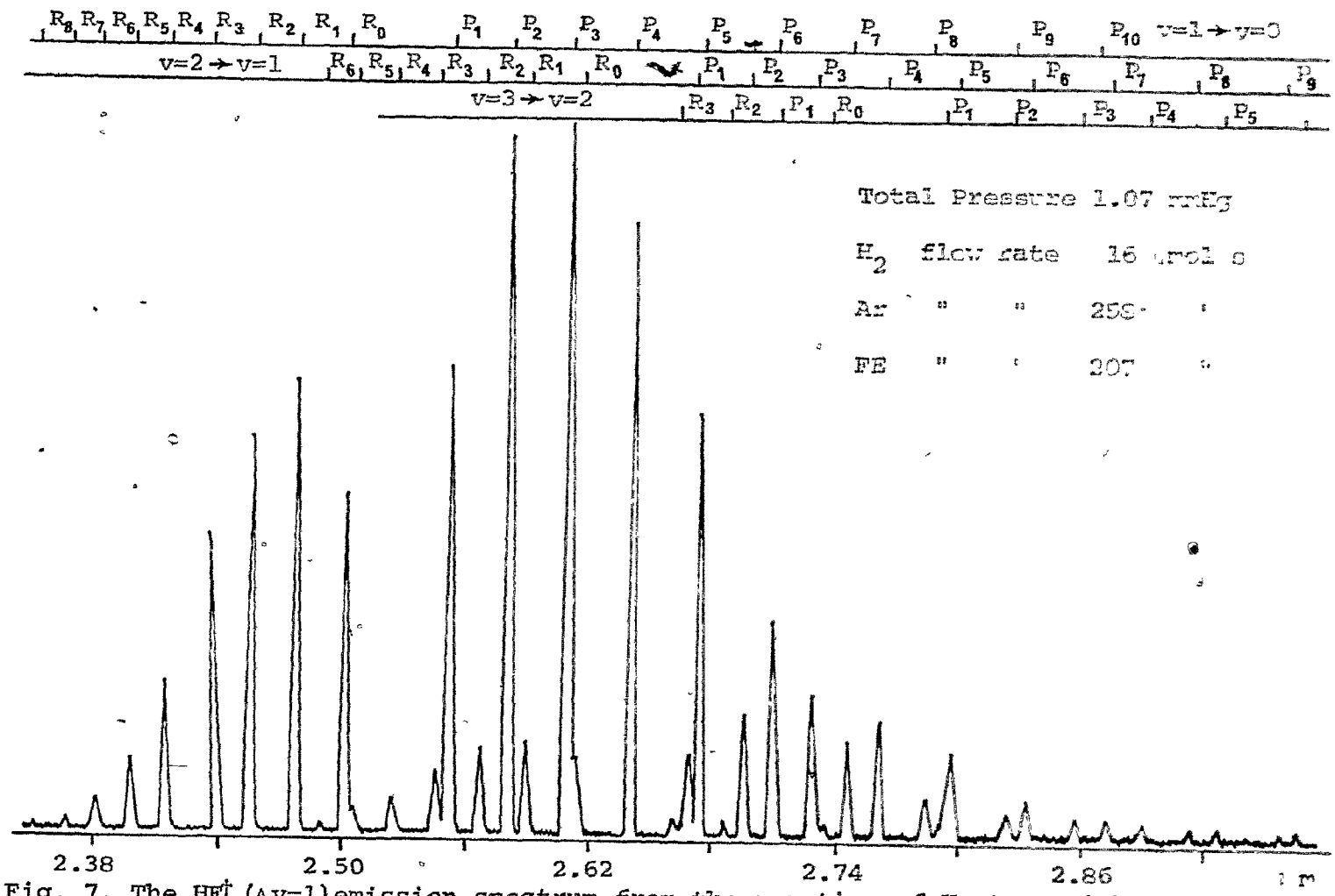

Fig. 7. The $HF^{\dagger}$ ($\Delta v=1$) emission spectrum from the reaction of H atoms with C_2F_4.

the average peaks and about 7% for the very small peaks. The areas obtained by these methods are presented in Appendices B1-B6. The sq. .01" was used as unit area. The relative intensities $I_{v''J''}^{v'J'}$ of the vibrational-rotational lines are proportional to these areas. The sensitivity of the detector and grating is different at various wavelengths, thus the experimental values were corrected by calibrating the detection system with a black-body at 617 ^{o}K.

2.1.4 Calculation of the Relative Stationary-State Rotational Populations.

The relative intensity $I_{v''J''}^{v'J'}$, divided by the transition probability $A_{v''J''}^{v'J'}$, gives the relative vibrational-rotational population (126, 127)

$$N_{v'J'} \propto \frac{I_{v''J''}^{v'J'}}{A_{v''J''}^{v'J'}} \propto \frac{I_{v''J''}^{v'J'}(2J'+1)}{\omega_J^4 S_J \left| M_{v''J''}^{v'J'} \right|^2} \qquad [46]$$

where, $N_{v'J'}$ is the relative population of the vibrational-rotational level v', J',

v is the vibrational quantum number,

J is the rotational quantum number,

ν_J is the frequency of the vibrational-rotational line,

S_J { is J' for the R branch
is J'+1 for the P branch and,

$M^{v'J'}_{v"J"}$ is the vibrational matrix element.

The double prime refers to the lower state.

The vibrational matrix element, $M^{v'J'}_{v"J"}$, calculated according to Herman and Wallis (126), is a function of the vibrational-rotational level

$$\left|M^{v'J'}_{v"J"}\right|^2 = \left|R^{v'}_{v"}\right|^2 \cdot F^{v'}_{v"}(m) \qquad [47]$$

where, $R^{v'}_{v"}$ is the vibrational matrix element for the harmonic oscillator and,

$F^{v'}_{v"}(m)$ is the vibration-rotation interaction.

The $F^1_0(m)$, $F^2_1(m)$, $M^{1\ J'}_{0,J"}$, and $M^{2\ J'}_{1,J"}$ were calculated as follows (126) :

$$F^1_0(m)=1-40\gamma m[1+3\gamma(1+5b/2\gamma^{1/2}-13b/120\gamma^{1/2}-1/80) \qquad [48]$$
$$-m(0\gamma-3\gamma/80-3b\gamma^{1/2}/40)]$$

$$F^2_1(m)=1-40\gamma m[1+6\gamma(1+5b/2\gamma^{1/2}-13b/120\gamma^{1/2}-1/80) \qquad [49]$$
$$-m(0\gamma-3\gamma/80-3b\gamma^{1/2}/40)]$$

$$M_0^1 \; {}^{J'}_{J''} = (M_1/[2\alpha]^{1/2})\{1-20\gamma m[1+15b\gamma^{1/2}/2+3\gamma-5b\gamma^{1/2}/20+ \quad [50]$$

$$+3b\gamma^{1/2}(m-1)/40+3\gamma(m-1)/80]\}$$

$$M_1^2 \; {}^{J'}_{J''} = (M_1/\alpha^{1/2})\{1-20\gamma m[1+15b\gamma^{1/2}+6\gamma-23b\gamma^{3/2}/40+ \quad [51]$$

$$+3b\gamma^{1/2}(m-1)/40+3\gamma(m-2)/80]\}$$

where,

$$m = \begin{cases} J'' + 1 & \text{for the R branch} \\ -J'' & \text{for the P branch} \end{cases} \quad [52]$$

$$\gamma = 2B_e/\omega_e \quad [53]$$

$$\alpha = 1/\gamma r_e^2 \quad [54]$$

$$b = -\gamma^{1/2}(1+\alpha_e/3\gamma B_e)/2 \quad [55]$$

Values used for the r_e, 0, α_e, M_1, B_e and ω_e are given in Table A1. From the calculated values of the vibrational matrix elements and the vibration-rotation interaction, the values of the transition moment $R_{v''}^{v'}$ were calculated for v=1 and v=2 vibrational levels as shown in Table 1.

Table 1

Transition Moments for HF.

Transition Moment	Calculated (Debye)	Ref. 128
R_0^1	.104	.105
R_1^2	.148	
R_1^2/R_0^1	1.423	1.438
R_2^3/R_0^1		1.792
R_3^4/R_0^1		2.106

For the same sequence, the vibration-rotation interaction is purely a function of m (128) (m is given by equation [52]), which can be seen from the calculated values of F_0^1 (m) and F_1^0 (m), Table 2. From the approximation $F_3^4 \simeq F_2^3 \simeq F_1^2$ and the values R_3^4/R_0^1 and R_2^3/R_0^1, the matrix elements $M_{3\ J''}^{4\ J'}(m)$ and $M_{2\ J''}^{3\ J'}(m)$ were calculated. Using these values, the relative population of the rotational levels with respect to the $N_{v'=1,J'=2}$ were calculated according to equation [46] and the results are shown graphically in Figures 8-11.

Table 2

Vibration-Rotation Interaction Factors for HF.

Transition	F_0^1	F_1^2
P(1)	1.05	1.05
P(2)	1.10	1.10
P(3)	1.15	1.14
P(4)	1.20	1.19
P(5)	1.25	1.24
P(6)	1.31	1.30
P(7)	1.36	1.35
P(8)	1.42	1.41
P(9)	1.48	
R(0)	.954	.956
R(1)	.910	.913
R(2)	.867	.871
R(3)	.826	.831
R(4)	.786	.793
R(5)	.748	
R(6)	.712	
R(7)	.677	

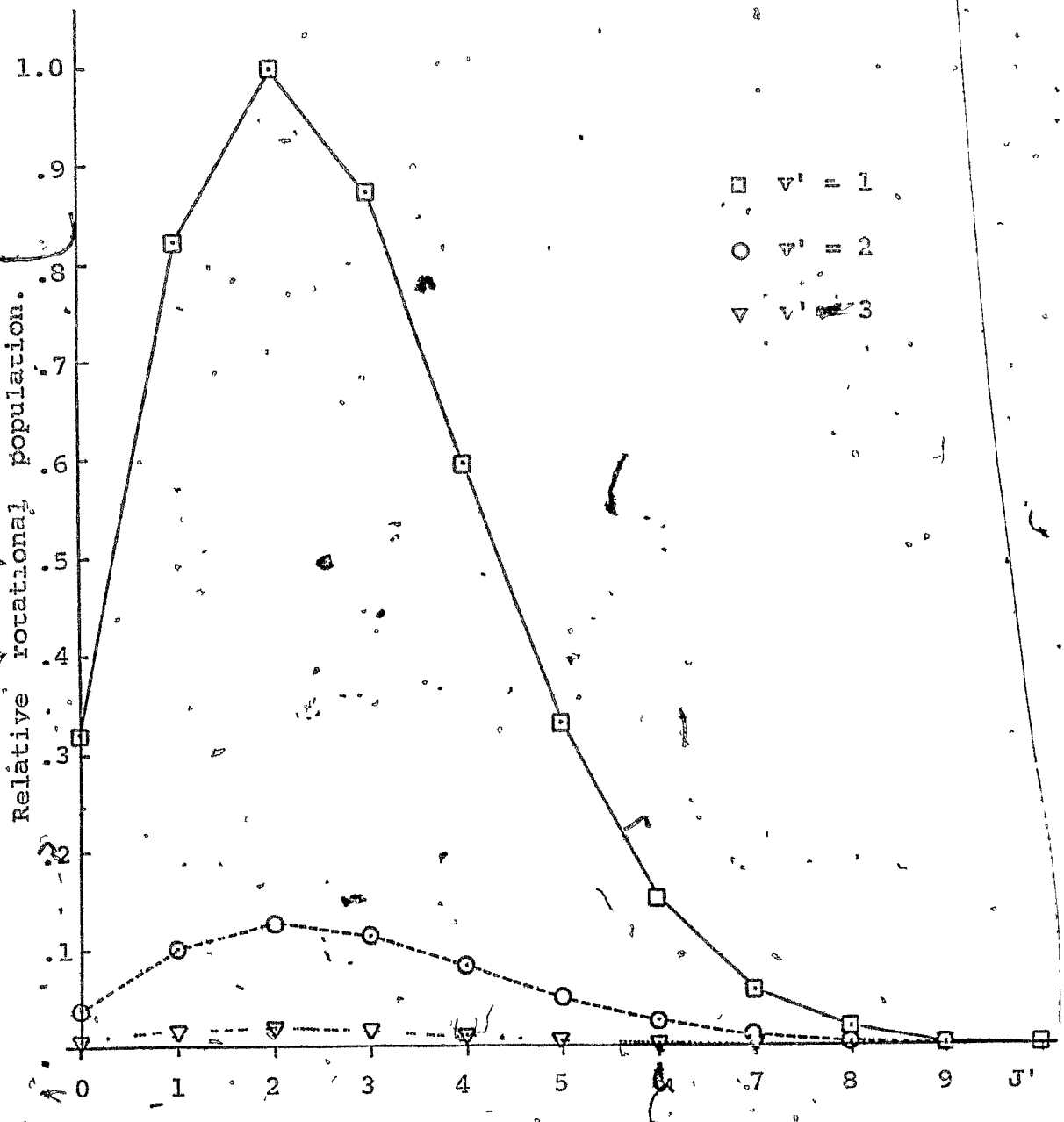

Fig. 8. The relative rotational population of HF from the reaction of H with C_2H_3F.

H_2 flow rate 16 μmol/s FE flow rate 207 μmol/s

Ar " " 258 " Total Pressure 1.07 mmHg

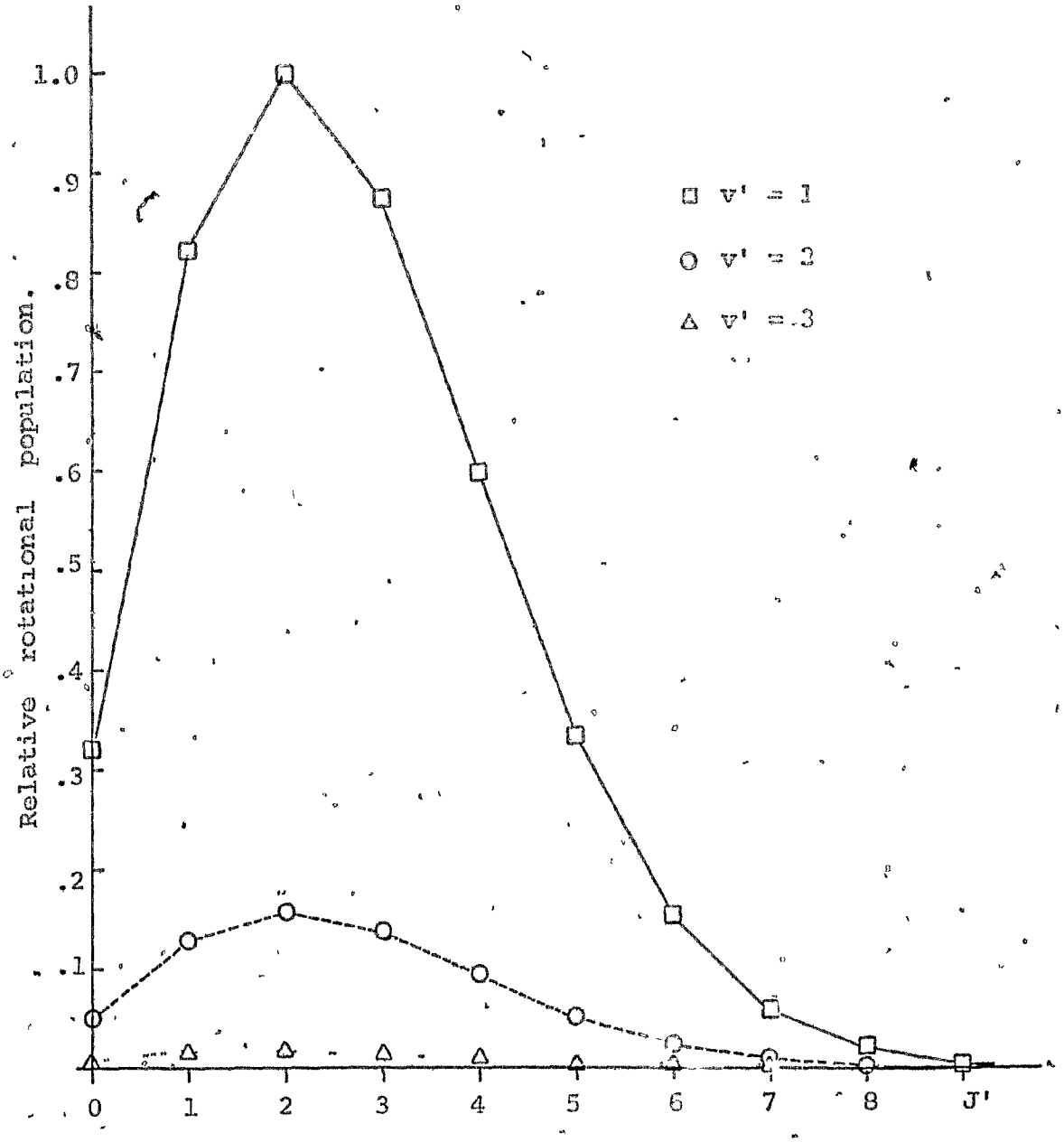

Fig. 9. The relative rotational population of HF from the reaction of H atoms with $1,1\text{-}C_2H_2F_2$.

H_2 flow rate 16 μmol/s , FE flow rate 207 μmol/s

Ar " " 258 " Total Pressure 1.07 mmHg

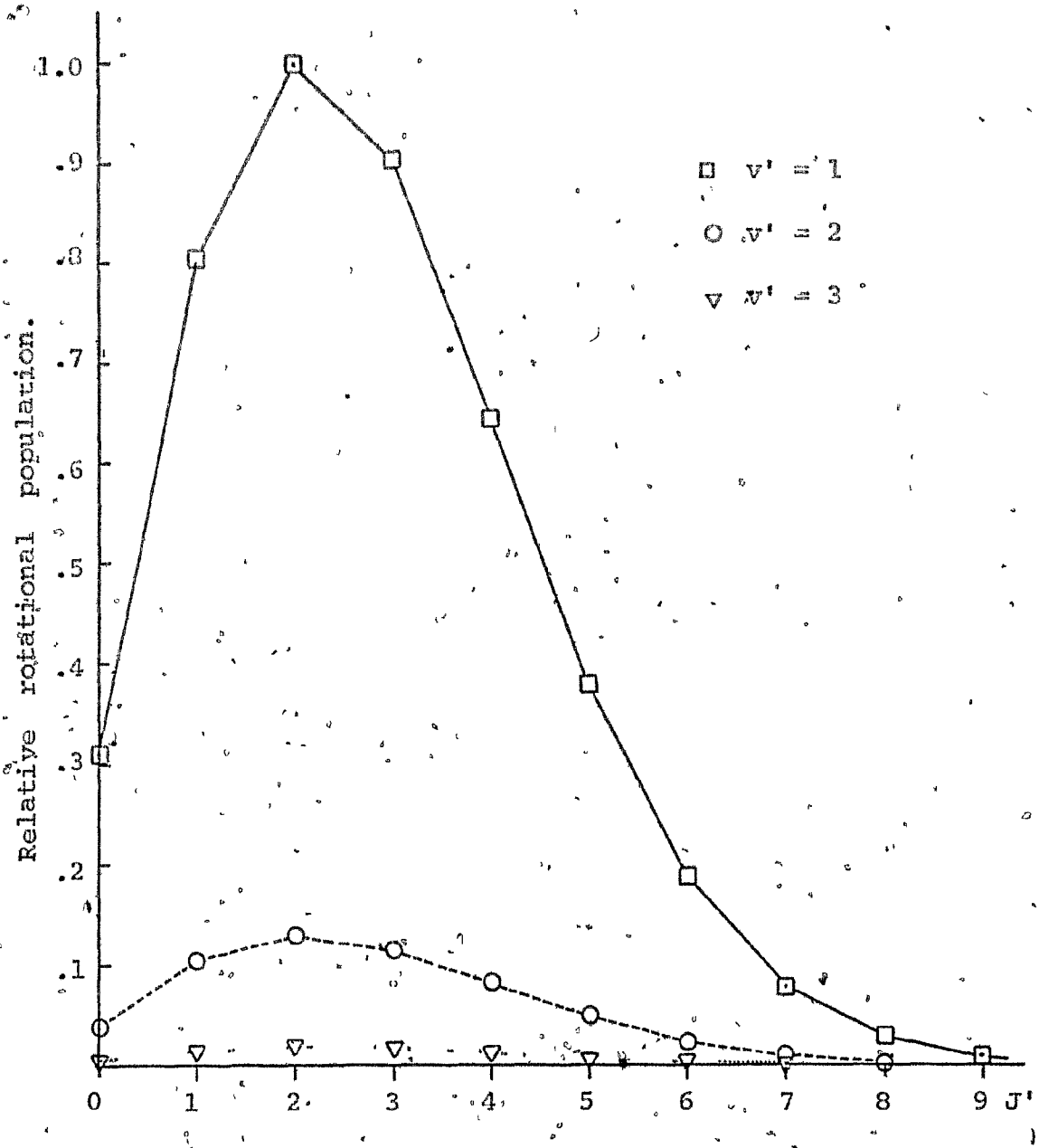

Fig. 10. The relative rotational population of HF from the reaction of H with C_2HF_3.

H_2 flow rate 16 μ mol/s FE flow rate 207 μ mol/s

Ar " " 258 " Total Pressure 1.07 mmHg

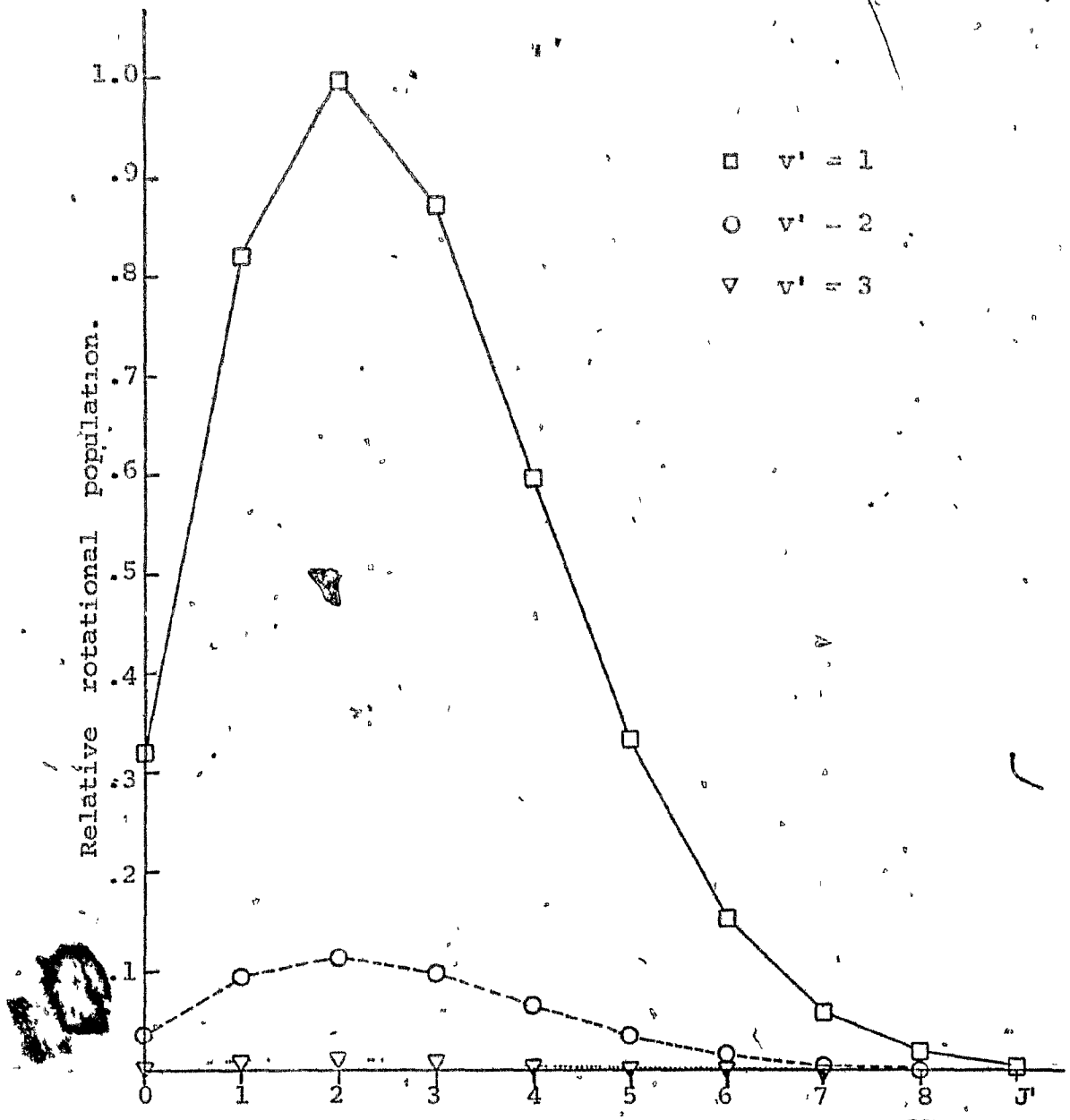

Fig. 11. The relative rotational population of HF from the reaction of H atoms with C_2F_4.

H_2 flow rate 16 μmol/s FE flow rate 207 μmol/s

Ar " " 258 " Total Pressure 1.07 mmHg

The rotational levels are close together, therefore a very small number of collisions is sufficient to give a Boltzmann equilibrium. Thus, there is a very fast relaxation between rotational levels (the relaxation of the translational levels is even faster) and the Boltzmann distribution between rotational levels applies (129).

$$N_{v'J'} = (2J'+1)\exp(-J'(J'+1)Bhc/kT_{rot}) \qquad [56]$$

Substituting in [46], rearranging, and taking logarithms, we have

$$\ln\left(I^{v'J'}_{v''J''}/\omega^4_J S_J \left|M^{v'J'}_{v''J''}\right|^2\right) = -Bhc(J'(J'+1))/kT_{rot} \qquad [57]$$

The logarithmic quantity on the left hand side of the equation [57] plotted against $J'(J'+1)$ should yield a straight line with slope equal to $-Bhc/kT_{rot}$. The constants h, c and, k have their usual meaning, Table A1.

Rotational Boltzmann plots for the three fundamental bands for the reactions of atomic hydrogen with vinyl fluoride, 1,1-difluoroethylene, trifluoroethylene and tetrafluoroethylene are given in Figures 12-15. Rotational temperatures are taken from the slopes of the lines using the least squares method. The average rotational temperatures are given in Table 3.

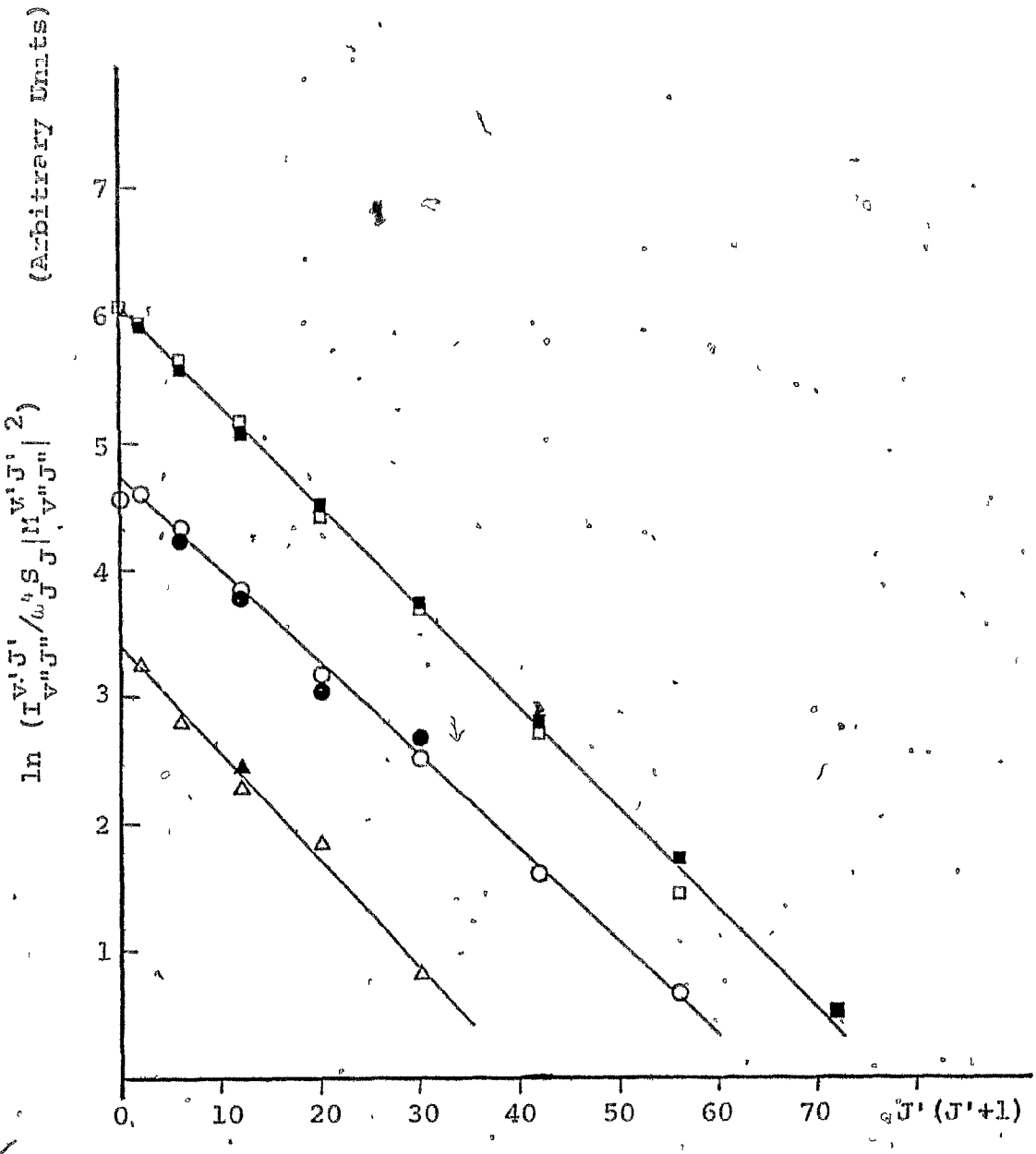

Fig. 12. Stationary-state distribution of HF among rotational states from the reaction of H atoms with C_2H_3F. □ from v(1→0), ○ from v(2→1), △ from v(3→2). Filled-in points from R branch lines, the remainder from P branch.

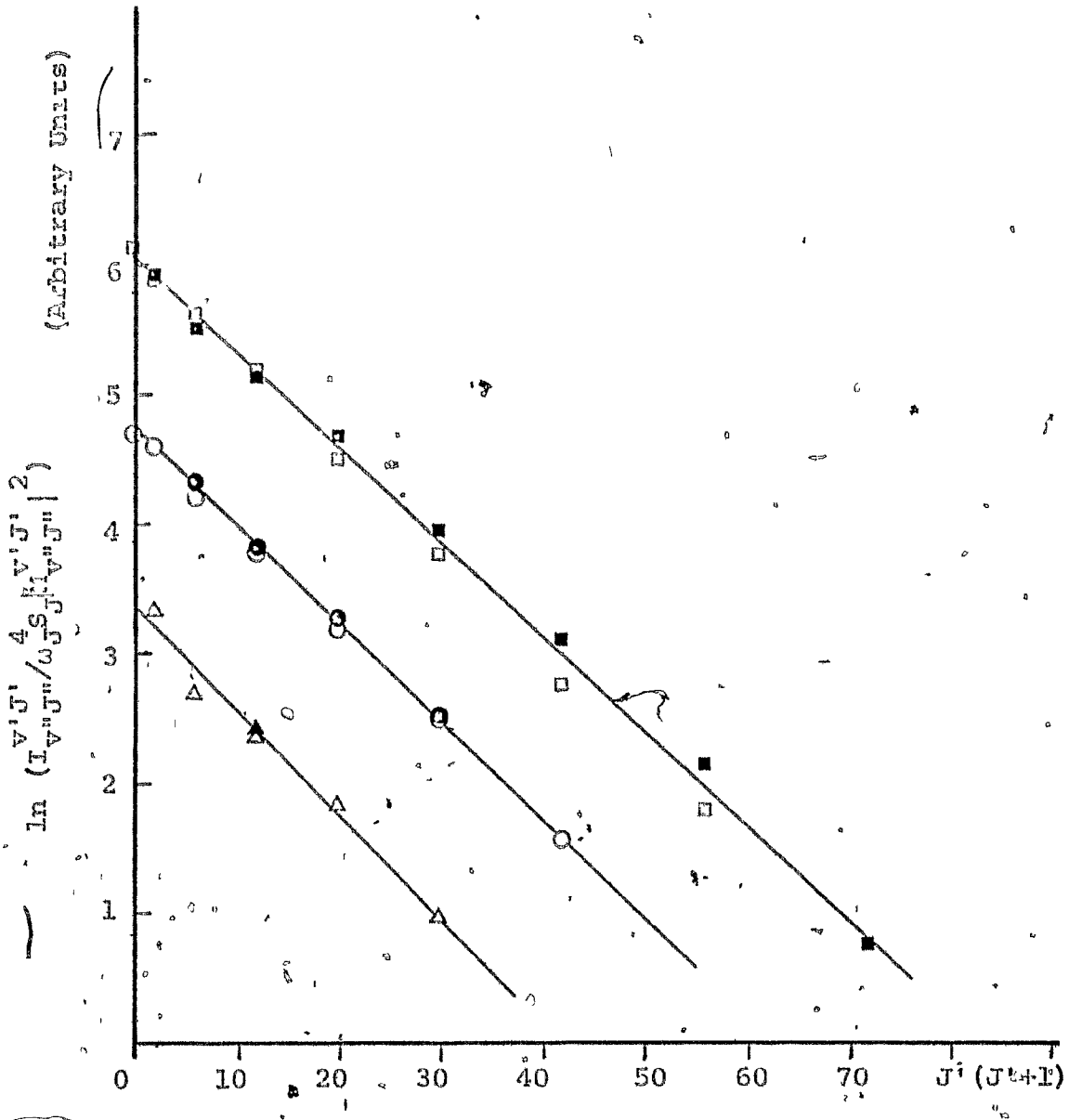

Fig. 13. Stationary-state distribution of HF' among rotational states from the reaction of H atoms with 1,1-$C_2H_2F_2$. □ from v(1→0), ○ from v(2→1), △ from v(3→2). Filled-in points from R branch lines, the remainder from the P branch.

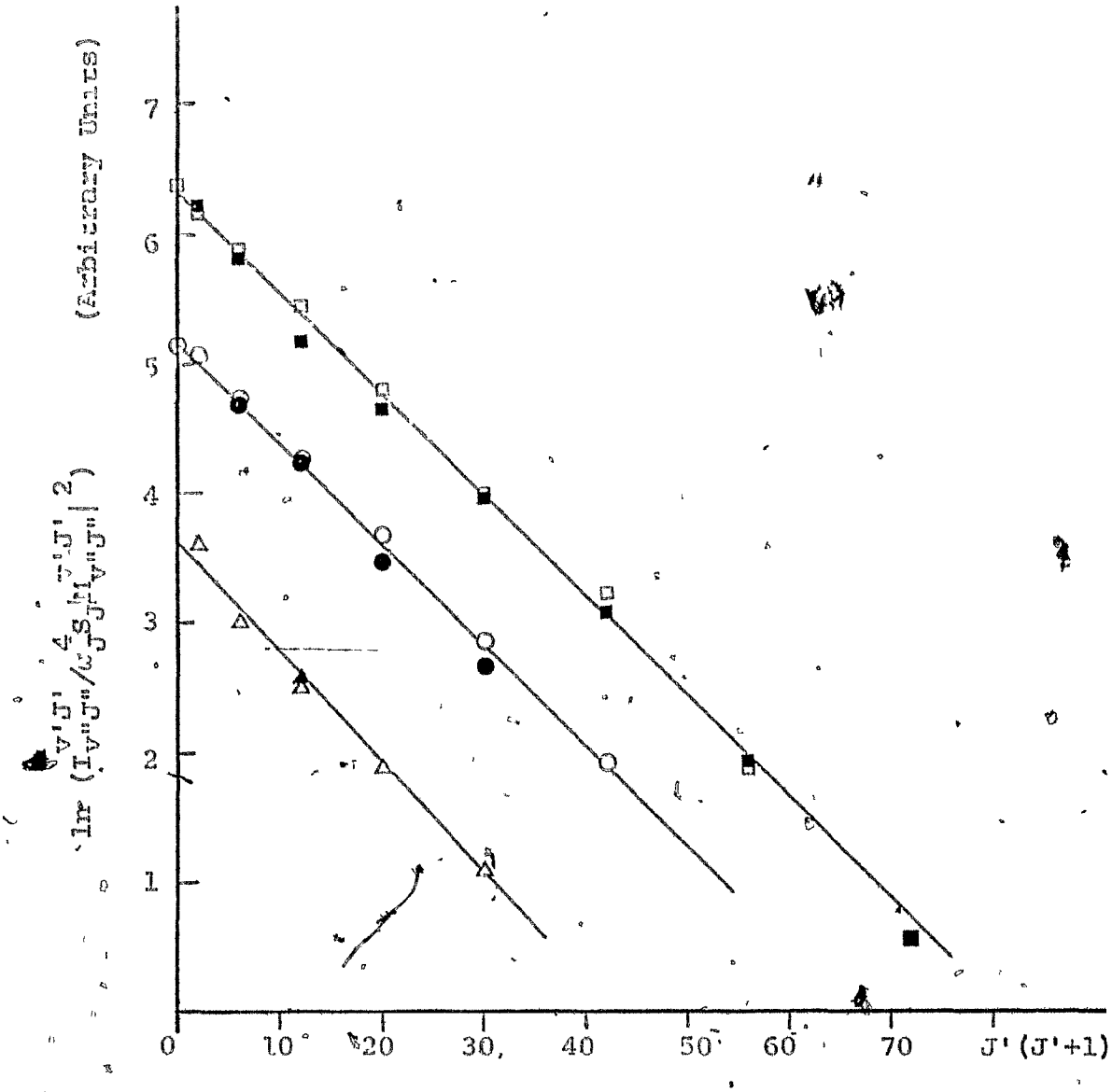

Fig. 14. Stationary-state distribution of HF† among rotational states from the reaction of H atoms with C_2HF_3. □ from v(1→0), ○ from v(2→1), △ from v(3→2). Filled-in points from R branch lines, the remainder from the P branch.

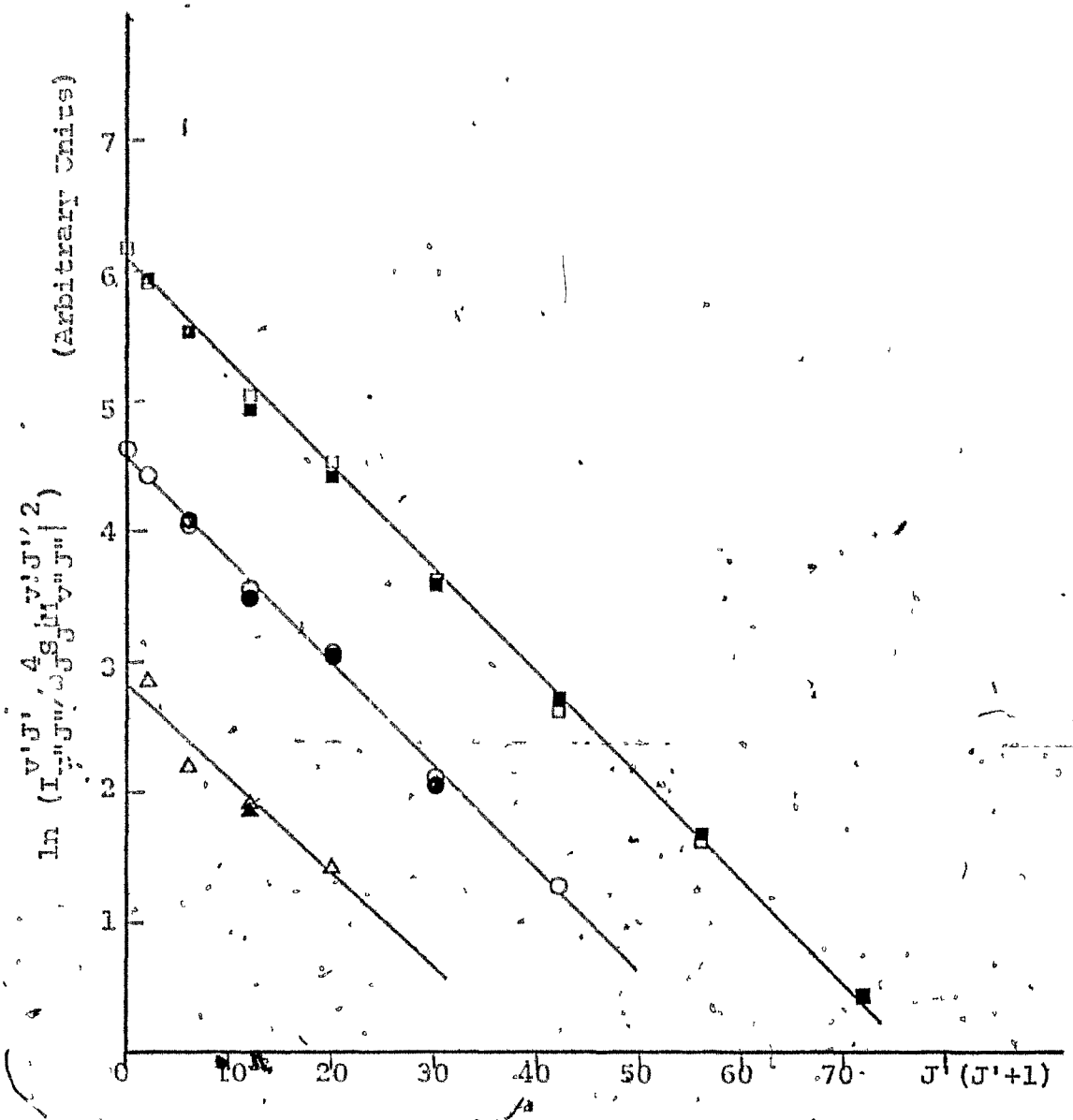

Fig. 15. Stationary-state distribution of $HF^{\dagger}$ among rotational states from the reaction of H atoms with C_2F_4. □ from v(1→0), O from v(2→1), △ from v(3→2). Filled-in points from R branch lines, the remainder from the P branch.

Table 3

Average Rotational Temperatures for the Reactions of H Atoms with Fluoroethylenes.

Vibrational Level	T_{rot}	±	Standard Error ^{o}K
1	346	±	4
2	343	±	4
3	381	±	19

The difference between the three rotational temperatures is very small and close to the temperature found experimentally for the reactions using a thermocouple (bath temperature 330-360 ^{o}K). This suggests the presence of a rotational-translational Boltzmann equilibrium. Therefore, assuming that there is no deviation from the Boltzmann equilibrium, the rotational Boltzmann plots (Figures 12-15) were used to find the relative population of the overlapped peaks by equations [56, 57].

2.1.5 Calculation of the Relative Stationary-State Vibrational Populations.

The relative stationary-state population in the various vibrational levels can be calculated by two methods. One method involves summing the intensities of all the lines arising from the same vibrational upper state

$$I_{v''}^{v'} = \sum_{J} I_{v''J''}^{v'J'} \qquad [58]$$

whereupon

$$N_{v} \propto I_{v''}^{v'} / (\omega_{v''}^{v'} A_{v''}^{v'}) \qquad [59]$$

Here, $\omega_{v''}^{v'}$ can be taken as the band origin frequency $(\omega_o)_{v''}^{v'}$ and,

$$A_{v''}^{v'} \propto (\omega_{v''}^{v'})^3 \left| R_{v''}^{v'} \right|^2 \qquad [60]$$

as the transition moment for the forbidden transition between the rotationless states $v', J' = 0 \rightarrow v'', J'' = 0$.

The second method, which is used when high resolution is available, as in the present work, gives the relative vibrational population from the general expression

$$N_{v} \propto \sum_{J} N_{v'J'} \propto \sum_{J} (2J'+1) I_{v''J''}^{v'J'} / (\omega_{J}^{4} S_{J} \left| M_{v''J''}^{v'J'} \right|^2) \qquad [61]$$

which requires a knowledge of the individual rotational line intensities $I^{v'J'}_{v''J''}$.

Using the second method [61] values were obtained for the stationary-state populations N_v expressed relative to N_1 and are listed in Tables 4-9.

If Boltzmann distribution among vibrational levels was obtained for HF, then, from the relation

$$N_v = (N/Q_v)\ \exp(-G_o(v)hc/kT_{vib}) \qquad [62]$$

where, N is the total population of hydrogen fluoride in all levels (including v=0) and $G_o(v)$ is the energy of level v relative to the zeroth level. A plot of $\log(N_1/N_v)$ against $G_o(v) - G_o(1)$ will yield a straight line of slope $0.625/T_{vib}$. The ω_o, $\omega_o x_o$, and $\omega_o y_o$ were calculated and from them the values of $G_o(v)$ for v=1,2 and 3 were calculated according to Herzberg (129) and are presented in Table 10.

$$G_o(v) = \omega_o v - \omega_o x_o v^2 + \omega_o y_o v^3 \qquad [63]$$

$$\omega_o = \omega_e - \omega_e x_e + 3\omega_e y_e/4 \qquad [64]$$

$$\omega_o x_o = \omega_e x_e - 3\omega_e y_e/2 \qquad [65]$$

$$\omega_o y_o = \omega_e y_e \qquad [66]$$

Table 4

Stationary-State Relative Vibrational Population at Total Pressure 1.07 mmHg.

H_2 flow rate 16 μmol/s FE* flow rate 207 μmol/s
Ar " " 258 "

Fluoro-ethylene	Experimental			Calculated Initial	
	N_1/N_1	N_2/N_1	N_3/N_1	R_2/R_1	R_3/R_1
C_2H_3F	1.	.135±.003	.020±.001	.19±.01	.042±.003
T_{rot}	361±4	382±9	317±17		
T_{vib}		2724	2728	3328	3361
1,1-$C_2H_2F_2$	1.	.131±.003	.019±.001	.19±.01	.040±.003
T_{rot}	389±7	369±5	334±23		
T_{vib}		2684	2692	3265	3304
C_2HF_3	1.	.157±.004	.019±.001	.24±.01	.041±.003
T_{rot}	362±5	348±9	306±17		
T_{vib}		2946	2692	3792	3332
C_2F_4	1.	.115±.002	.013±.001	.17±.01	.027±.002
T_{rot}	363±4	343±9	354±56		
T_{vib}		2522	2457	3053	2942

* FE = Fluoroethylene

Table 5

Stationary-State Relative Vibrational Population at

Total Pressure 0.83 mmHg.

H_2 flow rate 16 μmol/s FE* flow rate 207 μmol/s
Ar " " 258 "

Fluoro-ethylene	Experimental			Calculated Initial	
	N_1/N_1	N_2/N_1	N_3/N_1	R_2/R_1	R_3/R_1
C_2H_3F	1.	.166±.004	.024±.001	.24±.01	.049±.004
T_{rot}	347±5	356±10	374±4		
T_{vib}		3037	2861	3801	3528
$1,1\text{-}C_2H_2F_2$	1.	.171±.003	.023±.001	.25±.01	.047±.004
T_{rot}	349±4	359±6	332±11		
T_{vib}		3089	2829	3920	3485
C_2HF_3	1.	.226±.006	.026±.001	.35±.02	.056±.004
T_{rot}	326±6	322±6	345±19		
T_{vib}		3668	2924	5241	3699
C_2F_4	1.	.157±.005	.016±.001	.23±.01	.032±.003
T_{rot}	346±6	315±9	339±28		
T_{vib}		2946	2580	3731	3103

* FE = Fluoroethylene

Table 6

Stationary-State Relative Vibrational Population at Total Pressure .65 mmHg.

H_2 flow rate 16 μmol/s FE* flow rate 207 μmol/s
Ar " " 29 "

Fluoro-ethylene	Experimental			Calculated	Initial
	N_1/N_1	N_2/N_1	N_3/N_1	R_2/R_1	R_3/R_1
C_2H_3F	1.	.165±.005	.024±.001	.25±.01	.054±.004
T_{rot}	361±6	351±10	500±75		
T_{vib}		3027	2861	3890	3660
$1,1\text{-}C_2H_2F_2$	1.	.172±.007	.023±.001	.27±.02	.052±.004
T_{rot}	349±4	377±23	438±39		
T_{vib}		3099	2829	4153	3619
C_2HF_3	1.	.200±.004	.021±.001	.33±.02	.049±.004
T_{rot}	325±3	347±9	483±146		
T_{vib}		3389	2762	4959	3550
C_2F_4	1.	.154±.005	.014±.000	.25±.01	.031±.003
T_{rot}	354±6	355±10	364±24		
T_{vib}		2916	2500	3888	3078

* FE = Fluoroethylene

Table 7

Stationary-State Relative Vibrational Population at Total Pressure .63 mmHg.

H_2 flow rate 16 μmol/s FE* flow rate 207 μmol/s
Ar " " 29 "

Fluoro-ethylene	Experimental			Calculated Initial	
	N_1/N_1	N_2/N_1	N_3/N_1	R_2/R_1	R_3/R_1
C_2H_3F	1.	.192±.010	.023±.002	.31±.02	.052±.004
T_{rot}	357±6	361±28	298±53		
T_{vib}		3305	2829	4609	3615
$1,1\text{-}C_2H_2F_2$	1.	.200±.004	.026±.001	.32±.02	.060±.005
T_{rot}	345±5	363±8	420±53		
T_{vib}		3389	2924	4772	3784
C_2HF_3	1.	.215±.007	.020±.001	.36±.02	.047±.004
T_{rot}	343±4	347±11	398±48		
T_{vib}		3549	2728	5364	3481
C_2F_4	1.	.171±.006	.027±.001	.28±.02	.038±.003
T_{rot}	316±7	299±8			
T_{vib}		3109	2619	4234	3258

* FE = Fluoroethylene

Table 8

Stationary-State Relative Vibrational Population at Total Pressure .15 mmHg.

H_2 flow rate 13 μmol/s FE* flow rate 20 μmol/s
Ar " " 17 "

Fluoro-ethylene	Experimental			Calculated Initial	
	N_1/N_1	N_2/N_1	N_3/N_1	R_2/R_1	R_3/R_1
C_2H_3F	1.	.172±.009	.037±.002	.25±.02	.088±.007
T_{rot}	349±8	327±16	434±124		
T_{vib}		3099	3236	3965	4395
1,1-$C_2H_2F_2$	1.	.181±.009	.025±.003	.29±.02	.060±.005
T_{rot}	330±14	334±11	410±137		
T_{vib}		3191	2893	4446	3798
C_2HF_3	1.	.188±.006	.028±.004	.30±.02	.068±.005
T_{rot}	320±7	337±9	319±85		
T_{vib}		3264	2984	4581	3973
C_2F_4	1.	.157±.011	.028±.002	.23±.01	.068±.005
T_{rot}	346±15	361±33	374±35		
T_{vib}		2946	3014	3764	3972

* FE = Fluoroethylene

Table 9

Stationary-State Relative Vibrational Population at

Total Pressure .62 mmHg.

H_2 flow rate 26 μmol s FE* flow rate 281 μmol s
HF " " 29 "

Fluoro-ethylene	Experimental			Calculated Initial	
	N_1/N_1	N_2/N_1	N_3/N_1	R_2/P_1	R_3/R_1
C_2H_3F	1.	.220±.007	.034±.003	.33±.02	.074±.006
T_{rot}	349±8	330±10	326±70		
T_{vib}		3602	3136	4870	4096
$1,1\text{-}C_2H_2F_2$	1.	.247±.017	.033±.003	.39±.02	.074±.006
T_{rot}	362±20	322±21	396±118		
T_{vib}		3901	3128	5841	4094
C_2HF_3	1.	.264±.011	.026±.002	.44±.03	.059±.005
T_{rot}	334±10	319±10	337±56		
T_{vib}		4096	2924	6672	3776
C_2F_4	1.	.170±.005	.041±.002	.26±.01	.035±.003
T_{rot}	327±8	324±8	815±443		
T_{vib}		3078	2619	4018	3186

* FE = Fluoroethylene

The values for ω_o, $\omega_o x_o$, $\omega_o y_o$ are given in Table A1.

Table 10

Energy of the Vibrational Levels Relative to the Zeroth Level.

v	$G_o(v)$ cm^{-1}	o cm^{-1}	$\omega_o x_o$ cm^{-1}	$\omega_o y_o$ cm^{-1}
		4049.689	88.652	0.932
1	3961.969			
2	7752.226			
3	11376.363			

Figure 16 shows such a plot for the reaction of atomic hydrogen with vinyl fluoride at total pressure 0.63 mmHg. The straight lines follow from the Boltzmann equation [62]. The relative population after collisional relaxation were calculated using equation [61] and those before collisional relaxation were derived from the general equation [67].

The vibrational temperatures are given in Tables 4-9. The distribution deviates from Boltzmann in the sense that the population falls off towards higher vibrational levels (27), except for the results at pressure 1.07 mmHg.

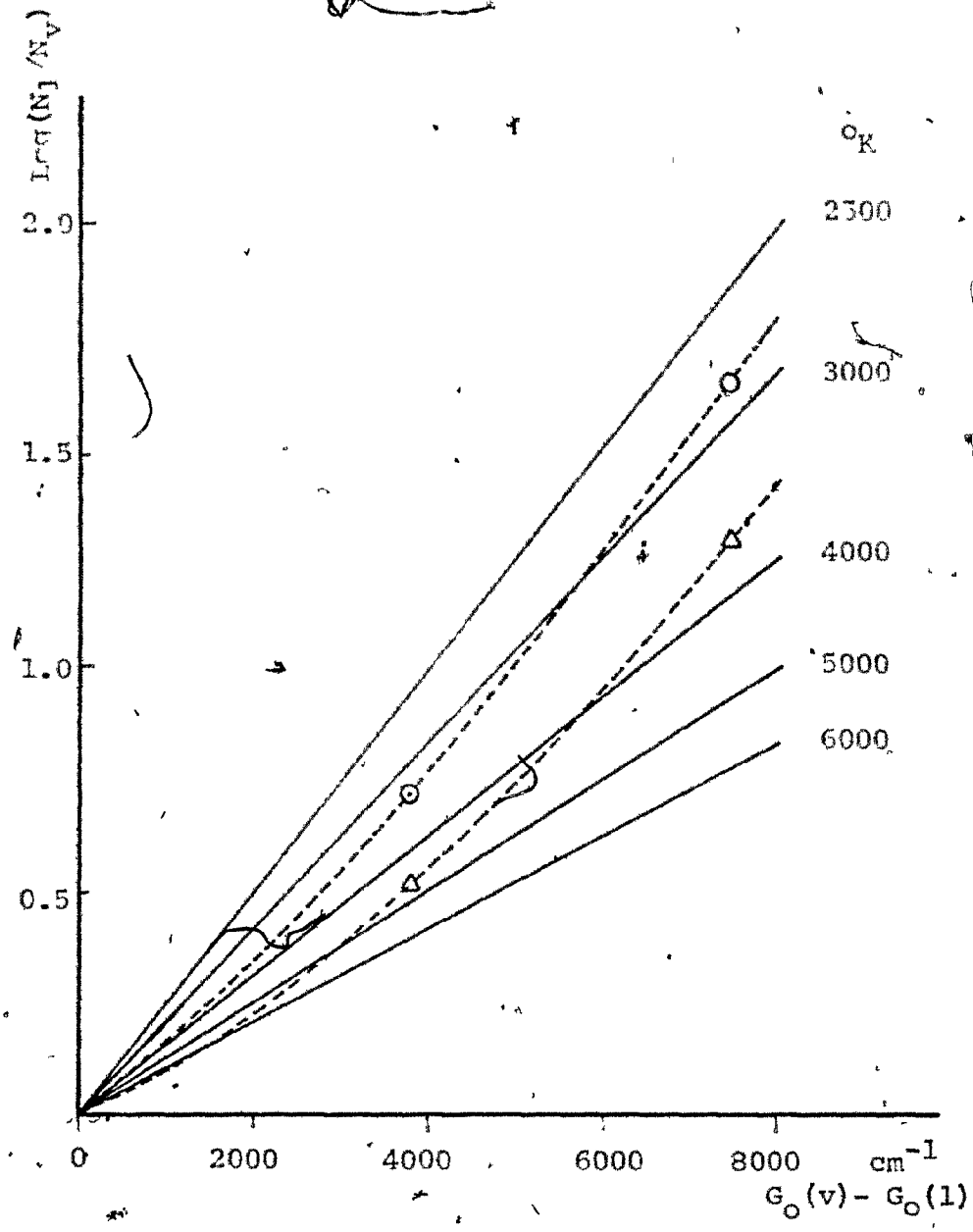

Fig. 16. Stationary-State Distribution of HF* among Vibrational States. Total Pressure .63 mmHg.

a) O After collisional relaxation.*

b) Δ Before collisional relaxation.*

* Values taken from Table 7.

2.1.6 Calculation of the Relative Rates of Formation R_v, from the Steady-State Populations N_v.

The values of N_v, obtained experimentally, are the relative stationary state vibrational populations during the time of observation (4 ms). Since the radiative lifetimes of vibrationally excited hydrogen fluoride are relatively short compared with the observation time (lifetimes: 4.6 ms for v=1, 2.6 ms for v=2, 1.9 ms for v=3 (41)), the method outlined by Charters and Polanyi (26) has been used to calculate the relative detailed rates of chemical reaction, R_v, into each vibrational level.

$$R_v = (A_{v,u} + ZP_{v,u} + zP^*_{v,0} + \tau^{-1})N_v - (A_{w,v}N_w + ZP_{w,v}N_w) \qquad [67]$$

where w , v >u.

$A_{v,u}$ = Einstein transition probability.

$P_{v,u}$ = Gas phase collisional transition probability

Z = Number of gas-collisions per second

$P^*_{v,o}$ = The collision transition probability for "quenching" at the walls and

τ = The residence time in the reaction cell.

The first four terms in the equation give the total rate of transfer of HF out of the level v; the remaining two terms give the rate of transfer into v with the exception of direct chemical formation. The difference denotes the rate of chemical formation into level v.

The first and fifth terms in equation [67] give the total rate of radiational transfer out of and into level v. The second and sixth terms give the total rates of collisional transfer out of and into level v. The third term gives the transfer out of level v, due to wall relaxation. The fourth term gives the transfer out of level v due to physical removal.

Absolute values of the Einstein coefficients, given in Table 11, were calculated from the relative values with respect to $A_{1,0}$ given by Cashion (128). The absolute Einstein transition probability, $A_{1,0}$, was calculated from the equation [68] according to Cashion (128).

$$A_{v',v''}=\frac{64\pi^4\nu^3}{3h}\left|R_{v''}^{v'}\right|^2 = 3.1366\times10^{-7}\times\nu^3\left|R_{v''}^{v'}\right|^2 \qquad [68]$$

where, ν is the band origin in cm^{-1} and R_0^1 in debye unit.

Table II

Einstein Transition Probabilities of Hydrogen Fluoride.

	Value relative to $A_{1,0}$ (ref 128)	Absolute Value s^{-1}
$A_{1,0}$	1.00	215 ± 4
$A_{2,1}$	1.81	389 ± 8
$A_{2,0}$	0.0632	13.6 ± .3
$A_{3,2}$	2.45	527 ± 10.
$A_{3,1}$	0.177	38.1 ± .8
$A_{3,0}$	0.00460	.99 ± .02
$A_{4,3}$	2.93	630 ± 12
$A_{4,2}$	0.330	71 ± 1.
$A_{4,1}$	0.0178	3.83 ± .07
$A_{4,0}$	0.000407	.0875 ± .0016

The collision deactivation probabilities were calculated using the Landau theory (130).

$$P_{i,j} = \begin{cases} iP_{1,0} & \text{for } i-j = 1 \\ 0 & \text{for } i-j \neq 1 \end{cases} \qquad [69]$$

Values for $P_{1,0}$ were taken from Green and Hancock (131).

Table 12

Collision Deactivation Probabilities of HF.

	Collisional Partner	Deactivation Probability (131)
$P_{1,0}$(vib-vib)	H_2	1.7×10^{-3}
$P_{1,0}$(vib-rot,trans)	H_2	7×10^{-5}
$P_{1,0}$(vib-trans)	Ar	1×10^{-5}
$P_{1,0}$(vib-trans)	He	5×10^{-6}

The relation [67] for the different vibrational states thus becomes.

$$R_3 = \{(A_{3,2}+A_{3,1}+A_{3,0})+3[P_{1,0(Ar-HF)}Z_{Ar-HF} + (P^{v-v}_{1,0(H_2-HF)}+P^{v-r,t}_{1,0(H_2-HF)})Z_{H_2-HF}]+\tau^{-1}\}N_3 \qquad [70]$$

$$R_2 = \{(A_{2,1}+A_{2,0})+2[P_{1,0(Ar-HF)}Z_{Ar-HF}+(P^{v-v}_{1,0(H_2-HF)} + P^{v-r,t}_{1,0(H_2-HF)})Z_{H_2-HF}]+\tau^{-1}\}N_2$$
$$-\{A_{3,2}N_3+3[P_{1,0(Ar-HF)}Z_{Ar-HF}+(P^{v-v}_{1,0(H_2-HF)} + P^{v-r,t}_{1,0(H_2-HF)})Z_{H_2-HF}]N_3\} \quad [71]$$

$$R_1 = \{A_{1,0}+[P_{1,0(Ar-HF)}Z_{Ar-HF}+(P^{v-v}_{1,0(H_2-HF} + P^{v-r,t}_{1,0(H_2-HF)})Z_{H_2-HF}]+\tau^{-1}\}N_1$$
$$-\{A_{3,1}N_3+A_{2,1}N_2+2[P_{1,0(Ar-HF)}Z_{Ar-HF} + P^{v-v}_{1,0(H_2-HF)}+P^{v-r,t}_{1,0(H_2-HF)})Z_{H_2-HF}]N_2\} \quad [72]$$

The number of collisions per second, were taken from Hirschfelder, Curtiss and Bird (132).

$$Z_{HF} = \sqrt{2}\pi d^2\sqrt{8\pi/k\mu T} \qquad \text{or,} \quad [73]$$

$$Z_{HF} = 6.24\times10^7 d^2_{M-HF}\, p_M\sqrt{1/T\mu} \quad [74]$$

where, $d_{M-HF} = (d_M+d_{HF})/2$ = The collisional diameter in Å

p_M = The partial pressure of the gas which collides with the HF.

T = Temperature in degrees K and,

μ = Reduced mass in atomic mass units.

The following collision diameters (in Å) were used: d_{HF}=2.5, d_{H_2}=2.9, d_{Ar}=3.4 and d_{He}=2.6 (123).

The possibility of vibrational exchange between HF molecules can be neglected since, for the low concentrations present in these experiments, the number of HF-HF collisions per molecule in the residence time is less than unity. Similarly, the deactivation of $HF^{\dagger}$ due to collisions with hydrogen atoms is negligible since the collisional deactivation of HF by atomic hydrogen is very small (133) and the concentration of atomic hydrogen is very small.

The collisional deactivation of vibrationally excited HF from other radicals and fluoroethylenes was not taken into account since the reactions are too complicated and there are no literature values for collisional deactivation by fluoroethylenes. By increasing the flow rate of hydrogen up to 16 µmol/s, the emission reaches a maximum and then decreases rapidly. On the other hand, even for a very large increase of the flow rate of the fluoroethylene, up to 300 µmol/s the emission reaches a maximum and does not decrease. Experimentally, this shows that the deactivation

to the fluoroethylene is much smaller than that due to hydrogen (the vibrational levels of H_2 are in resonance with those of HF).

Vibrational populations $R_{v'}$, assuming a small deactivation probability by fluoroethylenes (equal to that of argon are reported in AppendixE). In the same Appendix, vibrational populations are reported using a high value for deactivation of HF by fluoroethelenes (equal to that of C_2H_4).

Since HF reacts readily with silica, it seems reasonable to assume that vibrationally excited HF molecules which diffused to the wall were removed there by reaction, or at least completely deactivated, so that the observed steady-state distribution was not distorted by the wall relaxation (27). The effect of the wall removal on the importance of collisional relaxation is similar to the effect of physical removal. As the result of this excited molecules suffer fewer collisions with other molecules and atoms; hence, the effect of collisional deactivation becomes smaller.

The residence time τ was calculated according to Appendix C.

Using the equations [70, 71 and 72], the relative initial vibrational distributions were calculated and these values, $R_{v'}$, are given in Tables 4-9. The vibrational temperatures corresponding to the initial populations are also given in these Tables.

2.1.7 Berry Model Applied to the Elimination of HF from the Reaction of H Atoms with Vinyl Fluoride.

According to Teng and Jones, activated 1-fluoroethane is produced by successive addition of atomic hydrogen to vinyl fluoride (117). The Berry model was applied to the calculation of the probability vector for HF eliminated from fluoroethane. For comparison, the model was also applied to the elimination of HF from 1,1,1-trifluoroethane (27). In both reactions 1,2-elimination occurs (135).

The model allowed determination of values of $r_e^{\neq}$ and α which gave calculated probability ratios in good agreement with experimental values except at the threshold v'=4 (Table 13). The Berry model is known to give poor results for threshold values (89).

The "localized" available energies (136, 137) were calculated from the relation [33] and are given in Table 13. E_a are taken from ref 115.

$$E(^{Localized}_{Available}) = E_a - \Delta H^{\circ}_{react.} + 3RT \qquad [33]$$

The distribution of this energy $E(^{Localized}_{Available})$ (Fig. 17) over the quantum levels of the products was determined by the dynamics of the chemical reaction.

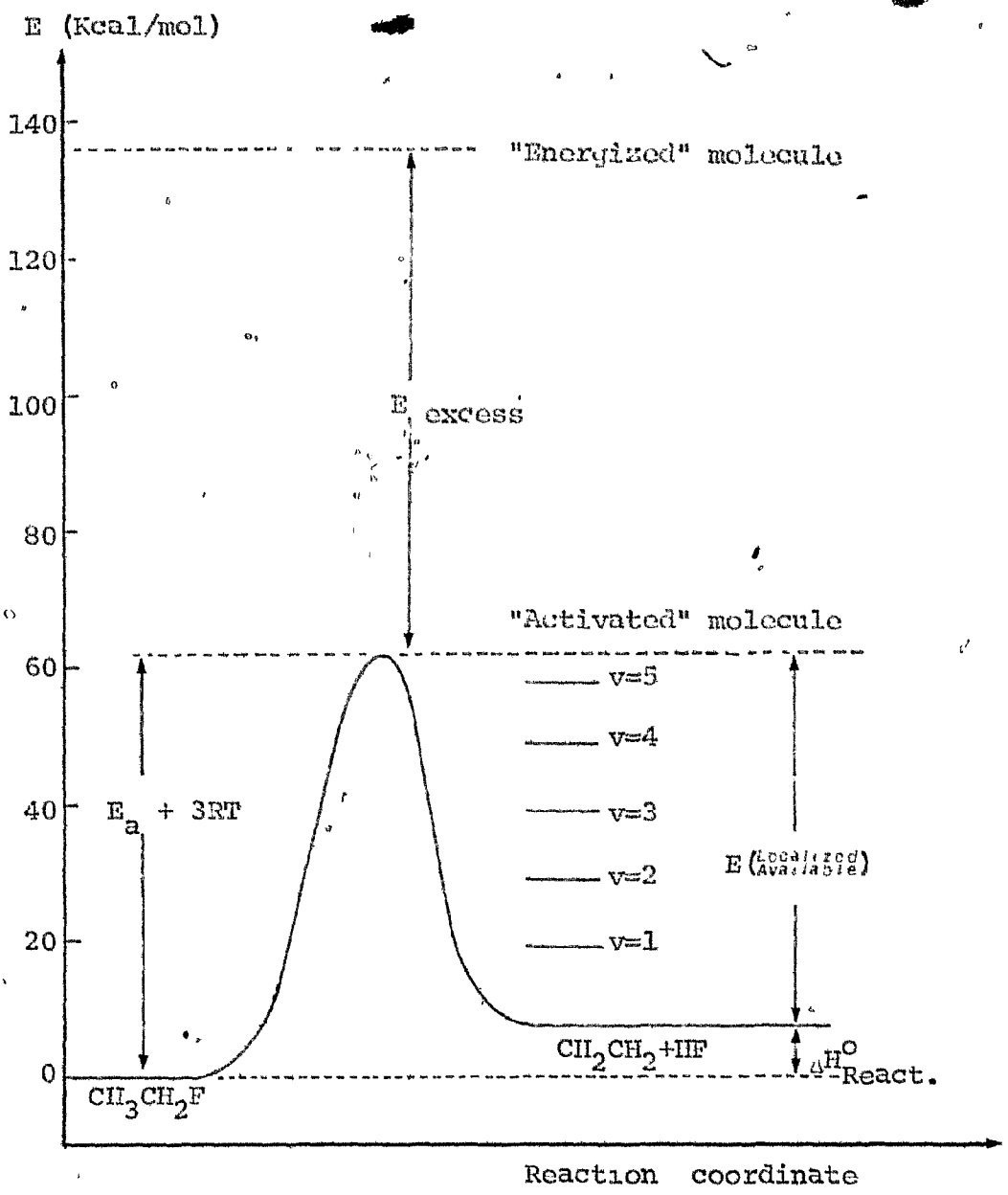

Fig. 17. Potential energy hypersurface along the reaction coordinate for $HF^{\dagger}$ elimination from ground electronic manifold CH_3CH_2F.

Table 13

Calculated Vibrational Probability Ratios for HF Eliminations and Fraction of the Available Energy Disposed in the Vibrations of HF.

P mmHg	CG	Probability Ratios 2/1	3/1	4/1	$r_e^{\neq}$ [2]	α [2] cm	τ [2]	$\langle f_{v'} \rangle$ [3]	$\langle f_v \rangle$ [4]	
0.15	Ar	0.28 (0.25)[1]	0.084 (0.088)		1.49	1×10^{-4}	4.50	0.72	0.07	CH_3CH_2F
0.62	He	0.34 (0.33)	0.074 (0.074)		1.23	1×10^{-6}	2.95	0.45	0.10	
0.63	Ar	0.31 (0.31)	0.052 (0.052)		1.39	1×10^{-3}	6.05	0.65	0.04	
1.07	Ar	0.20 (0.19)	0.042 (0.042)		1.41	1×10^{-4}	6.35	0.67	0.02	
0.35	Ar	0.38 (0.39)	0.11 (0.11)	0.003 (0.027)	1.41	1×10^{-5}	3.05	0.64	0.13	CH_3CF_3
0.55	Ar	0.34 (0.34)	0.085 (0.081)	0.002 (0.018)	1.41	1×10^{-6}	3.40	0.64	0.11	

[1] Experimental values corrected for radiational and collisional relaxation.

[2] $r_e^{\neq}$ is the bond length in Å of $HF^{\neq}$ at the transition state. α is the coupling constant for the Berry Model. τ is the time during relaxation by intercontinuum coupling.

[3] The fraction of available energy before relaxation by intercontinuum coupling.

[4] " " " " " after " " " " "

$E_{(Available)}^{(Localized)}$ for CH_3CH_2F = 53.7 Kcal/mol

" " CH_3CF_3 = 43.0 "

It was necessary to specify the dressed HF oscillator's properties in order to calculate vibronic overlap integrals. In order to calculate these properties, semi-empirical rules were used (138). The internuclear distance and the dissociation energy for the dressed oscillator HF were found in terms of the bond order n using Pauling's rule

$$r_e^{\neq} = r_e - 0.26\ \ln(n) \qquad [75]$$

and Johnston's rule

$$D_e^{\neq} = D_e n^p \qquad [76]$$

where, r_e and D_e are respectively the spectroscopic internuclear distance and dissociation energy for HF and $r_e^{\neq}$, $D_e^{\neq}$ the corresponding terms for the dressed HF, n is the bond order and p the bond index (138). The value (p=0.966) found from the re-evaluation of the BEBO method by Jordan and Kaufmann (141) was used for the bond index p.

Badger's rule was used to relate the dressed oscillator force constants $k_e^{\neq}$ to their bond lengths $r_e^{\neq}$ via empirical constants (a and b).

$$k_e = \exp[(a-r_e)/b] \qquad [77]$$

a and b were calculated from the least squares fit

of the equation [77] using the values of Table 14.

Table 14

Constant Values for the Calculation of the Empirical Constants of Badger's Rule.

Diatomic Molecule	r_e Å	ω_e cm^{-1}	$k_e \times 10^{-5}$ dynes/cm	Reduced mass	ref
B-H	1.236	2366.9	1.114648	0.92358	140
Be-H	1.297	2058.5	0.817024	0.90673	"
C-H	1.1202	2859.1	1.499446	0.93002	"
H-F	0.9168	4139.04	2.268011	0.95735	124
H-Li	1.5953	1405.4	0.025497	0.88151	140
O-H	0.9706	3735.21	2.053581	0.94838	"

Thus,

$$\ln(k^{\neq}/10^5) = -3.34065\ r_e^{\neq} + 5.269464 \qquad [78]$$

where, $r_e^{\neq}$ in Å and $k_e^{\neq}$ in dynes/cm.

At the bottom of the potential curve, a diatomic oscillator is essentially harmonic. Thus, the relation of the force constant k_e to the fundamental frequency ω_e and to the reduced mass μ is given by

$$k_e = 4\pi^2 \omega_e^2 c^2 \mu \qquad [79]$$

where c is the speed of light.

The equation [79] was used to calculate the force constant, k_e, of the spectroscopic state from ω_e and to find the fundamendal frequency, $\omega_e^{\neq}$, of the dressed oscillator $HF^{\neq}$ from the value of $k_e^{\neq}$.

To a first order approximation, the vibrational energy is given by (129),

$$E_{vib} = (v+\tfrac{1}{2})\omega_e - (v+\tfrac{1}{2})^2 \omega_e x_e \qquad [80]$$

and the vibrational wavefunctions are the eigenfunctions of the Schroedinger equation if the potential energy of the diatomic molecule follows a Morse curve. The Morse curves may be constructed analytically (127, 141) using spectroscopic data (Fig. 18 and 19). Morse wavefunctions were adopted in the present work as follows (56):

$$\psi_v(r) = A_v \exp(-z/2) z^{x/2} F_v(z) \qquad [81]$$

where

$$A_v = \{[(x+v)(x+v-1)\cdots(x+1)]v!\,\Gamma(x)\}^{\frac{1}{2}} \qquad [82]$$

$$F_v(z) = \sum_{i=0}^{v} \{(-1)^i \binom{v}{i} z^i / [(x+1)(x+2)\cdots(x+i)]\} \qquad [83]$$

$$x = k-2v-1 \qquad [84]$$

$$z = k \exp[-\beta(r-r_e)] \qquad [85]$$

$$k = 4D_e/\omega_e \qquad [86]$$

$$\beta = (k_e/2D_e)^{\frac{1}{2}} \qquad [87]$$

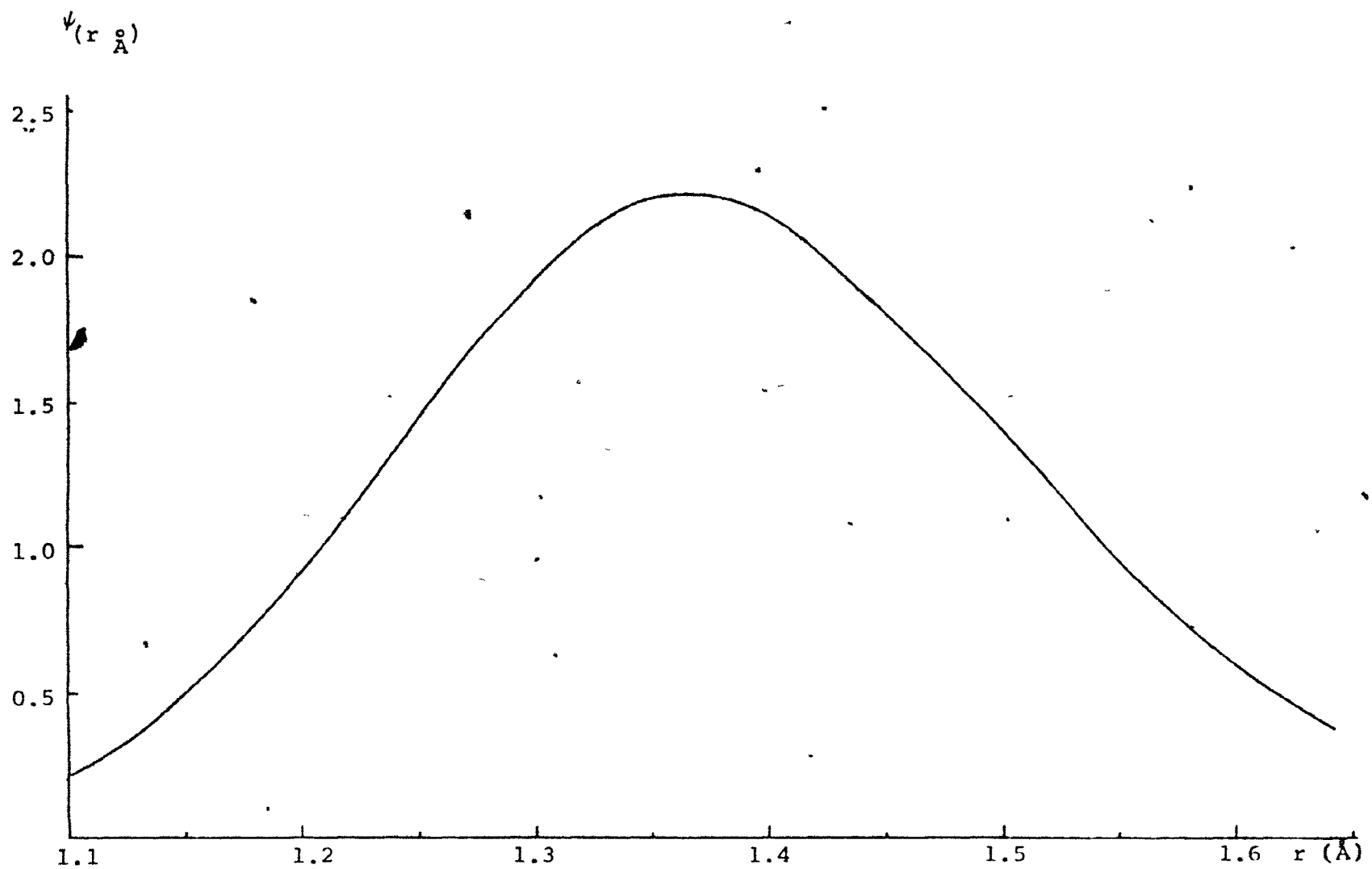

Fig. 18. Morse Wavefunction of the Dressed Oscillator $HF^{\neq}$ (v=0).

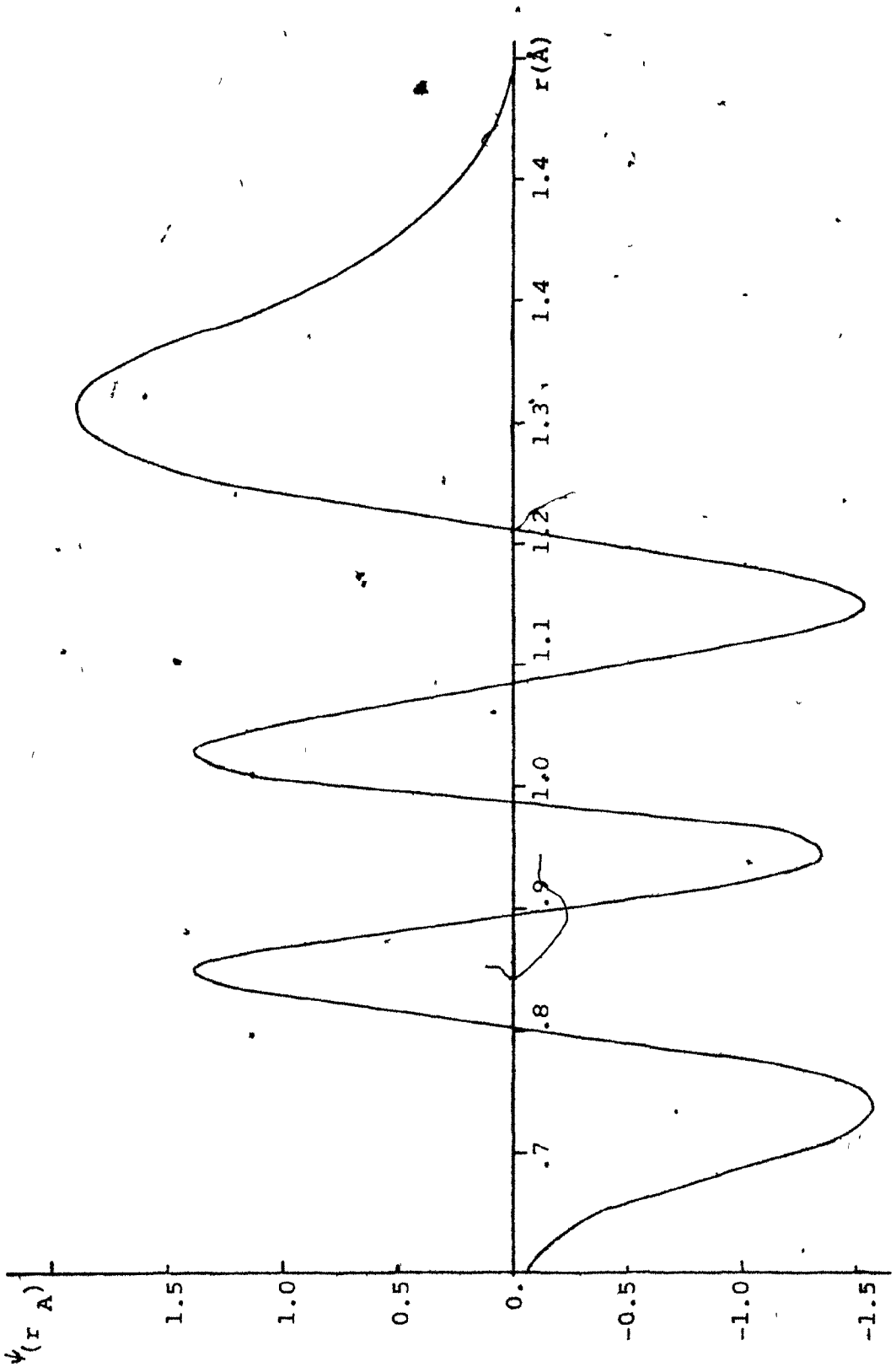

Fig. 19. Morse Wavefunction of the Undressed Oscillator HF^+ (v=5).

The evaluation of the relative transition rates between the discrete state and various final states is possible via Fermi's Golden Rule (142)

$$w_{i \to f} = (2\pi/\hbar) |\langle f|H'|i\rangle|^2 \rho_f(r) \qquad [88]$$

where, the matrix elements are taken to be proportional to the vibronic overlap integrals for initial and final oscillator states (131) and ρ_f is the number of final states with wavefunctions ψ_f.

$$\langle f|H'|i\rangle \propto \langle v'|v''=0\rangle \qquad [89]$$

Thus, finally

$$P_{v'} = w_{HF_{dressed}, v''=0 \to HF, v'} \propto |\int \psi_{v'(HF)} \psi_{v''} dr|^2 \rho_{v'} \qquad [90]$$

The proportionality constant includes the electronic matrix element which is the same for all these transitions in this approximation. The first factor in equation [90] is a Franck-Condon factor (143) between the lowest vibrational level of the dressed HF^* and the final vibrational level of the product HF. The second factor $\rho_{v'}$, is a statistical weighting factor. $\rho_{v'}$ is the number of rotational and translational states of the products for the quantum number v'.

It may be shown (90) that

$$f_{v'} \propto \{E(\text{Localized}) - (E_{v'} - E_{v=0})\}^{m/2} \quad [91]$$

$E_{v'}$ is the vibrational energy for the v' vibrational level, m is the number of translational degrees of freedom less 3 which follows from the Dirichlet integral (144).

Fig. 20 shows Franck-Condon factor arrays for HF dressed-undressed oscillator couplings parameterized as a function of dressed oscillator bond order for $E(\text{Localized})$ = 53.7 Kcal/mol. If the initial dressed oscillator is highly displaced, Franck-Condon factors favor highly excited product vibronic states (56). In Table 15 the values of $f_{v'}$ are given

$$f_{v'} = (E_{v'} - E_{v'=0}) / E(\text{Localized}) \quad [92]$$

where $E_{v'}$ is the vibrational energy of the vibrational level v'.

The distribution of available energy over the internal degrees of freedom of the olefin is taken into account in the Berry Model by assuming that undressed $HF^{\dagger}$ is partially relaxed by the olefin. The rate constants for the relaxation are given in the Berry Model for intercontinuum coupling as (56)

$$k_{v',v''} = \exp(-\alpha \Delta E_{v',v''}) \quad [34]$$

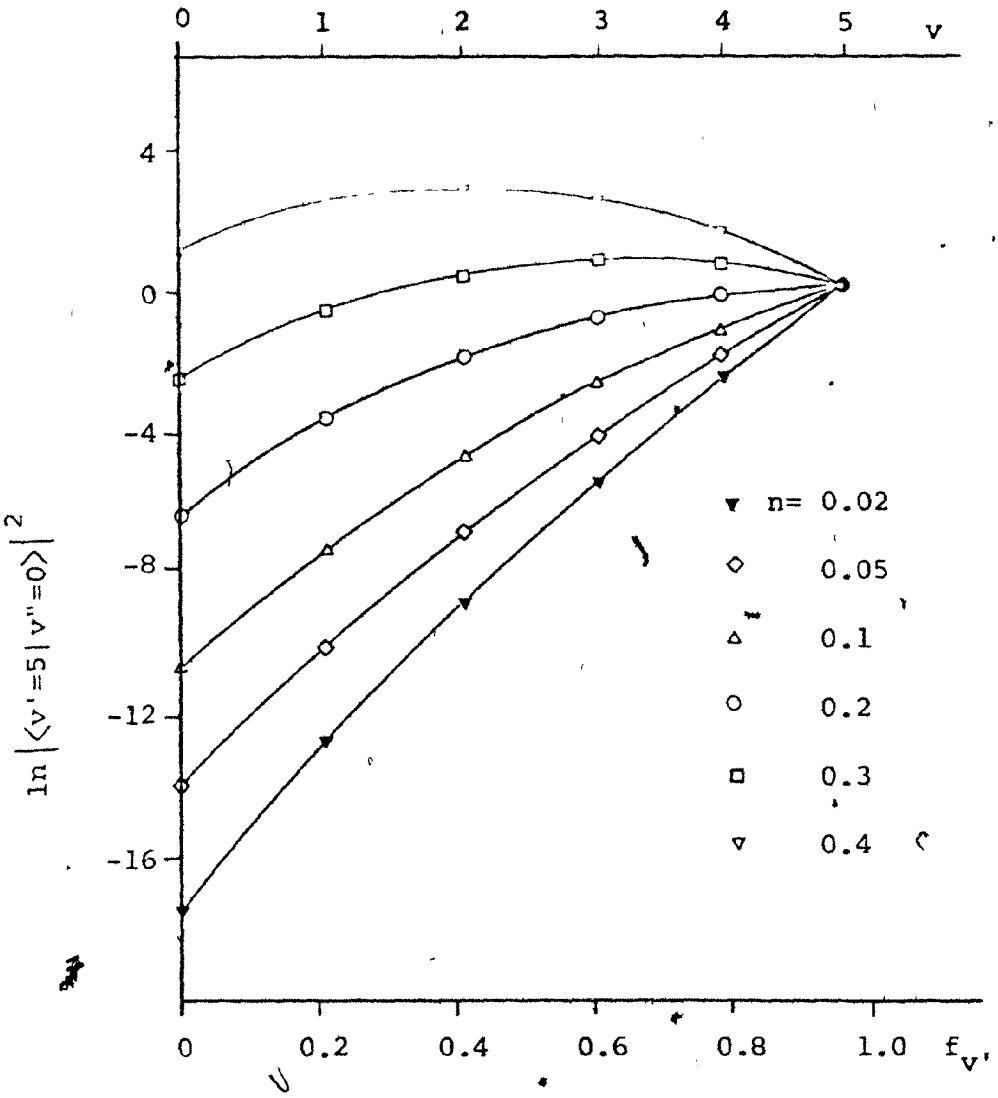

Fig. 20. HF dressed oscillator - HF undressed oscillator Franck-Condon factor arrays relative to v=5 for varying bond orders of initial dressed oscillator. (Localized available energy 53.7 Kcal/mol)

Table 15

Normalized Initial and Final Probabilities Calculated from Berry's Model for the Reaction $H + C_2H_3F$.

CG	P mmHg		Vibrational level					
			0	1	2	3	4	5
		f_v	0.	0.2110	0.412	0.604	0.786	0.958
		P_v^o	0.3985	0.2794	0.1797	0.0995	0.0396	0.0034
Ar	0.15	F.C.F.	0.	0.0007	0.0085	0.0561	0.2406	0.6940
		P (τ=0.)	0.0005	0.0102	0.0768	0.2879	0.4982	0.1263
		P (τ=4.50)	0.7713	0.1674	0.0465	0.0138	0.0034	0.0003
He	0.62	F.C.F.	0.0113	0.0758	0.2088	0.3069	0.2628	0.1343
		P (τ=0.)	0.0417	0.1999	0.3589	0.2946	0.1005	0.0044
		P (τ=2.95)	0.6423	0.2522	0.0847	0.0187	0.0020	0.0033
Ar	0.63	F.C.F.	0.0002	0.0038	0.0281	0.1176	0.3110	0.5392
		P (τ=0.)	0.0026	0.0322	0.1549	0.3644	0.3871	0.0588
		P (τ=6.05)	0.8471	0.1123	0.0344	0.0058	0.0004	0.0000
Ar	1.07	F.C.F.	0.	0.0005	0.0062	0.0471	0.2263	0.7198
		P (τ=0.)	0.0020	0.0264	0.1379	0.3536	0.4114	0.0688
		P (τ=6.35)	0.9059	0.0756	0.0148	0.0032	0.0005	0.0000

F.C.F. Normalized Franck-Condon Factor.

CG Carrier gas.

f_v Vibrational fraction of the available energy.

P_v^o A priori probability.

τ is the time during relaxation by intercontinuum coupling.

The final probability vectors, after relaxation from inter-continuum coupling, are given in Table 15. Calculated values of α are given in Table 13 (56).

The fraction of energy which is trapped in the vibrational levels of $HF^{\dagger}$ can be calculated from the equation [93]

$$\langle f_{v'} \rangle = \sum P_{v'} f_{v'} \qquad [93]$$

These values are also given in Table 13.

Figures 21 and 22 show the relaxation of the undressed oscillator $HF^{\dagger}$. The initial populations at time zero are calculated from [90] using $E_{(Available)}^{(Local;Zero)}$=53.7 Kcal/mol. The relaxed probabilities are calculated by solving the initial value problem with rate constants given by [34]. The relaxation proceeds until calculated probability ratios agree the experimental values corrected for deactivation according to equation [67]. The time scale for relaxation is given in units of the half-life of v=3. The results from the application of Berry Model are given in Table 13.

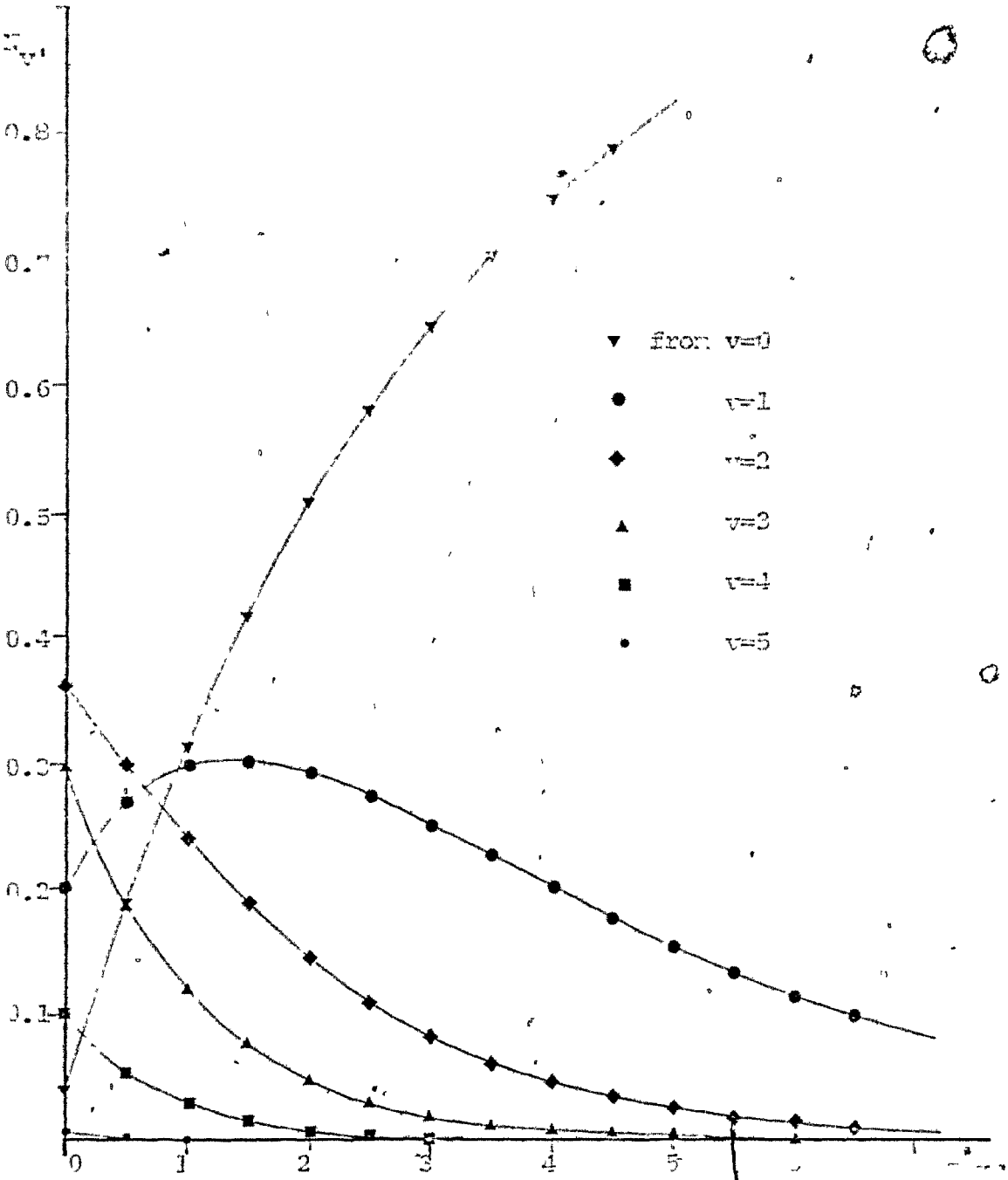

Fig. 21. Intramolecular relaxation of unrelaxed undressed oscillator HF* from the reaction H + C_2H_5F.

(Total pressure 0.62 mmHg. Carrier gas H_2)

* The time scale is given in units of v=3 lifetimes.

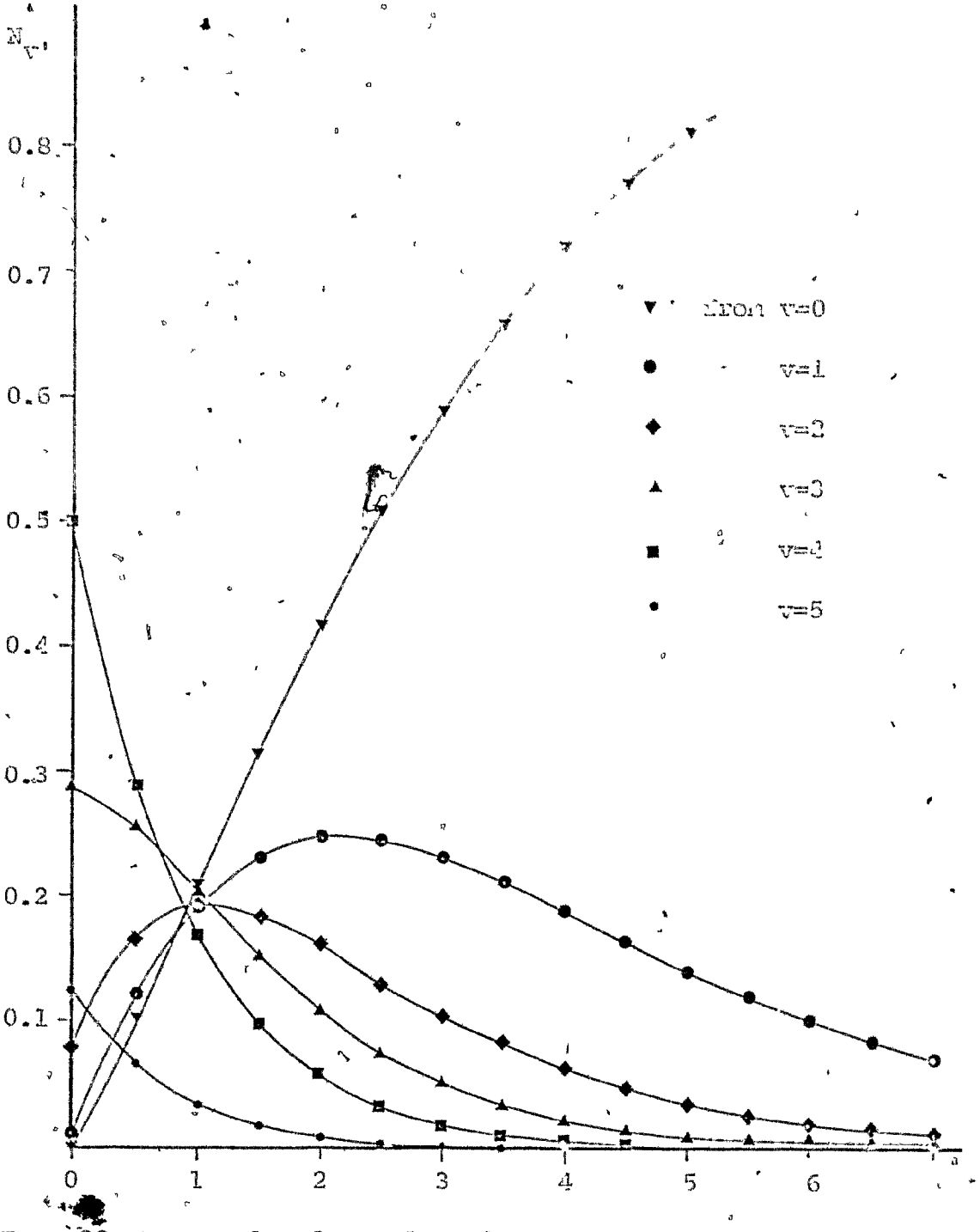

Fig. 22. Intramolecular relaxation of unrelaxed undressed oscillator HF from the reaction $H + C_2H_3F$.

(Total pressure 0.150 mmHg. Carrier gas Ar)

[a] The time scale is given in units of v=3 lifetimes.

2.1.3 Surprisals Analysis.

The surprisals, $I(f_v)$, of the calculated probabilities for HF eliminated from fluoroethane were examined as a function of f_v, the fraction of available energy in the vibrational level with quantum number v. This function may be analysed in terms of moments of f_v (99)

$$I(f_v) = -\ln(P_v/P_v^o) = \lambda_0 + \lambda_1 f_v \qquad [40]$$

where P_v^o, the a priori probability, is proportional to the density of states. In the case of argon pressure of 0.63 mmHg, fourth moments are required. For all the other probability vectors after relaxation and for all the initial probability vectors before relaxation by intercontinuum coupling, second moments are sufficient. The values for initial and final surprisals are given in Table 16. The values of moments and the standard deviations are given in the same Table. A representative plot for hydrogen fluoride eliminated from fluoroethane with argon pressure equal to 1.07 mmHg is shown in Fig. 23. In no case was a linear surprisal plot predicted. We must note that the surprisals analysis here is based upon the assumption that the a priori probabilities

Table 16

Initial and Final Surprisals for the Reaction H + C_2H_3F.

P [1] mmHg	τ [2]	Vibrational Level						Moments I(F)					Standard Deviation [3]
		0	1	2	3	4	5	λ_0	λ_1	λ_2	λ_3	λ_4	
Ar													
0.15	0.	6.59	3.31	0.85	-1.06	-2.53	-3.61	6.55	-16.20	5.97			6.08×10^{-4}
0.15	4.5	-0.66	0.51	1.35	1.97	2.47	2.14	-0.68	6.33	-3.11			8.33×10^{-2}
He													
0.62	0.	2.26	0.33	-0.69	-1.09	-0.93	-0.25	2.24	-10.56	8.32			3.20×10^{-2}
0.62	2.95	-0.48	0.10	0.75	1.67	2.98	4.65	-0.40	0.81	-1.57			1.8123
Ar													
0.63	0.	5.01	2.16	0.15	-1.36	-2.36	-2.84	4.98	-14.43	6.76			5.36×10^{-2}
0.63	6.05	-0.75	0.91	1.65	2.84	4.50	5.94	-0.75	13.95	-40.87	63.87	-30.97	6.62×10^{-3}
Ar													
1.07	0.	5.29	2.36	0.26	-1.27	-2.34	-3.00	5.25	-14.76	6.44			5.58×10^{-2}
1.07	6.35	-0.82	1.31	2.50	3.45	4.39	4.60	-0.73	9.56	-3.97			1.57×10^{-1}

[1] Total pressure in the reaction cell.
[2] is the time during relaxation by intermolecular coupling.
[3] Standard deviation from the least squares fit.

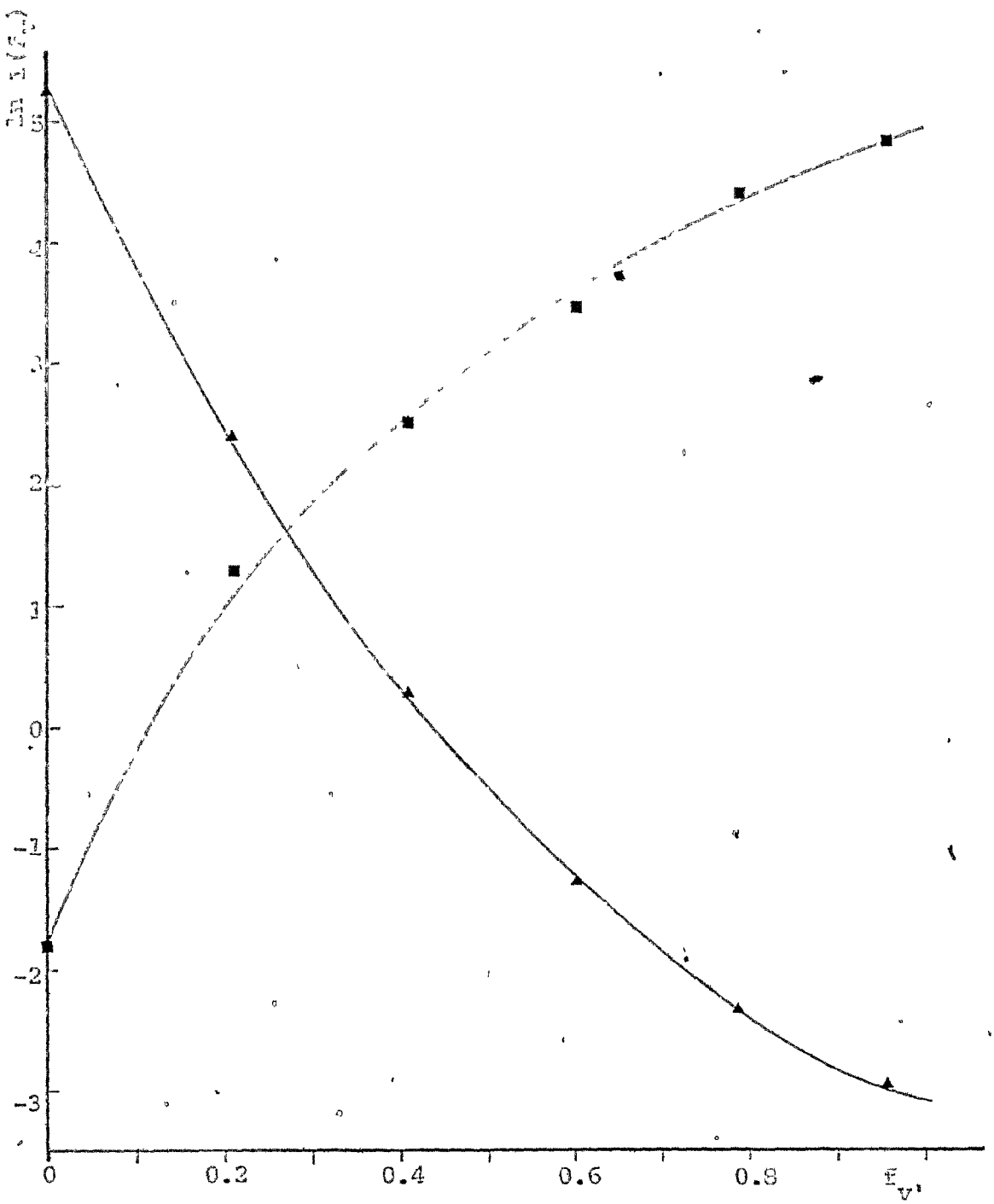

Fig. 23. HF (v) product vibronic reaction surprisals for H + C_2H_3F at total pressure 1.07 mmHg (Ar).

■ , Surprisals before intercontinuum relaxation.
▲ " " after " "

as determined by the energies of each of the states of the two-body system (56)

$$\rho_v' = (\epsilon - \epsilon_{v'})^{s-2} \qquad [94]$$

The internal degrees of freedom of the diatom have been ignored because the Barry Model is a localised model and because the same localised density of states has been used in the generalised form (10) of Barry's Model for unimolecular decomposition (56). The "elementary event" in this context is the formation of the diatomic product in the particular vibrational state in the simple two-body system. The criterion for this choice is that encoding densities of states, which include internal degrees of freedom, is tantamount to using another model from the set of statistical models for reaction dynamics. The successes and limitations of statistical models have been described in the introduction.

3.3.3 The Yield.

Item 17 shows the thermochemistry of the reaction of atomic hydrogen with vinyl fluoride. It is possible that the "energized" fluoroethane acquires energy of up to 136 Kcal/mol. The RRKM theory is essentially concerned with the transition of the decomposing molecules from the "energized" to the activated state and cannot predict product energy distributions when the activated molecule breaks up. A distinction can be made between the "critical energy" of the activated molecule, that is, the minimum energy needed for elimination and the "excess" energy possessed above this minimum. All of the excess energy is available to the products and is randomly distributed. Only part of the "critical energy" (the so called "localized" (56) energy about which the RRKM theory can make no prediction [33]) is available to the products. In many cases, it has been proven (27, 56) that the localized available energy must be contributing to the vibrational excitation in the HF.

From the thermochemistry of the reactions (Table 17), it seems that the energy of the energized molecule increases

Table 17

Thermochemistry of the Reactions of Atomic Hydrogen with the Fluoroethylenes.

Reaction	Total Energy kcal/mol	E(...) kcal/mol
$2H\cdot + C_2H_3F \longrightarrow C_2H_5F^{**}$	133.2	
$\quad\longrightarrow C_2H_4 + HF$		53.7
$2H\cdot + 1,1\text{-}C_2H_2F_2 \longrightarrow C_2H_4F_2^{**}$	139.[illegible]	
$\quad\longrightarrow C_2H_3F + HF$		46.6
$2H\cdot + C_2HF_3 \longrightarrow C_2H_3F_3^{**}$	146.4	
$\quad\longrightarrow C_2H_2F_2 + HF$		57.6
$2H\cdot + C_2F_4 \longrightarrow C_2H_2F_4^{**}$	153.3	
$\quad\longrightarrow C_2HF_3 + HF$		57.6

The total energy of "energized" molecule is calculated from ΔH_f of Table A2.

gradually from vinyl fluoride to tetrafluoroethylene. The difference between the total energies of the energized molecules and the localized energies is very small for the reactions of C_2H_3F and $1,1\text{-}C_2H_2F_2$; the former increases slightly while the latter decreases slightly. According to Teng and Jones (116, 117) the rate of addition of the second H and the rate of decomposition of the energized molecule is the same for C_2H_3F and $1,1\text{-}C_2H_2F_2$. For these reasons, it is probable that the relative initial population for v=2 (R_2/R_1) is approximately the same for the reactions of atomic hydrogen with vinyl fluoride and 1,1-difluoroethylene.

Because the localized available energy for 1,1,2,2-tetrafluoroethane is similar to that for fluoroethane (Table 17), we would expect similar population ratios for the reactions of atomic hydrogen with vinyl fluoride and tetrafluoroethylene. However, we observed that those for the reaction of atomic hydrogen with tetrafluoroethylene were considerably lower (Tables 4-9).

[illegible]. Setser [illegible] found that not all of the [illegible] able energy is available to the products of hydrogen abstraction reactions (57). In particular Setser found this to be the case in the formation of HF formed by abstraction of hydrogen from the methyl group of toluene by fluorine atoms (Fig. 24a). Setser suggested that the distribution of energy to HF is finished before the organic radical re-hybridizes (Stage I of Fig. 24a). Thus, the stabilization energy of the benzyl radical, gained in the step I → II (Fig. 24a), is not available to HF.

A similar suggestion may be made for elimination of hydrogen fluoride for 1,1,2,2-tetrafluoroethane (Fig. 24b). In this reaction the distribution of localized available energy may be complete at stage I. The step I → II of Fig. 24b may be delayed for stereoelectronic and stereochemical reasons. In the first place donation from the lone pairs of fluorine into the empty hybrids of [illegible] (Fig. 24b) may be stereoelectronically favorable. In the second place torsion about the C=C double bond of the olefin becomes less unfavourable energetically as fluorine substitution increases (145). Thus, as fluorine substitution increases the energy gained in step I → II (Fig. 24b) may not be available to HF. This is in agreement of the observation of lower population

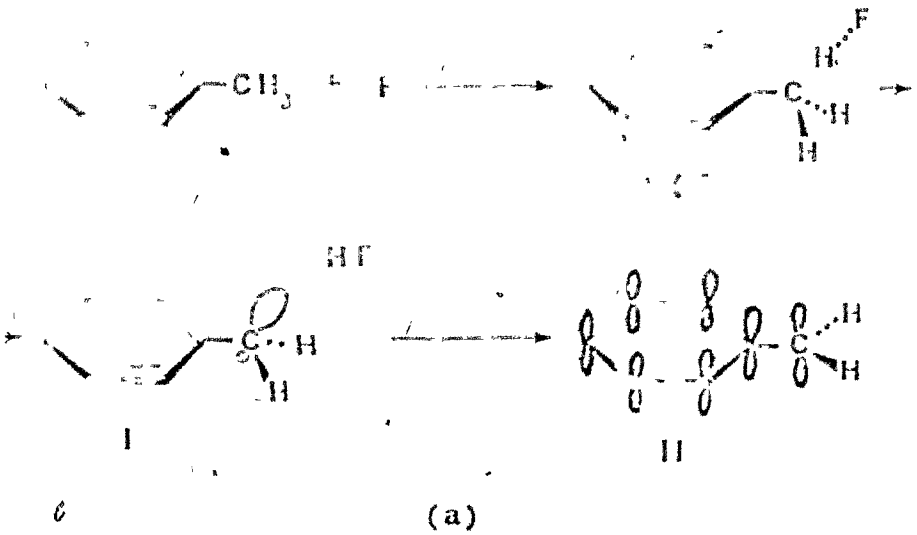

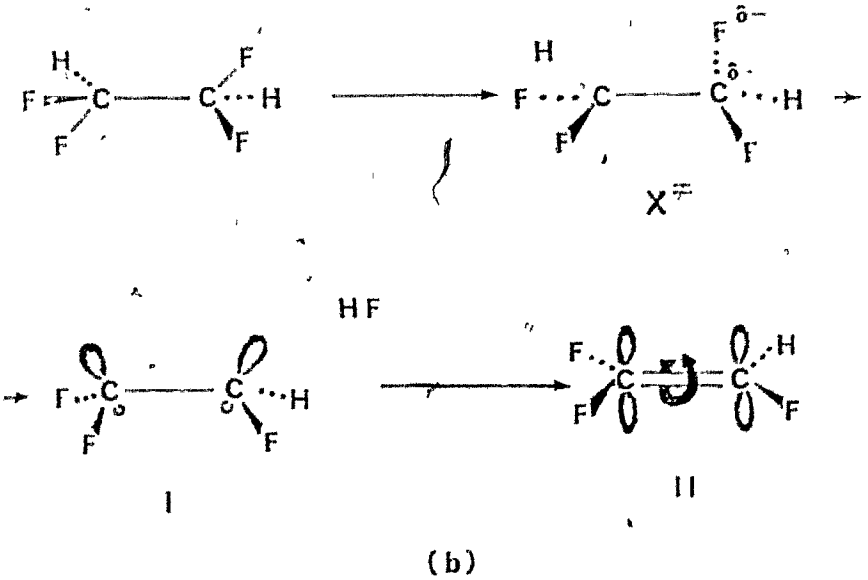

Fig. 24. (a) Hydrogen abstraction by F atoms from toluene.

(b) HF elimination from tetrafluoroethylene.

relative to the C_2H_4 reaction than for C_2H_3F and 1,1-$C_2H_2F_2$ reactions.

Since the ratio P_2/P_1 is highest for the reaction of atomic hydrogen with C_2HF_3 it appears that this reaction must be faster than the others. These conclusions are in agreement with the results of Pennbern and Sandoval (112) who found the following relative velocities with respect to ethylene; C_2H_4:1,1-$C_2H_2F_2$:C_2HF_3 1:1.41:1.67.

Another reason for the relative initial population P_2/P_1 for C_2HF_3 to be highest is that the reaction has available much higher "localized" energy than the others (Table 17).

The ratios P_3/P_1 do not show appreciable differences between C_2H_3F, 1,1-$C_2H_2F_2$ and C_2HF_3 within the error limits which are larger for R_3/R_1 than for R_2/P_1 (Table 4-9).

Comparison of the series of runs at pressures 1.07 and 0.83 mmHg shows that the relative initial populations are higher at the lower pressure which is expected since the energized molecule suffers fewer collisions at lower pressure. This cannot be due to an error in the calculation of the relaxation of HF since, the pumping is quite fast allowing the only appreciable relaxation to be caused by radiation.

In this pressure region, the relative vibrational population for v=1 increases (Tables 4-8) except for the lowest pressure, 0.13 mm Hg for which the ratio P_2/P_1 decreases. This is explained by the fact that since the pressure 0.13 mHg is much lower than the high pressure limit, the rate constant of decomposition would show a falling off (15, 140).

The relaxation of hydrogen fluoride due to Ar or He is almost negligible. Therefore, assuming the use of the same mechanism, independent of the inert gas, the emission would be expected to be the same when either gas is used. However, in this work, it was found that the total emission intensity of the reaction when He was used as the inert gas was half the emission intensity when Ar was used (Tables B4 and B6). On the other hand, the ratios P_3/P_1 and P_2/P_1, were larger for He than for Ar. Since this difference cannot be due to a change in mechanism or to the collisional deactivation of HF , it must be due to the history of the energized molecule before it decomposes to give HF.

The ratio of the collision frequencies Z_{He-E}/Z_{Ar-E} for helium and argon with the energized molecule vary from 5 to 8 depending on the mass and diameter of the energized molecule formed from the reaction (Table 17).

The energized molecule thus undergoes many more collisions when He is present and would thus be more relaxed (less total energy) than when Ar is present. The rate constant of a unimolecular decomposition according to the RRKM theory is given as a function of the total energy, E, of the "energized" molecule

$$k(E) = A(1 - E_a/E)^{s-1} \qquad [95]$$

where s is the number of active modes which may be smaller or equal to the number of internal degrees of freedom (15). Since the rate constant, k(E), depends on the total energy, E, it is smaller for the case where He is used as inert gas than for Ar at the same pressure and therefore the chemical yield and the emission intensity must be less when He is used.

Even though the emission intensity is lower for He the population ratio R_2/R_1 is higher for He. The lower emission intensity has just been explained using semi-classical arguments. The distribution of E([illegible]) over the vibrational levels can be explained by means of the theories described in the introduction (1.3-1.5). Polanyi has shown that the random statistical model (section 1.5) cannot quantitatively account for the values of the relative vibrational populations of HF.

chloroethane (27), Kassel, Slater Model calculations (36) were carried out. In these calculations the bond length of hydrogen fluoride at the transition state, r_2^*, and intercontinuum coupling constant, ω, are used as parameters to fit the observed ratios P_2/P_1 and R_2/P_1. As result of these calculations the average fractional energy disposed in the vibration of HF has been found to have the lowest value before relaxation by intercontinuum coupling when He is used as carrier gas (Table 13). This agrees with the prediction of lower excess energy with He because of a higher collision frequency of the energized molecule. Remarkably, the Berry Model also shows that f_v^* for hydrogen fluoride after relaxation by intercontinuum coupling is the highest with He (Table 13). This is because the time for intercontinuum coupling in the case of helium at pressure .62 mMy is less than the corresponding time for argon at any pressure. This explains the highest relative populations of HF with He as carrier gas.

Using Berry Model, a bond order of n=.15 was found. This agrees with models of the activated complex which best fit the observed kinetics of unimolecular eliminations of RRKM treatments (147, 148, 149). In the RRKM model, the formation of the C=C double bond is taken

to be almost complete, while the HF bond order is only n=.1 to .2 of a single bond. In this case the available energy is inefficiently channelled into HF vibration. If, on the other hand, the available energy becomes translational energy of the products, this suggests that the energy is released along the coordinate of separation of hydrogen fluoride from the rest of the molecule rather than being released during the approach of H to F. This is analogous to the "repulsive" type of energy-release in exchange reactions

$$A + BC \longrightarrow AB + C \qquad [5]$$

The energy-release is termed "repulsive" when it occurs as the products separate and tends to be less efficient in channeling reaction energy into product vibration (11). This is due to the fact that the forces on A and B are not sufficiently different to produce internal motion. Therefore, in the repulsive type of energy-release, the available energy is disposed in translation and rotation. Since rotationally excited HF was not observed, then an energy release on a repulsive surface must dispose most of the available energy in translation. However, if the available energy became only translational energy, the separation of the hydrogen fluoride from the rest of the molecule would

be too rapid for intersystem crossing.

An alternative is that the energy of the reaction may be deposited in vibration of the C—C bond. This suggests a type of "attractive" energy-release, in which the change in C—C bond length corresponds to the coordinate of descent on the potential energy hypersurface in the course of forming a double bond.

When argon is used as inert gas, for hydrogen fluoride elimination from both 1,1,1-trifluoroethane and fluoroethane, the application of Berry Model gives approximately the same internuclear distance for the dressed oscillator $HF^{\neq}$ at all pressures (Table 13). Also, the fractional energy disposed in the dressed oscillator is approximately the same ($\langle f_{v'} \rangle$=.65 at .63 mmHg and $\langle f_{v'} \rangle$= .67 at 1.07 mmHg for CH_3CH_2F and $\langle f_v \rangle$ =.64 for CH_3CF_3 at pressure .35-.55 mmHg with Ar as inert gas) (Table 13). This indicates a similarity in the hydrogen fluoride elimination from the activated complex of the two compounds. This is in agreement with the results of Kirk, Setser and Holmes who have proven that 1,2-elimination is the exclusive path for elimination of HF from fluoroethane (135) as it must be for 1,1,1-trifluoroethane.

2.2

REACTIONS OF ACTIVE NITROGEN WITH VINYL FLUORIDE, 1,1-DIFLUOROETHYLENE AND, TRIFLUOROETHYLENE.

3.3.1 General.

The reaction of active nitrogen with hydrocarbons has been the subject of many studies. Generally, such reactions show very complex features.

Strutt (150) found that many organic compounds introduced into a stream of active nitrogen produced brilliant glows in the region downstream from the point of mixing. Winkler et al (151) studied the products formed by the reaction of active nitrogen with organic compounds and found that most organic substances yield HCN as the major product. The electronic, vibrational and rotational intensity distribution in the CN bands of the reaction flames was studied by Broida et al (152). Emission from CH and NH were also observed although they were relatively weak. The C_2 Swan bands were also present.

The outstanding feature of these reaction systems is the similarity of the reactions with different hydrocarbons. The reason for this behavior is that all hydrocarbons are degraded to nearly the same simple radicals by reaction with active nitrogen. Because of this similarity, Safrany classified them into three

groups according to their visual and kinetic behaviour (150).

Group I. Reactions with alkenes, dienes and alkynes, with the exception of acetylene.

Group II. Reactions with alkanes and cycloalkanes.

Group III. Reactions with substances denoted as "anomalous" (154), that is acetylene, HCN and $(CN)_2$.

The only major difference between groups I and II is that the reactions with alkanes are much slower at room temperature (131, 155-158). Group III is distinguished from groups I and II by strong emission from the CN-red band system in whitish reaction flames.

Active nitrogen is produced by an electric or microwave discharge in molecular nitrogen or mixtures of N_2 with Ar or He. The main active species present are atomic nitrogen in the ground state $N(^4S)$, molecular $N_2(A^3\Sigma_u^+)$ and vibrationally excited molecular nitrogen. Other metastable species $N(^2D)$, $N(^2P)$ and molecular N_2 in $B(^3\Pi_g)$, $B(^3\Delta_u)$, $B'(^3\Sigma_u^-)$ and $a'(^1\Sigma_u^-)$ states formed in the discharge, are less important due to their short life time (134). The reactions of active nitrogen with most of the hydrocarbons and their derivatives have been studied by many workers.

Winkler and coworkers have suggested addition

followed by unimolecular decomposition as the mechanism of the reaction of active nitrogen with ethylene (150).

$$CH_2{=}CH_2 \quad N \rightarrow [\cdot C_2H_4] \rightarrow HCN + CH_3 \qquad [96]$$

A few reactions of active nitrogen with halocarbons have been studied. Jennings et al (150) photographed the spectra of flames produced by introducing CH_4 or CH_3Cl into a stream of active nitrogen. Winkler and coworkers (160, 161) studied reactions of active nitrogen with chlorocarbons. They suggested the following mechanism for the reaction of active nitrogen with vinyl chloride (161)

$$CH_2CHCl + N \rightarrow [N \cdot CH_2CHCl] \rightarrow HCl + N \cdot C_2H_2 \qquad [97]$$

$$N \cdot C_2H_2 + N \rightarrow N_2 + C_2H_2 \qquad [98]$$

$$N + N \cdot C_2H_2 \rightarrow 2HCN \qquad [99]$$

Jones and coworkers (162) have proposed the following primary steps for the reaction of atomic nitrogen with tetrachloroethylene

$$N(^4S) + C_2Cl_4 \rightarrow [N \cdot C_2Cl_4] \quad \text{Products} \qquad [100]$$

$$N_2(A^3\Sigma_u^+) + C_2Cl_4 \rightarrow N_2(X^1\Sigma_g^+) + C_2Cl_4^* \qquad [101]$$

Regarding the reactions with fluorocarbons, Johnson

and Tamres (160) have studied the chemiluminescence of C, CN and CH from the reaction of active nitrogen with tetrafluoroethylene. They observed chemiluminescence from CN ($B^2\Sigma^+ \rightarrow A^2\Pi$, 388 nm), CH ($C^2\Sigma^+ \rightarrow A^2\Delta$) and C (156.1, 165.8 and 193 nm). Ground state and metastable C (^3P, ^1D) were detected and studied via resonance fluorescence.

Jones and coworkers (164, 165) studied the reactions of active nitrogen with perfluorocarbons. For the reaction of active nitrogen with tetrafluoroethylene, the following main steps have been proposed by Madhavan and Jones (164).

$$C_2F_4 + N \rightarrow CF_2N + CF_2 \qquad [102]$$

$$C_2F_4 + N \rightarrow FCN + CF_3 \qquad [103]$$

$$CF_2N \rightarrow FCN + F \qquad [104]$$

$$CF_2 + N \rightarrow FCN + F \qquad [105]$$

$$CF_3 + N \rightarrow FCN + 2F \qquad [106]$$

$$C_2F_4 + FCN \rightarrow (C_3F_5N)_n \quad \text{Polymer} \qquad [107]$$

So far, no reactions of active nitrogen with partially fluorinated ethylene have been studied. In the present work, the flames of the reactions of active nitrogen with vinyl fluoride, 1,1-difluoroethylene and

[illegible] nitrogen was photographed in the visible region. The [illegible] vibrationally excited nitrogen molecules produced from these reactions has also been studied.

3.2.3 Fluorine.

Atomic nitrogen was produced by microwave discharge (2450 MHz) in a 5:6 mixture of nitrogen and argon. At the study of the visible emission, the total pressure in the reaction zone was 1.2 mmHg. When a small amount of fluoroethylene was introduced into the active nitrogen stream, the nitrogen afterglow was quenched completely and a vari-coloured emission was produced. Three zones appeared in the flame. The first zone, close to the fluoroethylene inlet jet, had a bright pink glow. The second zone had a short length and a weak pinkish-white glow. The third zone had a bright blue emission. By increasing the fluoroethylene flow, the first zone retained roughly the same size, colour and intensity but the colour of the third zone changed from a bright blue to a bright pinkish-white colour giving it the same appearance as the second zone. The spectra of these flames are presented in Fig. 25.

By decreasing the flow rate of the fluoroethylene

Figure 25

Spectra of the Flames of the Reactions of Active Nitrogen with:

(a) C_2H_3F

(b) 1,1-$C_2H_2F_2$

(c) C_2HF_3

(d) C_2H_3F in the presence of atomic oxygen.

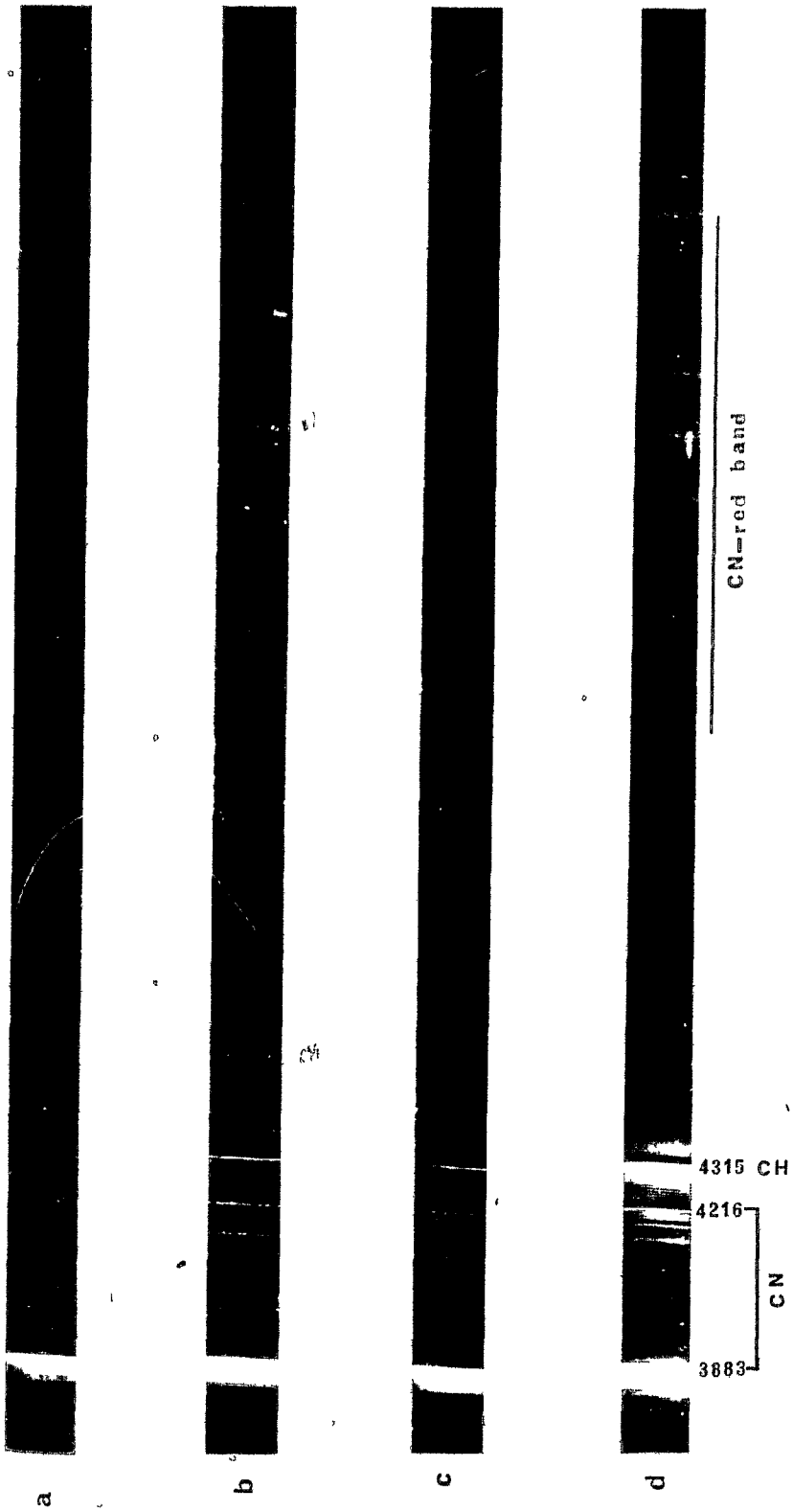
CN-red band
4315 CH
4216
CN
3883
a
b
c
d

the zones were filled with a uniform weak yellow glow, thus making the definition of the zones very ambiguous. In all cases, the emission appeared to oscillate.

The visible spectra emitted by the reaction flames were recorded on an Ilford HP4 film (400 ASA) with a 1.5 m Bausch and Lomb concave grating spectrograph. The exposure time was two hours. The exposed film was developed in exactly the same way each time in order that the band intensities could be compared. The violet degraded bands with heads at 3883 and 4216 Å result from CN emission ($B^2\Sigma^+ \rightarrow X^2\Sigma^+$) and are the sequences $\Delta v=0$ and -1, respectively. These bands were observed to be quite perturbed in the photographs because the intensity of some rotational lines were much stronger than the others. It is impossible to say whether the C_2 Swan bands were present or not, because of the emission of the CN red system in the region of 5000-6400 A. The 0-0 band from CH emission ($A^2\Delta \rightarrow X^2\Pi$) was also present in the spectra. In general, the CH radical is formed in hydrocarbon flames supported by active nitrogen as a product of the reaction (166)

$$C_2 + NH \longrightarrow CH^* + CN \qquad [108]$$

The emission in the infra-red region in the range 2-3 microns was studied by using the same system as was

used to study the reactions of atomic hydrogen with the fluoroethylenes. When fluoroethylene was introduced in the stream of active nitrogen, the luminescence in the IR region from vibrationally excited HF was recorded. By increasing the flow rate of fluoroethylene, the intensity of the hydrogen fluoride emission was increased and reached a maximum. This maximum intensity is very weak for low nitrogen flow rates. Therefore, a high nitrogen flow rate and a larger slit width had to be used for quantitative measurements. The total pressure in the reaction zone was 4.47 mmHg, measured with an oil manometer. Under these conditions, HF was introduced in the active nitrogen stream. No emission was observed. This lack of emission proves that we do not have HF emission due to energy transfer from active nitrogen. The IR emission spectra of the vibrationally excited hydrogen fluoride are presented in Fig. 26, 27 and 28. The data were treated in the same way as for the reactions of atomic hydrogen with the fluoroethylenes (section 2.1). The areas representing the intensity of the rotational lines are given in Table B7.

In the reactions of active nitrogen with vinyl fluoride and 1,1-difluoroethylene emission from only v=1 and v=2 was observed, while with trifluoroethylene, an extremely weak emission from v=3 was observed.

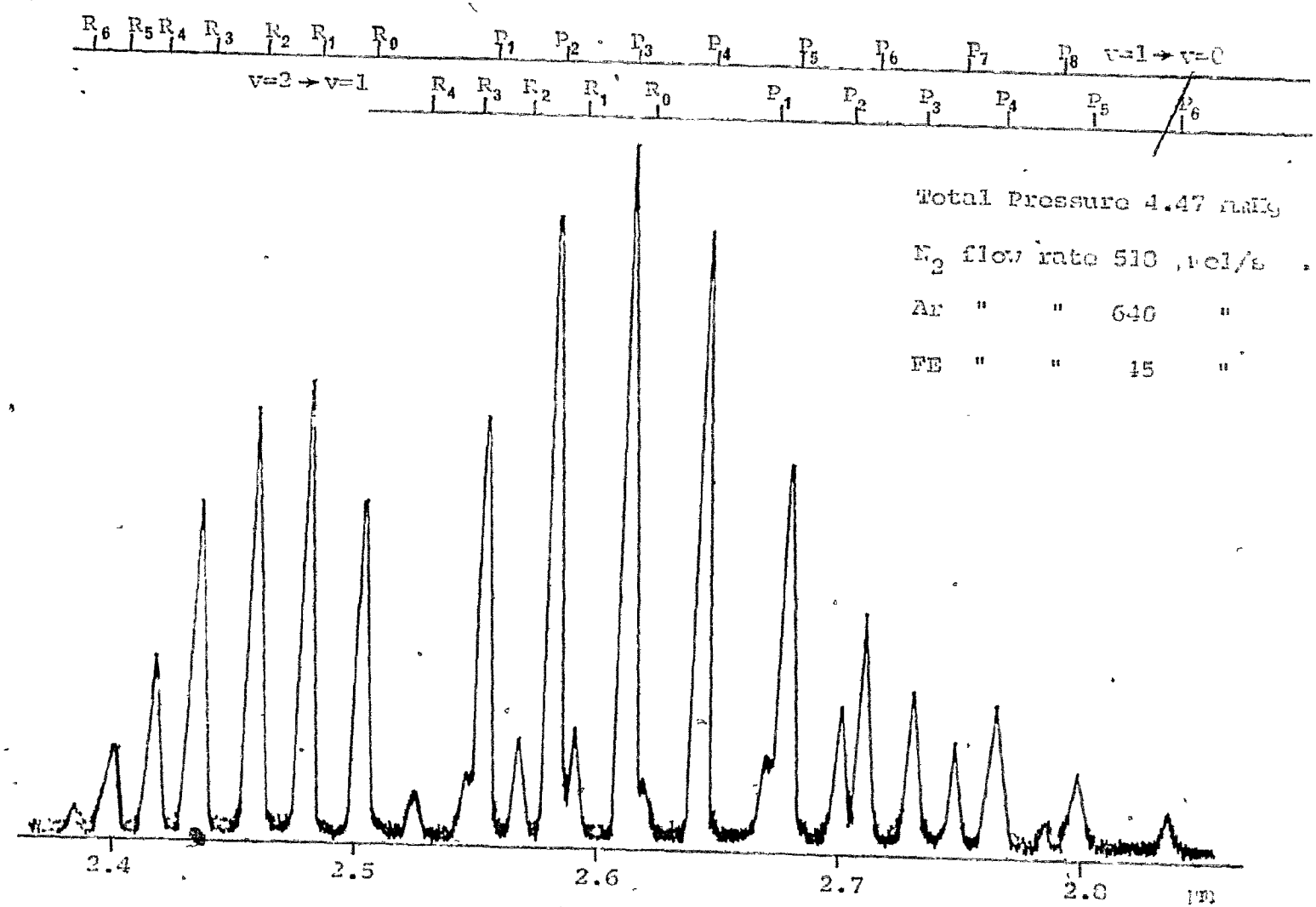

Fig. 26. The HF^1(Δv=1) emission spectrum from the reaction of N atoms with C_2H_3F.

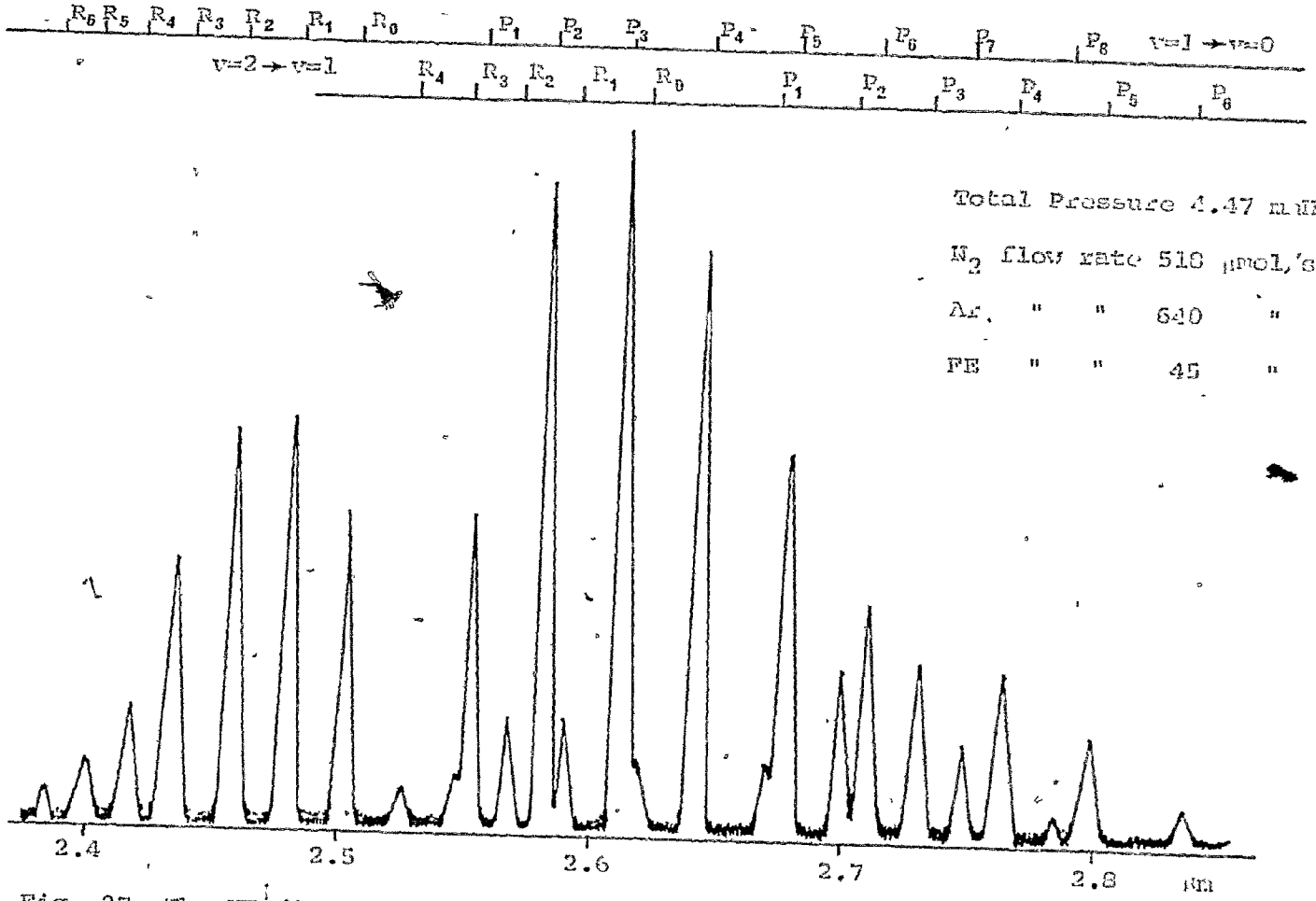

Fig. 27. The HF^{1} ($\Delta v=1$) emission spectrum from the reaction of N atoms with $1,1\text{-}C_2H_2F_2$.

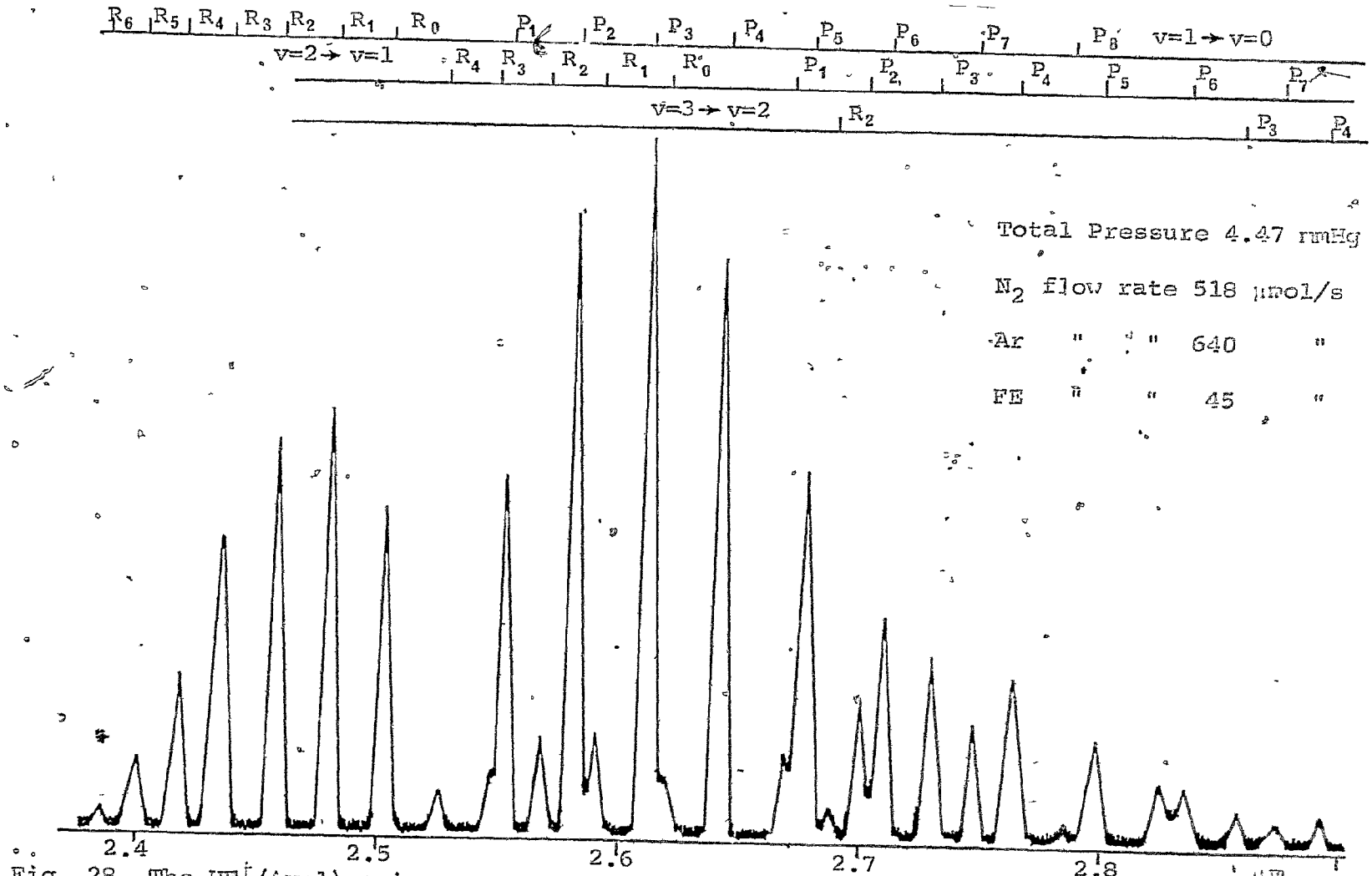

Fig. 28. The $HF^{\dagger}(\Delta v=1)$ emission spectrum from the reaction of N atoms with C_2HF_3.

Relative stationary-state rotational populations were calculated and plotted against values of J' in Fig. 29, 30 and 31. From the rotational Boltzmann plots (Fig. 32, 33 and 34), the rotational temperatures were calculated for the two vibrational levels. These values are given in Table 18 and are close to the reaction zone temperature, 340-360 ^{o}K, as measured with a thermocouple.

From the sum of the rotational populations over all rotational levels in a vibrational state, the experimental stationary-state relative vibrational populations were calculated. The same collisional model for relaxation was used as in the reactions of hydrogen atoms with the fluoroethylenes. The collisional deactivation probability $P_{1,0(HF-N_2)} = 1.8 \times 10^{-5}$ for deactivation of vibrationally excited hydrogen fluoride (v=1) by molecular nitrogen is given by Green and Hancock (131). The corrected vibrational populations and vibrational temperatures are also given in Table 18.

A dark yellow-brown polymer of type $(C_3F_5N)_n$ has been found for the reaction of active nitrogen with C_2F_4 (164). On the other hand, a white polymer is formed from the reaction of active nitrogen with ethylene (153). Similarly, during the reactions of active nitrogen with partially fluorinated ethylenes polymers were formed on the walls of the reaction cell. A whitish-yellow polymer was formed from the

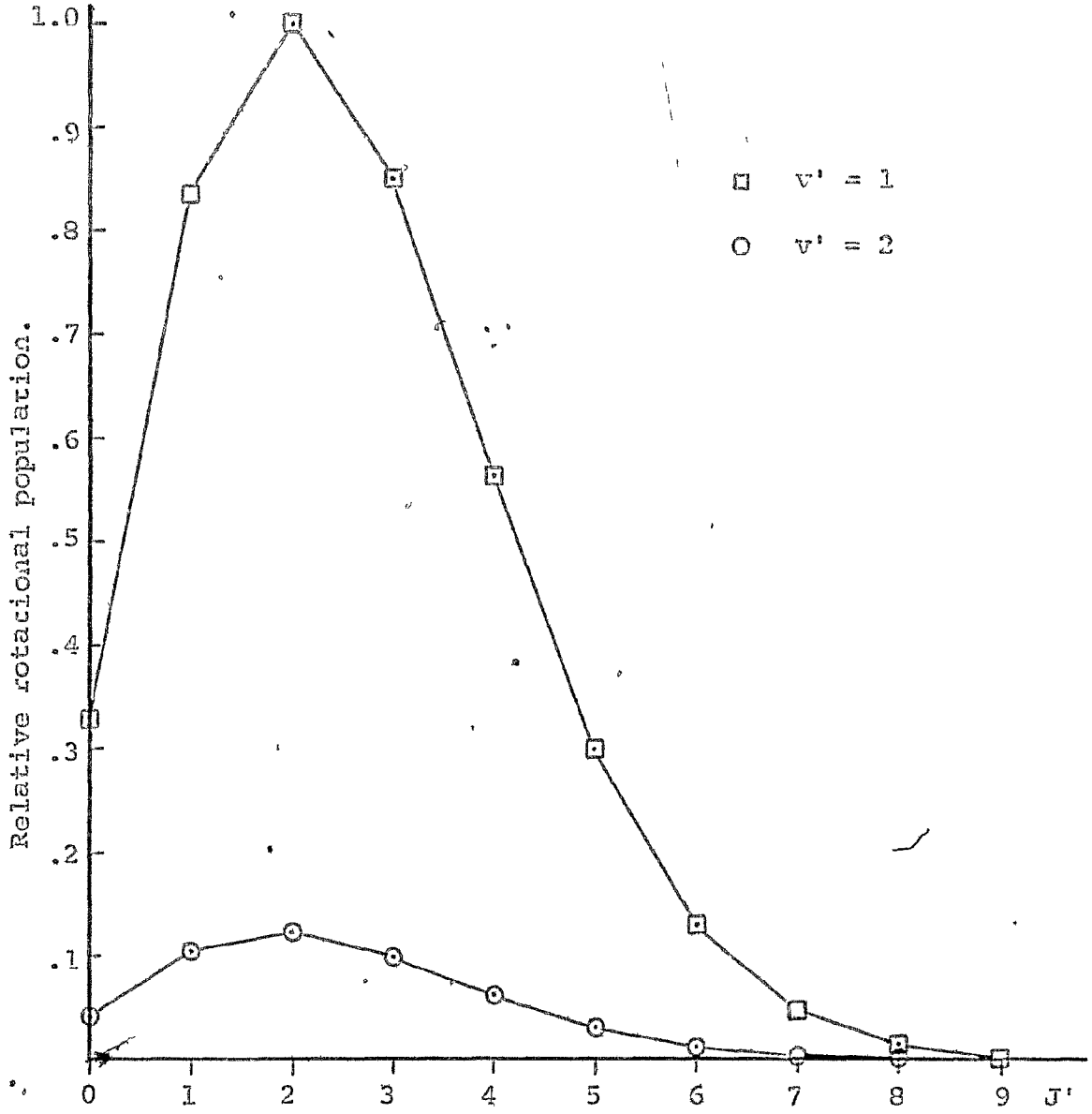

Fig. 29. The relative rotational population of HF from the reaction of active nitrogen with C_2H_3F.

N_2 flow rate 518 μmol/s FE flow rate 45 μmol/s

Ar " " 640 " Total Pressure 4.47 mmHg

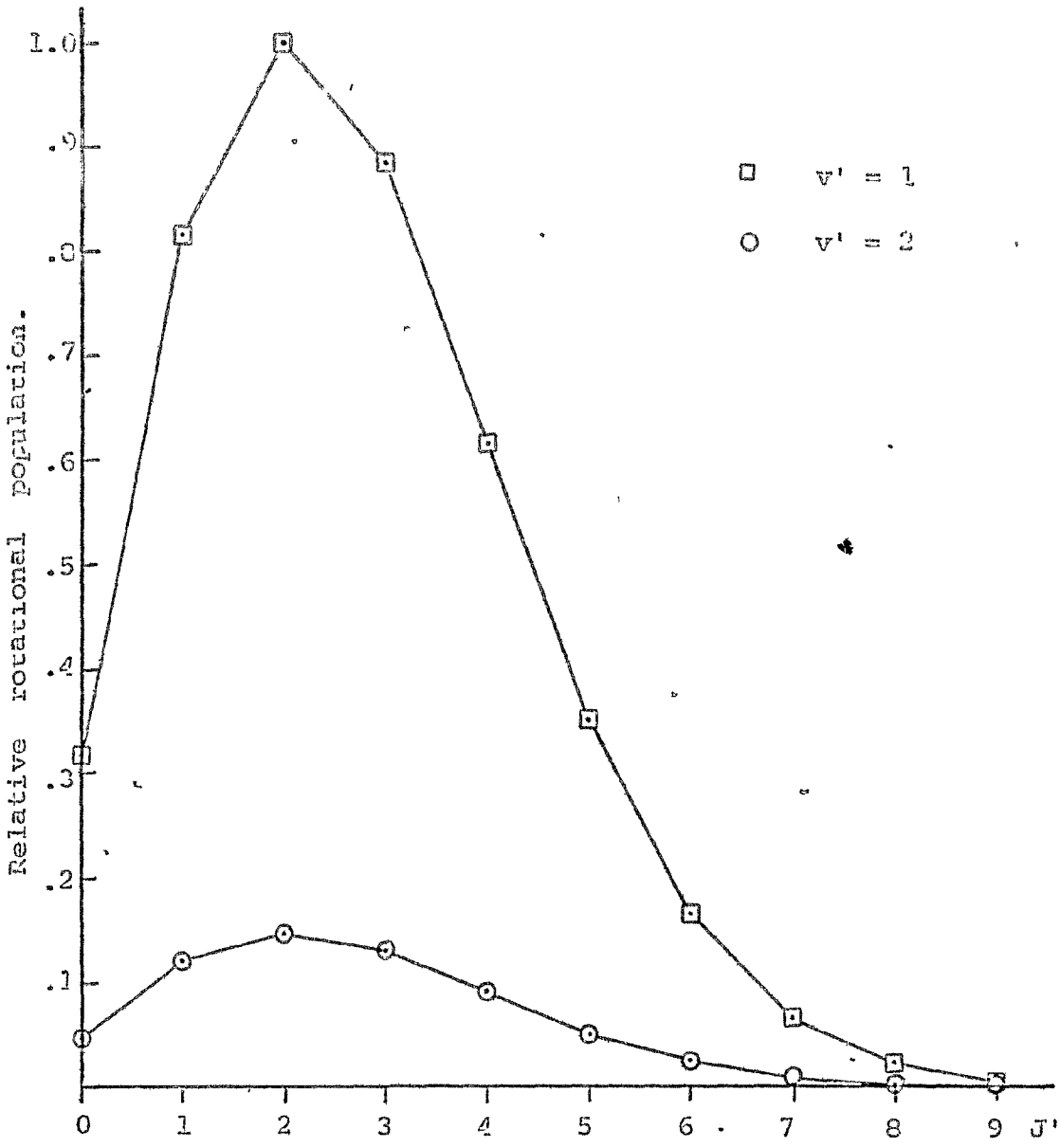

Fig. 30. The relative rotational population of HF from the reaction of active nitrogen with 1,1-$C_2H_2F_2$.

N_2 flow rate 518 μmol/s FE flow rate 45 μmol/s

Ar " " 640 " Total Pressure 4.47 mmHg

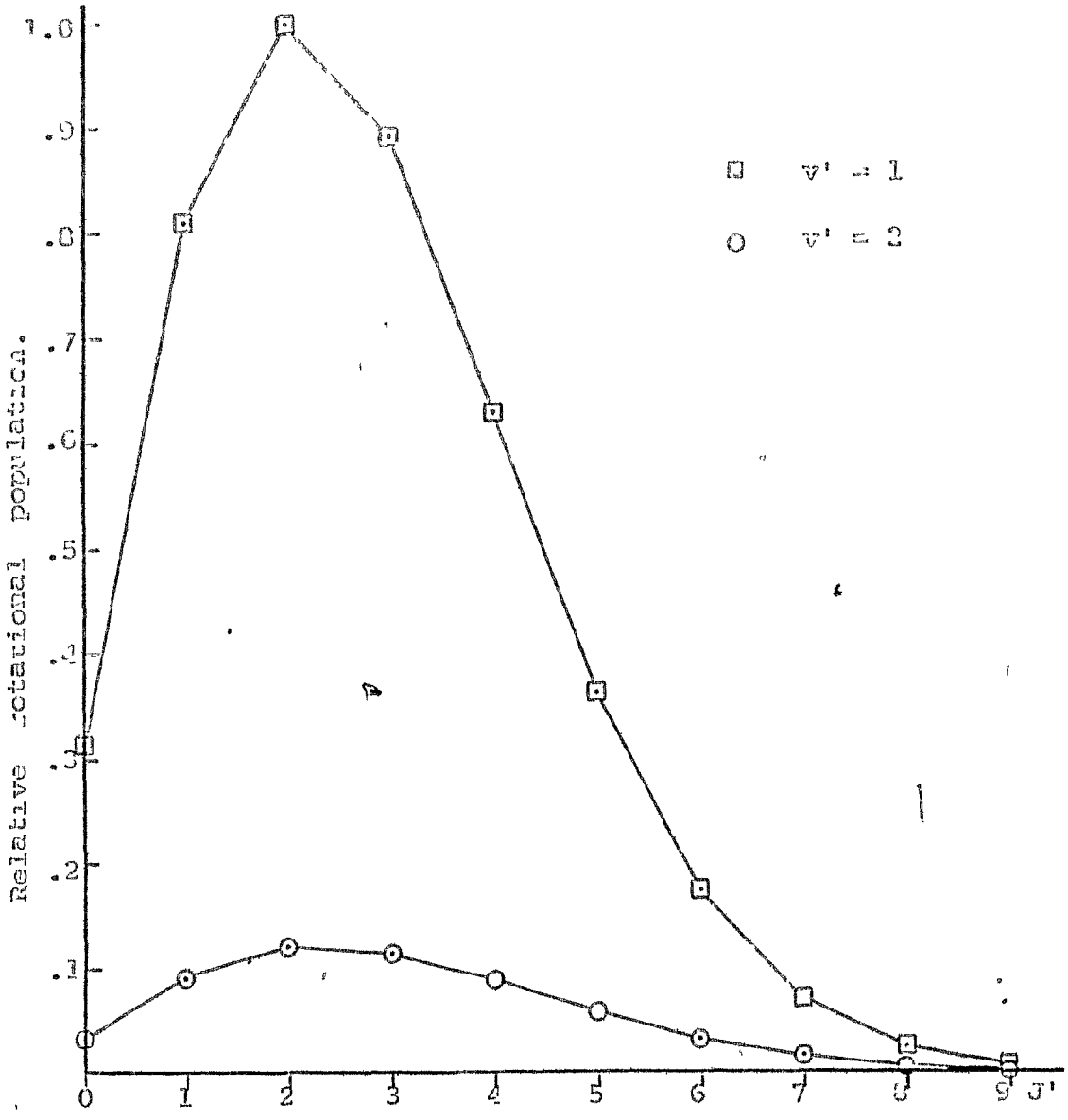

Fig. 31. The relative rotational population of HF from the reaction of active nitrogen with C_2HF_3.

N_2 flow rate 518 μmol/s HF flow rate 45 μmol/s

Ar " " 640 " Total Pressure 4.47 mmHg

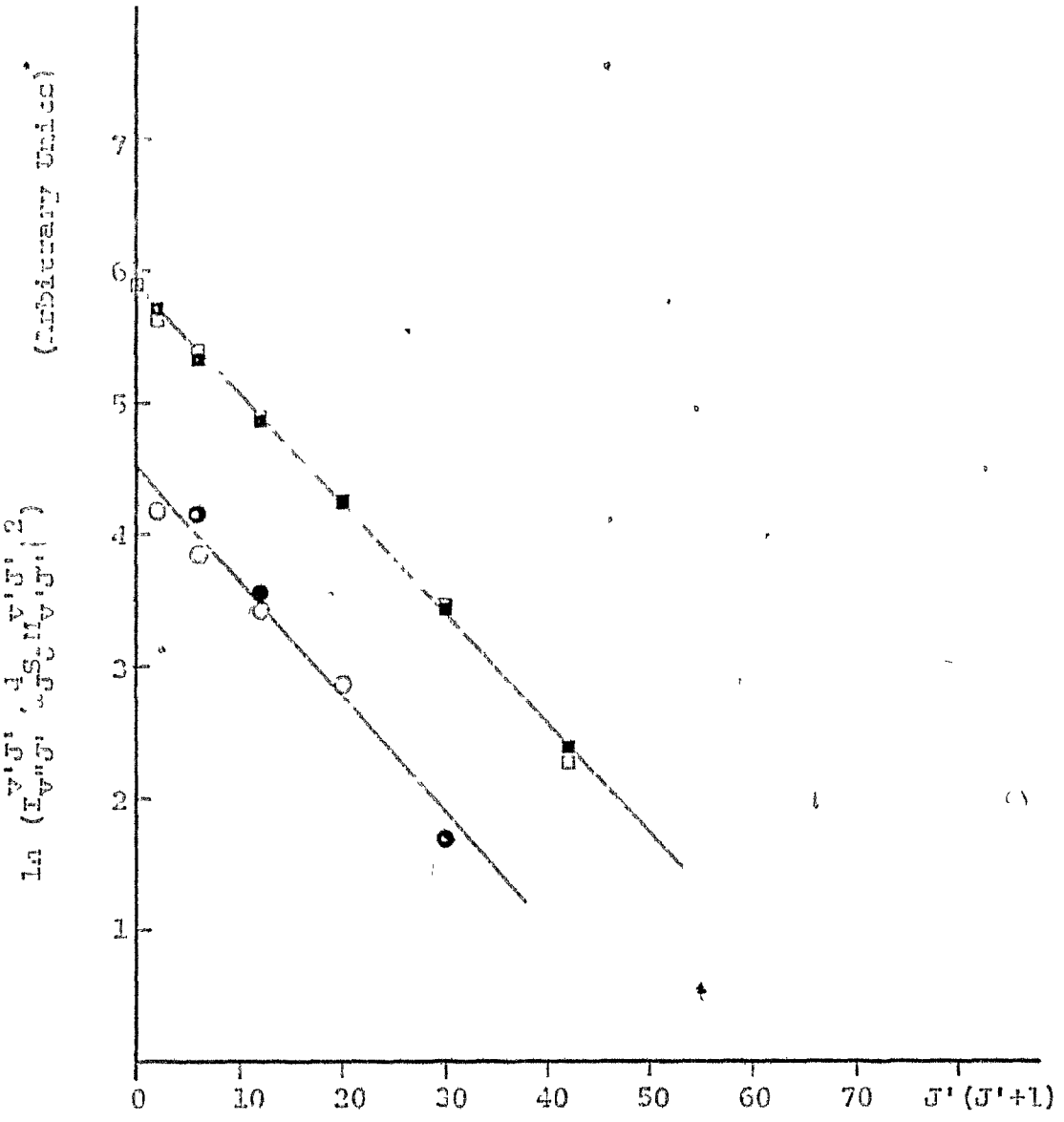

Fig. 32. Stationary-state distribution of HF among rotational states from the reaction of active nitrogen with C_2H_3F. □ from v(1→0), O from v(2→1). Filled-in points from R branch lines, the remainder from the P branch.

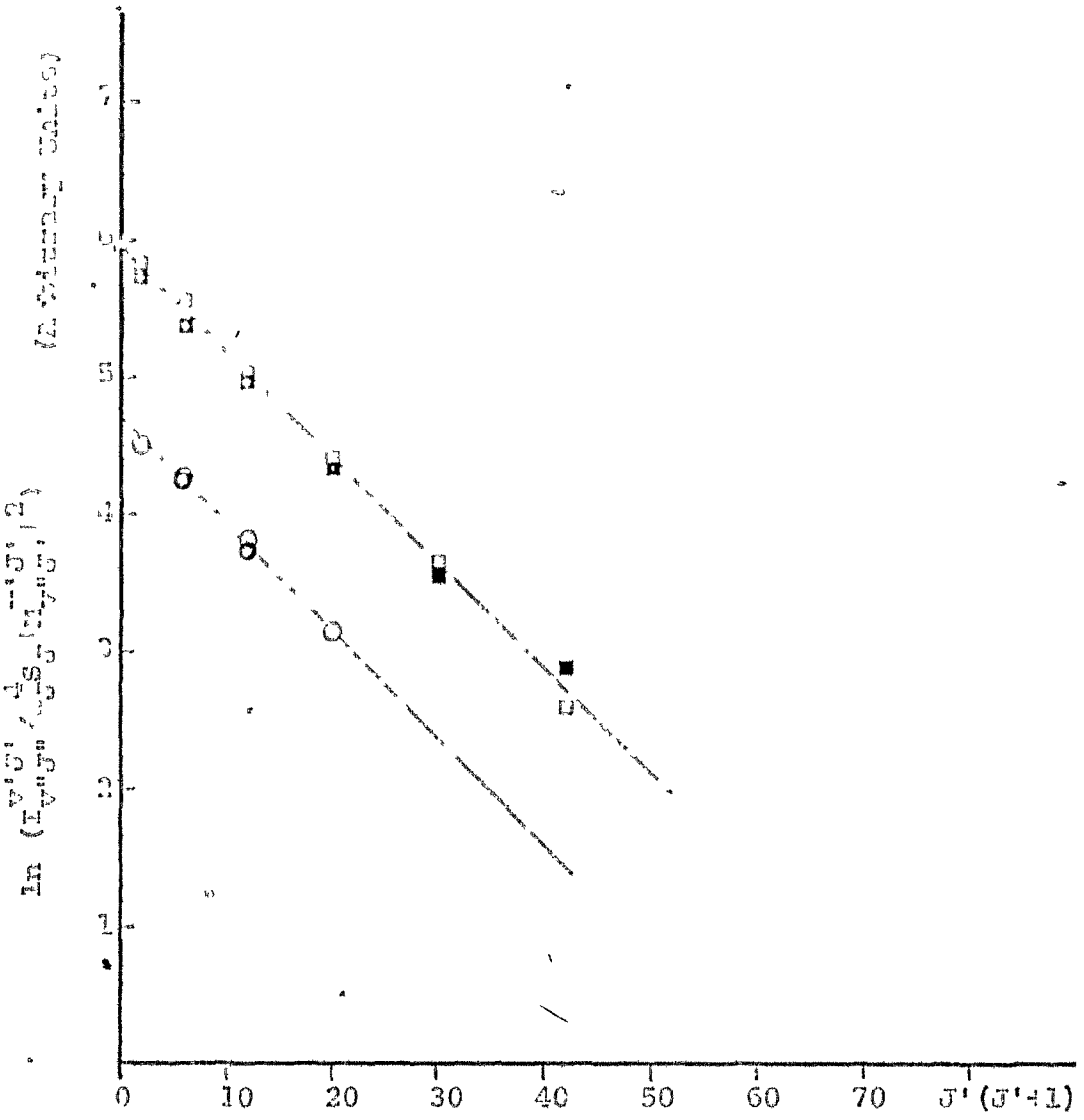

Fig. 33. Stationary-state distribution of HF' among rotational states from the reaction of active nitrogen with 1,1-$C_2H_2F_2$. □ from v(1→0), O from v(2→1). Filled-in points from R branch lines, the remainder from the P branch.

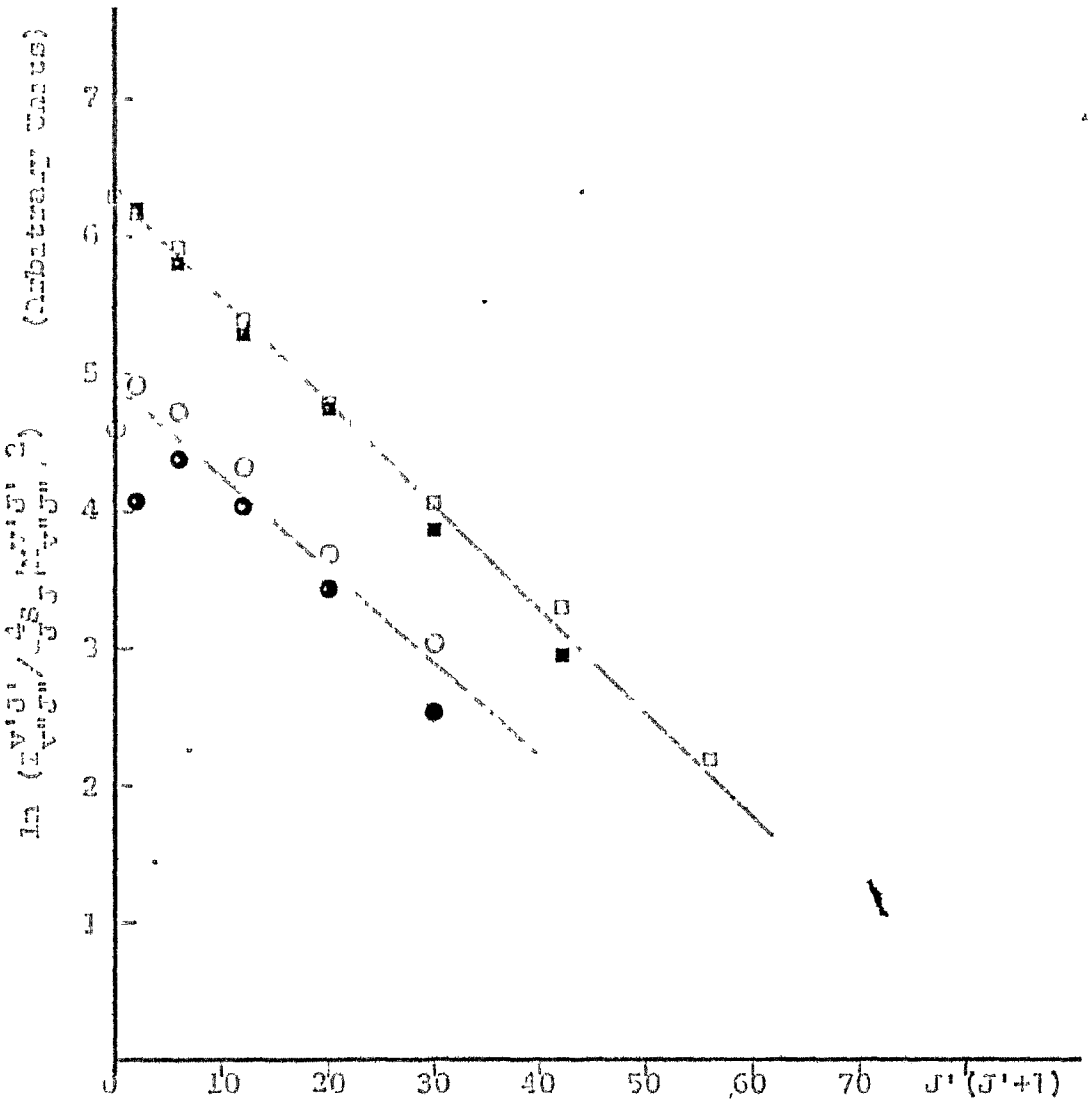

Fig. 34.- Stationary-state distribution of HF among rotational states from the reaction of active nitrogen with C_2HF_3. □ from v(1→0), O from v(2→1). Filled-in points from R branch lines, the remainder from the P branch.

Table II

Steady-State Relative Vibrational Populations for the Reactions of Active Nitrogen with Fluoroethylenes.

N_2 Flow rate 510 μmol/s FE Flow rate 15 μmol/s
Ar " " 600 " Total pressure 4.47 mmHg

Fluoro-ethylene	Experimental		Calculated initial
	N_1/N_1	N_2/N_1	R_2/R_1
C_2H_3F	1.	.133±.000	.25±.02
T_{rot}	379±8	440±63	
T_{vib}		3694	3935
1,1-$C_2H_2F_2$	1.	.147±.003	.27±.01
T_{rot}	372±9	356±14	
T_{vib}		3845	4166
C_2HF_3	1.	.119±.005	.22±.01
T_{rot}	343±5	305±23	
T_{vib}		2563	3602

FE = Fluoroethylene

[illegible] with 1,1-difluoroethylene and a comparison [illegible] with trifluoroethylene.

The comparison, the reaction of active nitrogen with ethylene was carried out under the same conditions as those with fluoroethylenes. The violet [illegible] bands for this reaction were observed to be perturbed and a white polymer was deposited on the walls of the reaction cell.

3.2.3 Discussion.

Since, from the observation of the visible emission, the second and third zones of the reaction region have a whitish colour, this is an indication that from the first step of the reaction an acetylenic product is formed which undergoes a secondary reaction with the active nitrogen. Another indication supporting this is the oscillation of the flame. The rate of reaction of active nitrogen with acetylene is small and increases very rapidly when the concentration of acecylene becomes larger than a certain value (153). The stationary-state concentration of the acetylenic derivative increases and when a certain concentration is reached, the acetylenic derivative reacts rapidly with active nitrogen as a result of which its concentration decreases to give an oscillatory effect.

Therefore, the initial step can be considered to be the one as that suggested by Winkler and coworkers (161) for the reaction of atomic nitrogen with vinyl chloride. That is,

$$C_2H_3X + N \longrightarrow [\cdot C_2H_3NX] \longrightarrow HF + \cdot C_2H_2N \qquad [109]$$

where X = F or H. The exothermicity of this reaction is around 50 Kcal/mol which is sufficient to produce vibrationally excited hydrogen fluoride. The fact that the relative population of the v=2 vibrational level is approximately the same for all reactions, is in accord with the mechanism, since the available energy is distributed first in the complex and finally the hydrogen fluoride is eliminated with approximately the same probability of excitation in each case.

A secondary mechanism is the one proposed by Jones and coworkers(164) for the reaction of active nitrogen with tetrafluoroethylene (equations [102-107]). This mechanism is more important for the reactions of 1,1-difluoroethylene and trifluoroethylene since the C=C bond energy drops with increasing degree of fluorination from 171 Kcal/mol in C_2H_4 to 70 Kcal/mol in C_2F_4 (167). Both π and σ bond energies are lowered (168) so that the increasing degree of fluorination makes the decomposition

in c radicals a more likely process. Since the radicals react more easily and faster, the visible intensity for 1,1-$C_2H_2F_2$ and C_2HF_3 is expected to be stronger and this agrees with the present experimental results. In addition, this fragmentation increases the stationary-state concentration of fluorine atoms, especially for trifluoroethylene. In this case, the very small emission of the transition HF' ($v=3 \rightarrow v=2$) observed in the reaction of active nitrogen with trifluoroethylene may be due to hydrogen abstraction from trifluoroethylene by fluorine atoms.

The fact that the strong emission for 1,1-$C_2H_2F_2$ and C_2HF_3 is due to radicals is further supported by the observation that the emission from the vinyl fluoride becomes very strong when a small amount of oxygen is mixed with the nitrogen (Fig. 25). In this case, a larger number of free radicals is present from the reaction of O atoms with vinyl fluoride.

Perturbations of the CN violet bands were observed only in flames of hydrocarbons supported by N at low pressures (169-172). They were caused jointly (169) by (a) a chemical property of the flame: the highly preferential formation of CN in the $A^2\Pi$ levels as compared to $B^2\Sigma^+$ levels and, (b) a physical property of the CN molecule itself: the long radiative lifetime of the $A^2\Pi$

levels (6×10^{-7}s , radiative life time for v'=10) compared to the $B^2\Sigma^+$ levels (8.5×10^{-8}s radiative life time for v'=0). The perturbation of the violet CN bands observed in the present work was probably due to the same reasons. This was further supported by the fact that the same perturbation was shown by the reaction of active nitrogen with ethylene.

REACTIONS OF ATOMIC OXYGEN (^3P) WITH VINYL FLUORIDE, 1,1-DIFLUOROETHYLENE AND TRIFLUOROETHYLENE.

2.3.1 General.

The reactions of atomic oxygen with haloethylenes have long been recognized as important steps in the thermal and photochemical combustion mechanisms and as a route to a better understanding of the mechanism of the reactions of atomic oxygen with olefins. Recently, these reactions received great attention, especially the reactions of oxygen atoms with fluoroethylenes, since they proceed via the formation of extremely energy-rich adducts which are capable of decomposing or undergoing rapid internal rearrangements giving potential chemical lasers (173).

The reaction of oxygen atoms with olefins has been studied extensively (174-179). By photolysis of nitrogen dioxide at different wavelengths, it was possible to produce atomic oxygen in either its ground electronic state, O (^{3}P), or in its first excited state, O (^{1}D), so that the comparative chemical behavior could be investigated (181). Jarvie and Cvetanovic (182) have also compared the results obtained by a discharge flow technique with those obtained by the photolysis technique.

In 1970, Cvetanovic (183) proposed a general scheme

for the reaction of atomic oxygen with an olefin. In the first step, the oxygen atom adds to one side of the double bond, preferentially at the less substituted carbon atom:

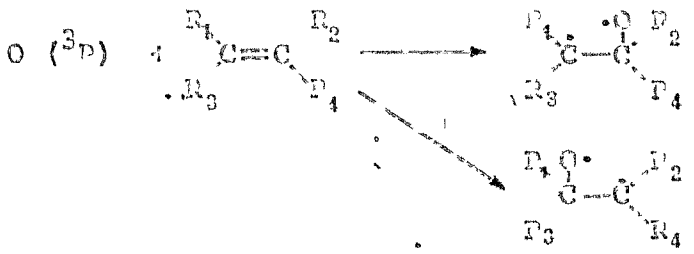

[110]

This intermediate was visualised as a triplet biradical, in which the electrons need not be completely localized. This excited triplet biradical may (i) undergo ring closure to an excited epoxide [111a], which may be stabilized or may fragment, (ii) rearrange to an excited carbonyl compound [111b], which may also be stabilized or fragment or, (iii) undergo pressure independent fragmentation [111c]

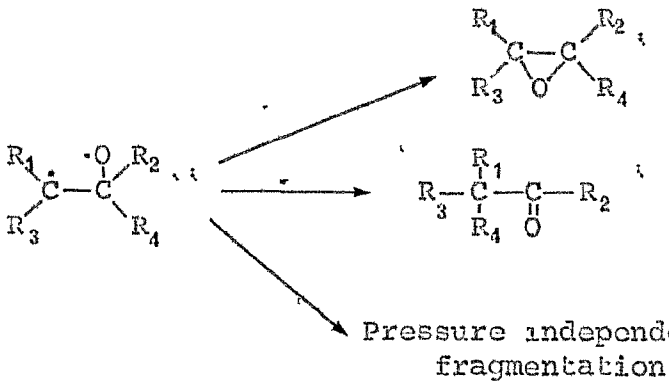

[111a]

[111b]

[111c]

The product yield from reactions [111a, 111b] will depend upon the total pressure, while that resulting from

the direct decomposition of the intermediate biradical [111c] will show no pressure dependence.

In order to explain the product ratios from cis- and trans-2-butene Scheer and Klein (184) postulated a different model of attack of the oxygen atom on the olefin. Rather than approaching the double bond in the plane of the π electrons and becoming localized on one carbon atom, the oxygen atom approaches in the plane of the molecule, becomes loosely bound to both carbon atoms, and interacts with the adjacent hydrogen atoms:

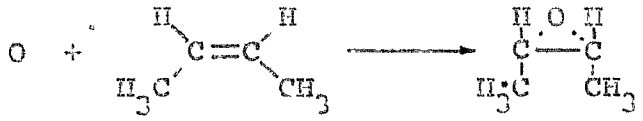
cis [112]

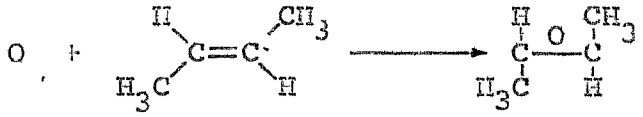
trans [113]

Arguments based on product analysis do not support conclusively one mechanism or the other since each, with a few additional assumptions, has been able to account for all of the observations. A serious failing of the Scheer-Klein mechanism is that it predicts that reaction is more favorable at unsubstituted olefinic carbon atoms, contrary to observation.

The reactions of atomic oxygen with perfluoroalkenes

and 1,1-difluoroethene were first investigated and a very simple mechanism was used to explain the products (183-187).

$$O + C_2F_4 \longrightarrow CF_2 + CF_2O \qquad [114]$$

$$O + \begin{matrix} F & X \\ & C=C \\ F & Y \end{matrix} \longrightarrow \begin{matrix} F & O & X \\ & C-C \\ F & & Y \end{matrix} \longrightarrow CF_2O + CXY \qquad [115a]$$

$$\longrightarrow \begin{matrix} F & O & X \\ & C-C \\ F & & Y \end{matrix} \longrightarrow CF_2 + CXYO \qquad [115b]$$

where X,Y = Br, Cl.

Since then, different methods have been used to determine the rate constants in the reactions of oxygen atoms with fluoroethylenes (188-191). From these studies, it became obvious that this simple mechanism [115] is the only one for the fluoroethylenes of the type CF_2CXY (X, Y = F, Cl and Br). For other fluoroethylenes, the evidence supports a mechanism which involves the production of an aldehyde and a carbene in the initial step (192). In the reaction of atomic oxygen with ethylene, however, considerable evidence indicates that the initial step produces a formyl and methyl radical. The observation of CO as a major reaction product in the C_2H_3F system (189) indicates that this reaction also produces a formyl radical.

Recently, Gutman and coworkers tried to identify

Recently the reactive rate constants from the reactions of atomic oxygen with the fluoroethylenes in crossed jet experiments (160). They give the general scheme of Fig. 35 for the reactions. This scheme is the composite of the two mechanisms for the oxidation of ethylene and tetrafluoroethylene by oxygen atoms. The reaction of tetrafluoroethylene with atomic oxygen proceeds exclusively by direct C—C bond cleavage [114]. The reaction of oxygen atoms with ethylene proceeds by two routes. [116a] is the principal route involving internal H atom migration in the $O \cdot C_2H_4$ adduct followed by decomposition into two free radicals whereas, [116b] is a secondary route in which hydrogen is eliminated from the excited adducts (193).

$$O + C_2H_4 \longrightarrow [C_2H_4O]^* \begin{cases} \longrightarrow CH_3 + CHO & [116a] \\ \longrightarrow CH_2{=}C{=}O + H_2 & [116b] \end{cases}$$

Recently, Lin and coworkers (173) obtained chemical hydrogen fluoride laser emission from the reaction of O (^3P) atoms with vinyl fluoride. This is the only study of IR chemiluminescence from the reactions of atomic oxygen with fluoroethylenes.

In the present work, we have studied the IR chemiluminescence of the reactions of atomic oxygen with C_2H_3F, 1,1-$C_2H_2F_2$ and C_2HF_3. Vibrational population distribu-

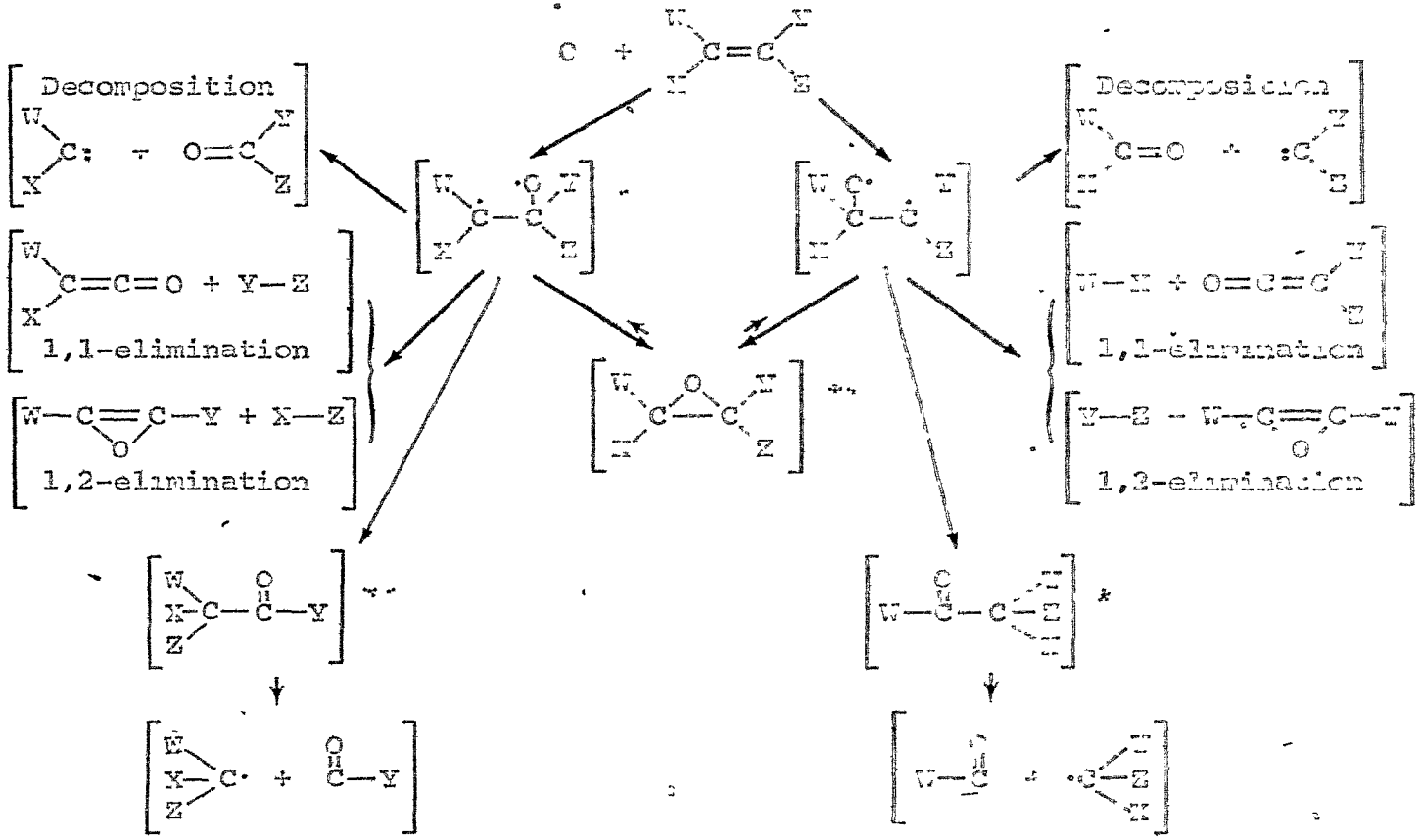

Fig. 35. Mechanistic scheme for the reaction of oxygen atoms with the fluoroethylenes. W, X, Y and Z represent H or F atoms. The migrating group is always a H atom.

tion were measured in all reactions. A preliminary survey of the visible emission resulting from chemically excited species was also made.

2.3.3 Results.

When the fluoroethylenes (C_2H_3F, 1,1-$C_2H_2F_2$ and C_2HF_3) were introduced into an oxygen atom stream, visible chemiluminescence attributed to the molecules CH, C_2, HCF was observed. Several additional bands which have not yet been identified were also observed. Atomic oxygen was produced by microwave discharge in molecular oxygen using the apparatus described in the Experimental Section. The colour of the flame changed, depending upon the fluoroethylene used. A spectrographic investigation showed that the strongest bands resulted from the CH radical. With C_2H_3F, the CH ($A^2\Delta$-$X^2\Pi$) and ($B^2\Sigma^-$-$X^2\Pi$) bands are the strong ones. With 1,1-$C_2H_2F_2$, they become weaker. With C_2HF_3 the ($A^2\Delta$-$X^2\Pi$) band becomes even weaker while the ($B^2\Sigma^-$-$X^2\Pi$) can barely be seen. The same intensity change is observed for the C_2 Swan bands ($A^1\Pi_g$-$X^1\Pi_u$). For C_2H_3F, all the sequences $\Delta v=1$, 0, -1 are quite strong, whereas, for the 1,1-$C_2H_2F_2$ only the sequences $\Delta v=1$ and 0 can be seen. In contrast, the emission of HCF is weak in all reactions.

however, it appears to be somewhat stronger for C_2HF_3 and decreases gradually in intensity from C_2HF_3 to C_2H_3F. Due to these differences, the color of the flame of C_2HF_3 with O atoms is observed to be green. The flame of 1,1-$C_2H_2F_2$ is blue-green and the flame of C_2H_3F appears blue. The spectra of CH and C_2 are well known and were easily identified by comparison of the wavelengths of the band heads with those given by Pearse (194). The identification of HCF was more difficult. The present work is the first observation of this radical in emission. Moore and Travis (195) have observed the absorption spectrum of the HCF free radical in the flash photolysis of dibromofluoromethane, $HCFBr_2$, and have analyzed the rotational structure of the vibrational bands 000-000 and 010-000.

The spectra of the flames are given in Fig. 36. These spectra are reproduced from films obtained with a 1.5 m Bausch and Lomb spectrograph. The spectrum of the flame of the reaction of atomic oxygen with ethylene is also given. Each spectrum was photographed under the same conditions (Table 7B) with HP4 film (ASA 400). Two hours exposure time and the same developing procedure were used in each case to allow relative comparison of the intensities. The intensity of the unidentified bands is stronger for the reaction with C_2HF_3 and weaker for the reaction

Figure 36

Visible Spectra of the Reaction of Atomic Oxygen with

a. Trifluoroethylene

b. 1,1-Difluoroethylene

c. Vinyl Fluoride

d. Ethylene.

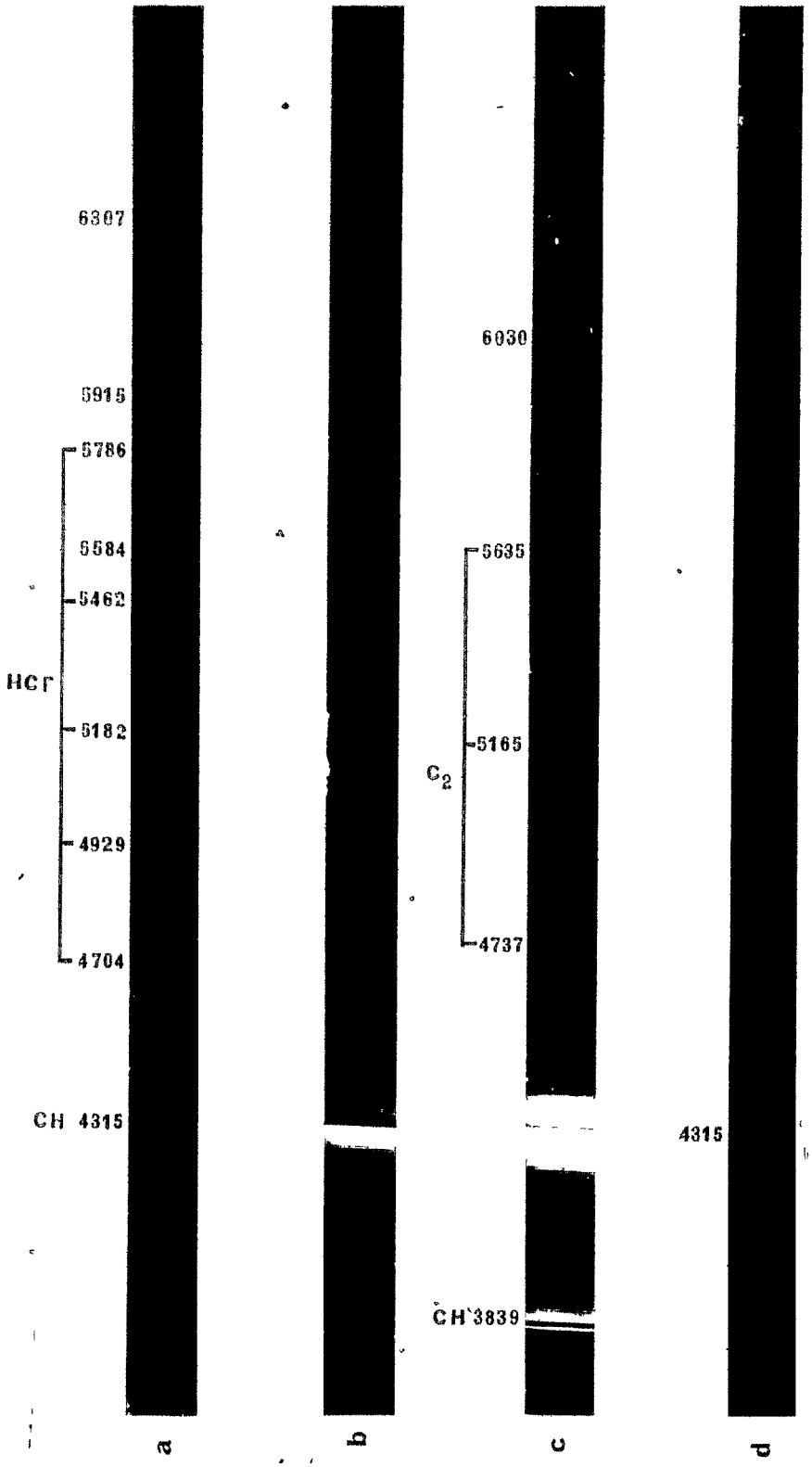
6307
5915
5786
5584
5462
HCr
5182
4929
4704
CH 4315
a
b
6030
5635
C2
5165
4737
CH 3839
c
4315
d

with $C_2H_2F_2$. The observed bands are given in Table 19.

Infrared chemiluminescence was observed in the reactions of oxygen atoms with fluoroethylenes due to vibrationally excited hydrogen fluoride. The flow rates of the reactants were adjusted to optimize the conditions for HF* emission and in order to achieve emission from vibrationally excited CO^*. It is known (196) that the reaction of atomic oxygen with chloroethylenes gives vibrationally excited HCl* and CO^*. However, no emission from vibrationally excited CO^* was observed under any conditions in the reactions of atomic oxygen with fluoroethylenes.

We did the same tests as in the reactions of atomic hydrogen and nitrogen to ascertain that the emission was from the products of the reactions and not from energy transfer processes. The experimental conditions were the same for all the reactions of atomic oxygen with the fluoroethylenes to give comparable results; total pressure 1.03 mmHg, O_2 flow rate 532 μmol/s, O atom flow rate 22.6 μmol/s, fluoroethylene (FE) flow rate 29.2 μmol/s. The flow rate of O atoms was determined by titration with NO_2.

$$O + NO_2 \longrightarrow O_2 + NO^* \qquad [117]$$

Reaction [117] is used for the chemiluminescence "titration" of O atoms (197). In the titration a gradu-

Table 19

Observed Emission Bands from the Reaction of O Atoms with Fluoroethylenes.

	Electronic Transition	Vibracional Band	Å	Intensity C_2H_3F	$C_2H_2F_2$	C_2HF_3
HCF	$\tilde{A}\,^1A'' \rightarrow \tilde{X}\,^1A'$	000-000	5786	VW	W	M
		010-000	5462	VW	W	W
		020-000	5182	VW	VW	W
		030-000	4929	EW	EW	W
		040-000	4704	-	EW	VW
CH	$A^2\Delta \rightarrow X^2\Pi$	0-0	4315	VS	S	M
	$B^2\Sigma^- \rightarrow X^2\Pi$	0-0	3889	S	M	-
C_2	$A^3\Pi_g \rightarrow X^3\Pi_u$	0-1	5635	M	-	-
		0-0	5165	S	M	W
		1-0	4737	S	W	W
?			6307	VW	VW	W
?			6030	VW	EW	
?			5915	EW	VW	W
?			5584	-	EW	W

S=Strong, M=Medium, W=Weak, V=Very and, E=Extrcmely

ally increasing flow of NO_2 is fed into the stream of the gas under investigation. As a result of reaction [117], the concentration of atomic oxygen decreases and that of NO increases. The intensity of the chemiluminescence, which is proportional to the product [O][NO], passes through a maximum. With a further increase in the flow of NO_2, the intensity of the chemiluminescence decreases sharply. The end-point of the titration corresponds to the complete disappearance of the chemiluminescence in the tube. At this point the flow of NO_2 is equal to the concentration of O atoms.

The oxidation of trifluoroethylene gives the strongest hydrogen fluoride emission while the reaction of the vinyl fluoride gives the weakest.

The emission spectra of the reactions of atomic oxygen with C_2H_3F, 1,1-$C_2H_2F_2$ and C_2HF_3 are given in Figures 37, 38 and 39. As can be seen, emission from the vibrational levels v=1, 2, 3 and 4 is observed from the reactions of trifluoroethylene and 1,1-difluoroethylene.

In order to calculate rotational populations, the same procedure was followed as with hydrogen. The area of the peaks representing the transition intensities are given in Table B8. The relative stationary-state population of the rotational levels with respect to $N_{v'=1,\ J'=2}$,

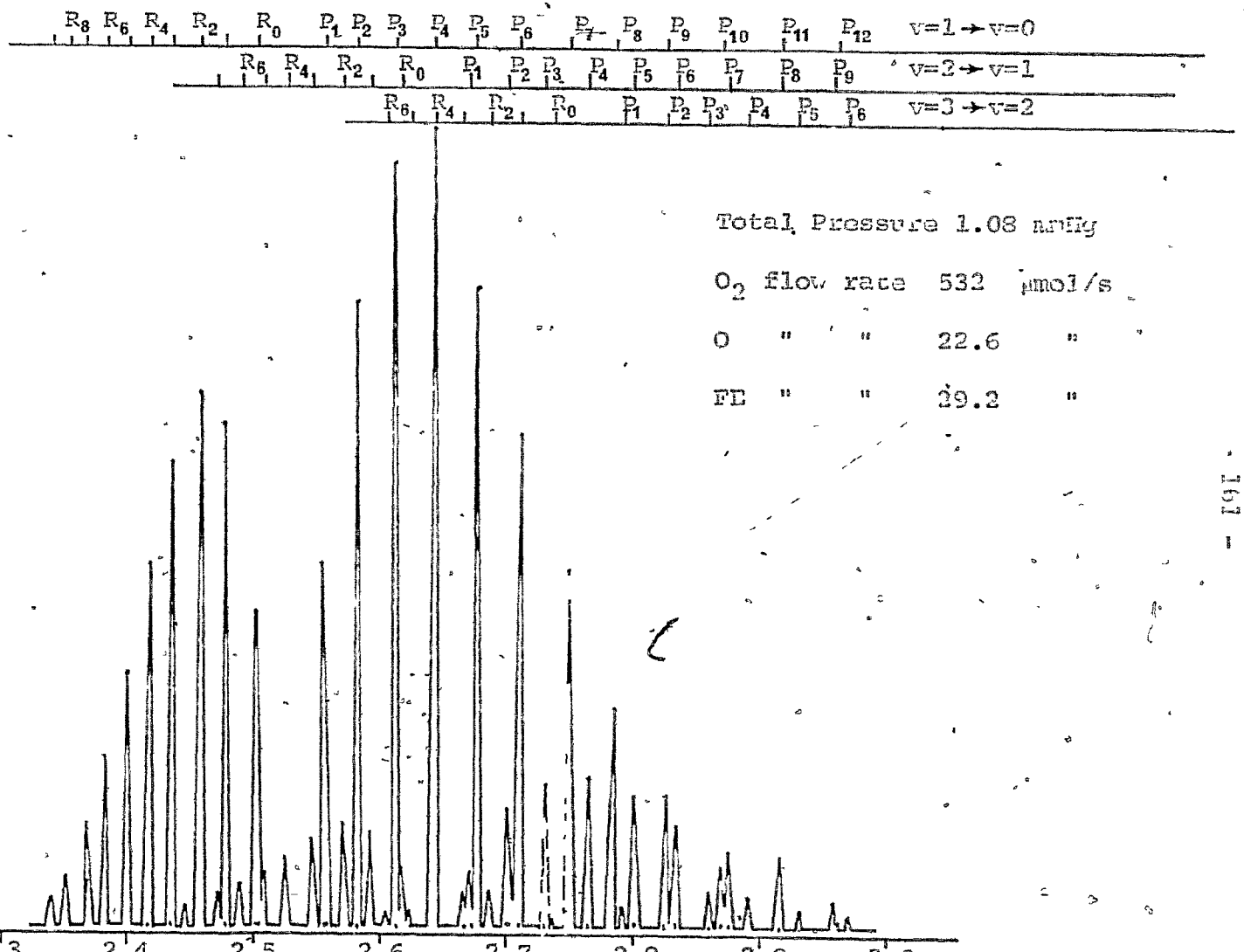

Fig. 37. The HF' ($\Delta v=1$) emission spectrum from the reaction of O atoms with C_2H_3F.

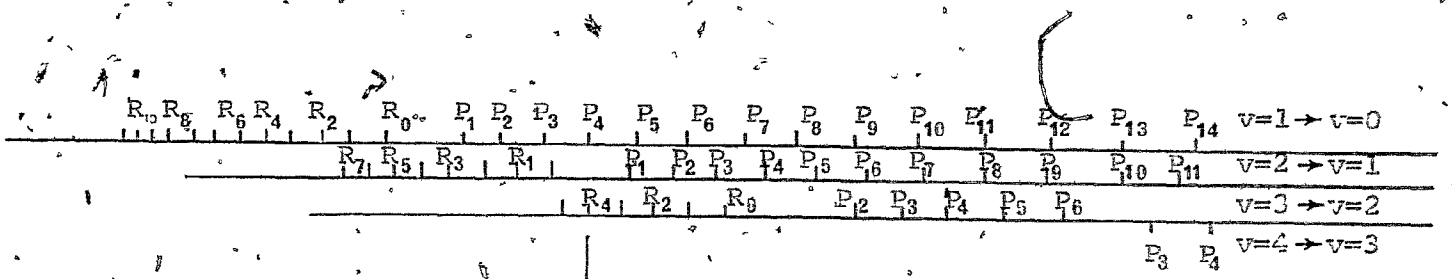

Total Pressure 1.08 mmHg

O_2 flow rate 532 μmol/s

O " " 22.6 "

FE " " 29.2 "

2.2 2.3 2.4 2.5 2.6 2.7 2.8 2.9 3.0 3.1 μm

Fig. 38. The HF (Δv=1) emission spectrum from the reaction of O atoms with 1,1-$C_2H_2F_2$.

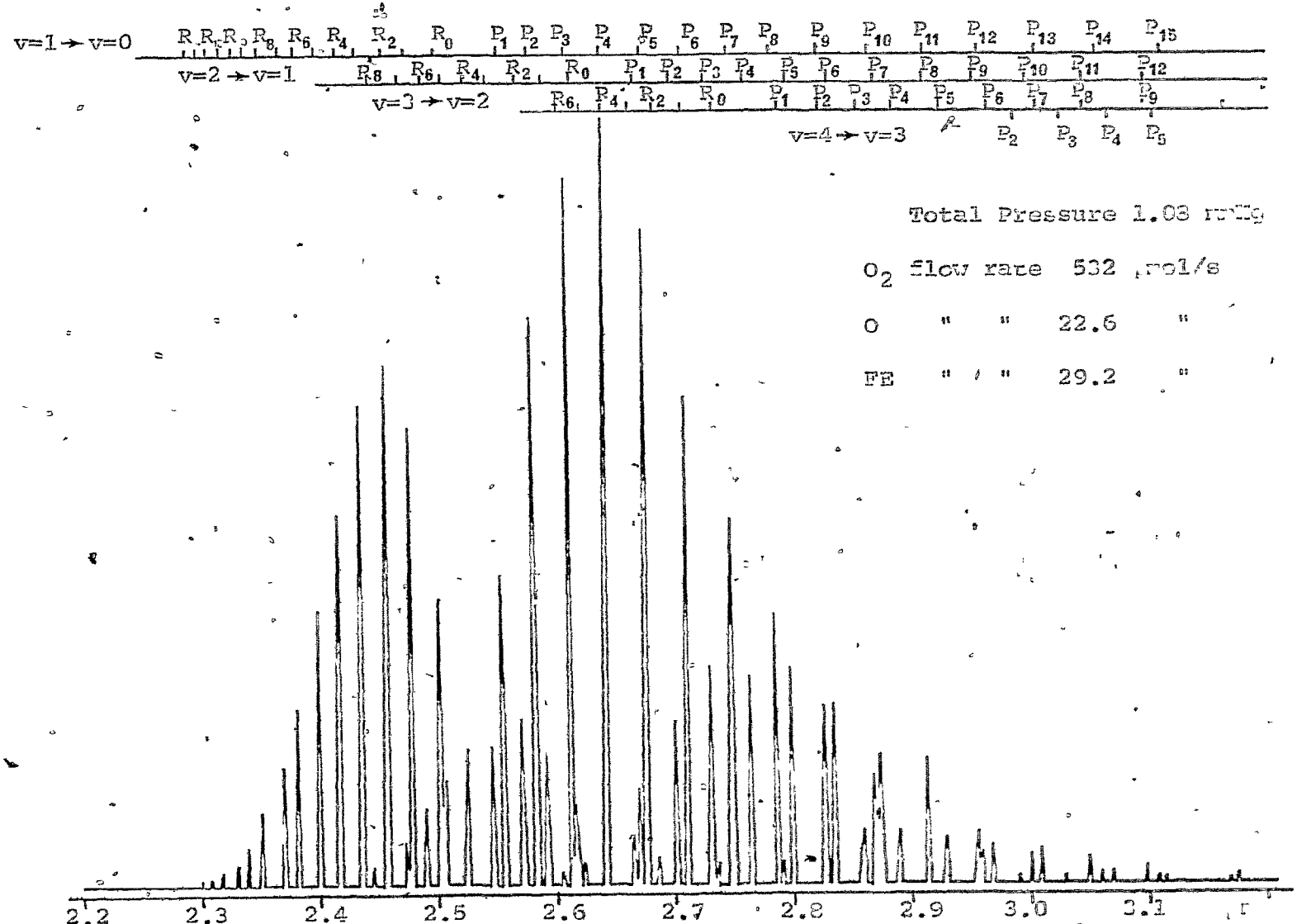

Fig. 39. The HF (Δv=1) emission spectrum from the reaction of O atoms with C_2HF_3.

were calculated according to equation [46] and the results are shown graphically in Figures 40, 41, 42.

$$N_{v'J'} \propto I^{v'J'}_{v''J''}(2J'+1)/\nu^4 S_J |M^{v'J'}_{v''J''}|^2 \qquad [46]$$

The values obtained for the relative populations of v=4 are poor since the intensity of the v'=4→v"=3 band is low and most of the lines overlap. In addition, the sensitivity of the detection system is low for wavelengths greater than 3 microns.

Rotational Boltzmann plots for the three fundamental bands are reproduced in Figures 43, 44, 45. Table 20 lists rotational temperatures taken from the slope of the lines in their linear region.

The stationary-state populations were calculated from the equation [61].

$$N_{v'} \propto \sum_{J'} N_{v'J'} \qquad [61]$$

For the vibrational level, v=4, the stationary-state vibrational population was estimated from the rotational population as being approximately one sixth of the population of the vibrational level v=3.

Vibrational Boltzmann temperatures were calculated from the relation [62].

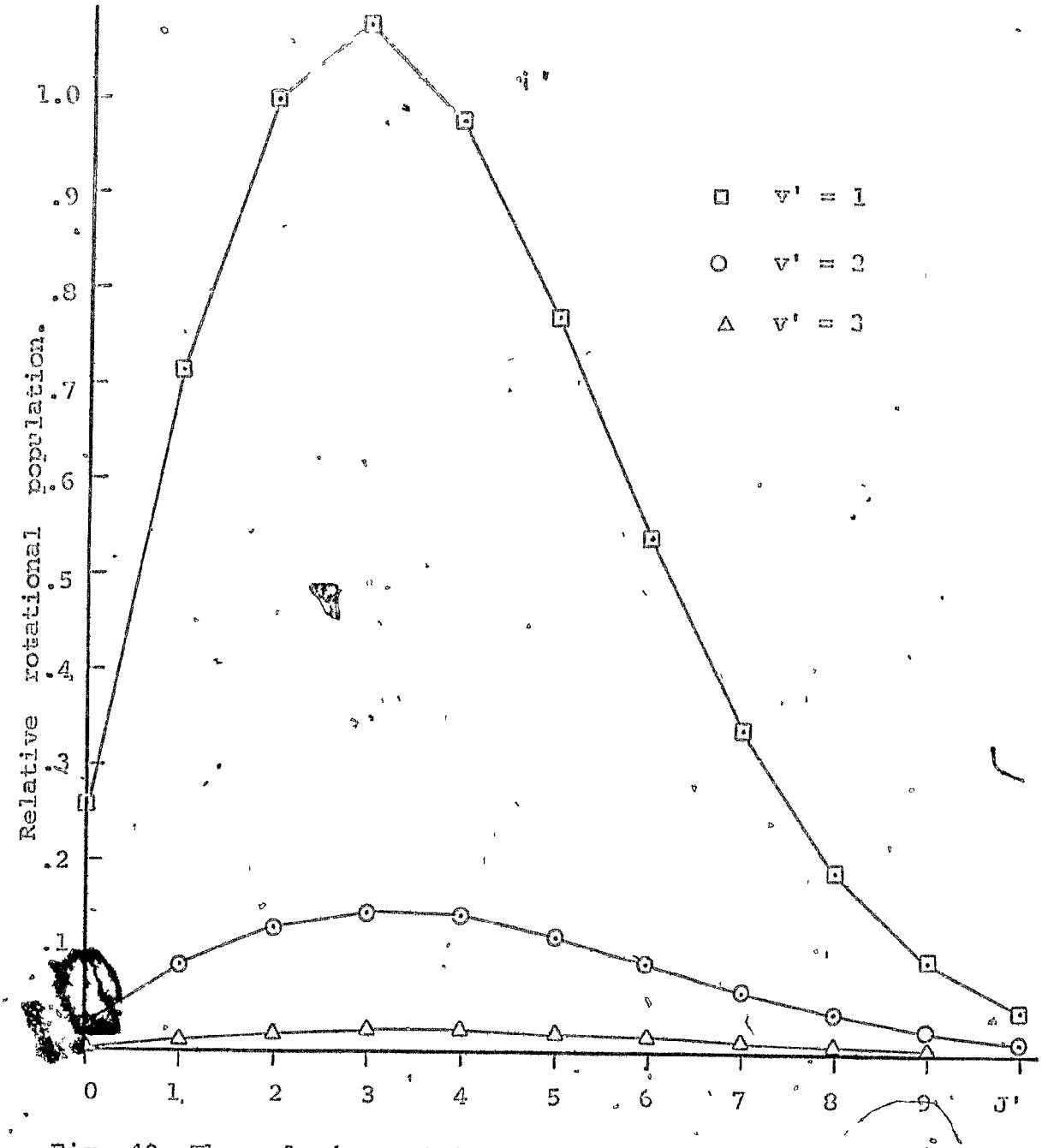

Fig. 40. The relative rotational population of HF from the reaction of O atoms with C_2H_3F.

F_2 Flow rate 533 μmol/s HF Flow rate 29.2 μmol/s

O " " 22.6 " Total Pressure 1.08 mmHg

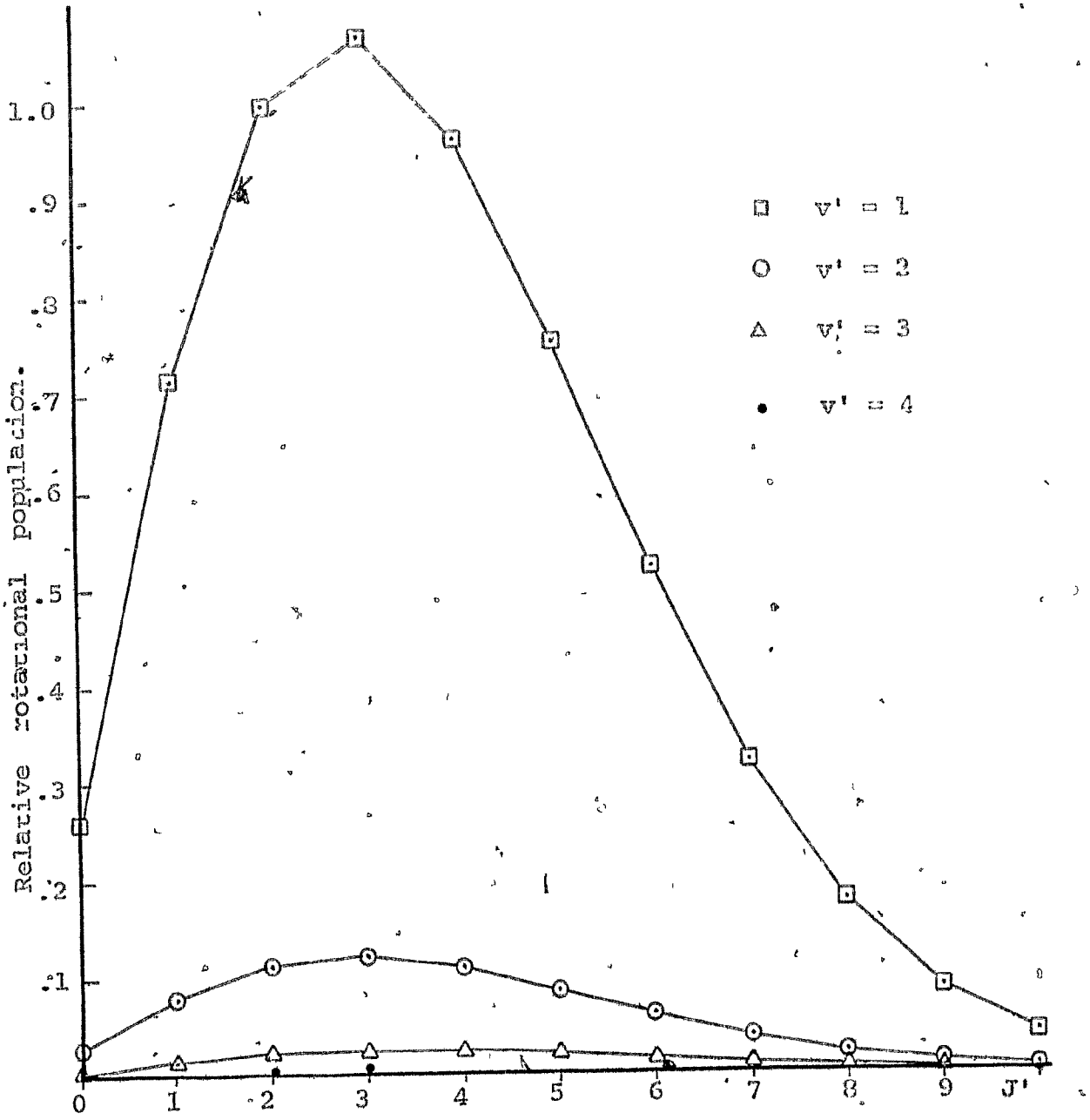

Fig. 41. The relative rotational population of HF from the reaction of O atoms with 1,1-$C_2H_2F_2$.

O_2 flow rate 532 μmol/s FE flow rate 29.2 μmol/s

O " " 22.6 " Total Pressure 1.08 mmHg

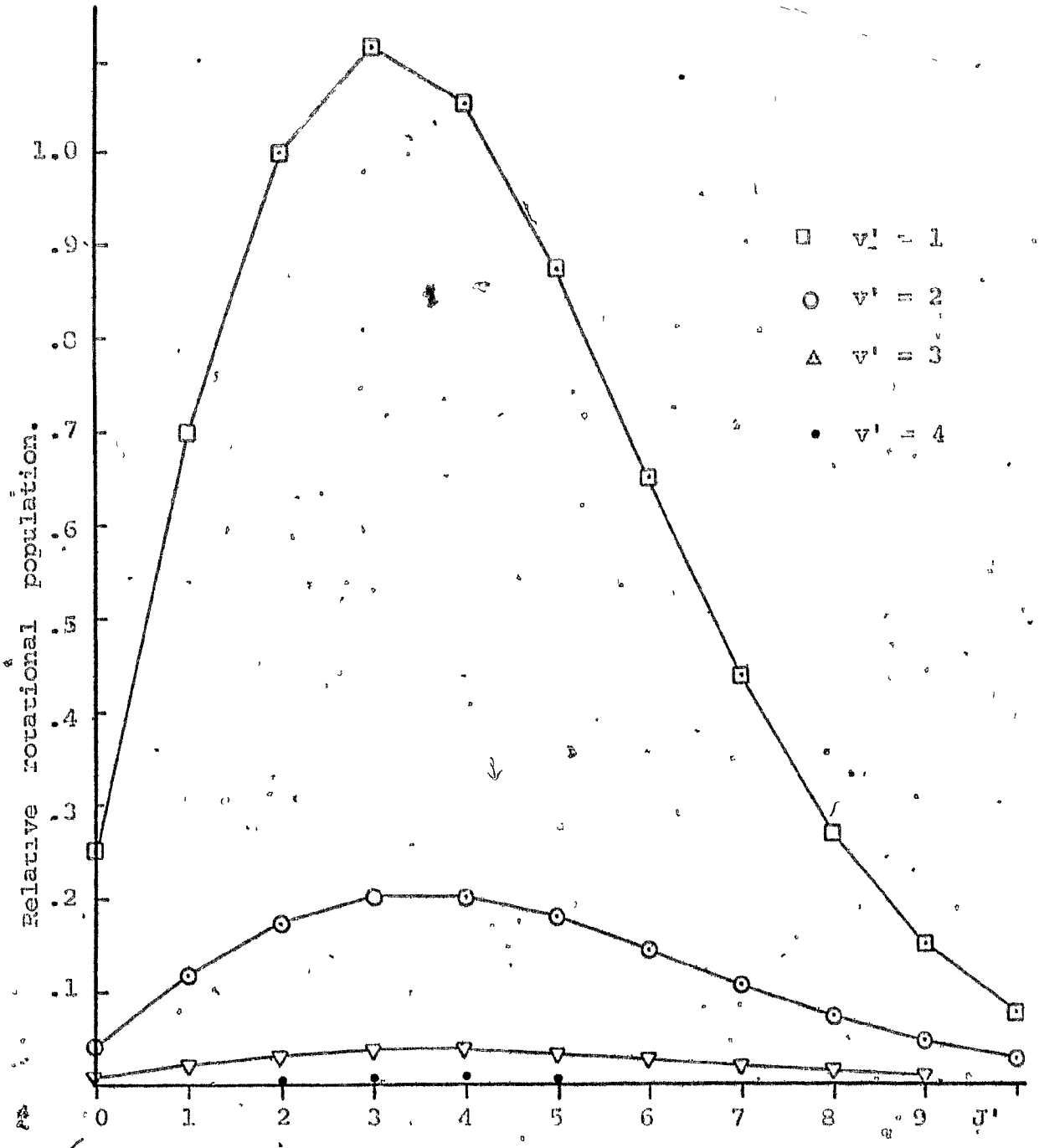

Fig. 42. The relative rotational population of HF from the reaction of O atoms with C_2HF_3.

O_2 flow rate 532 μmol/s FE flow rate 29.2 μmol/s

O " " 22.6 " Total Pressure 1.08 mmHg

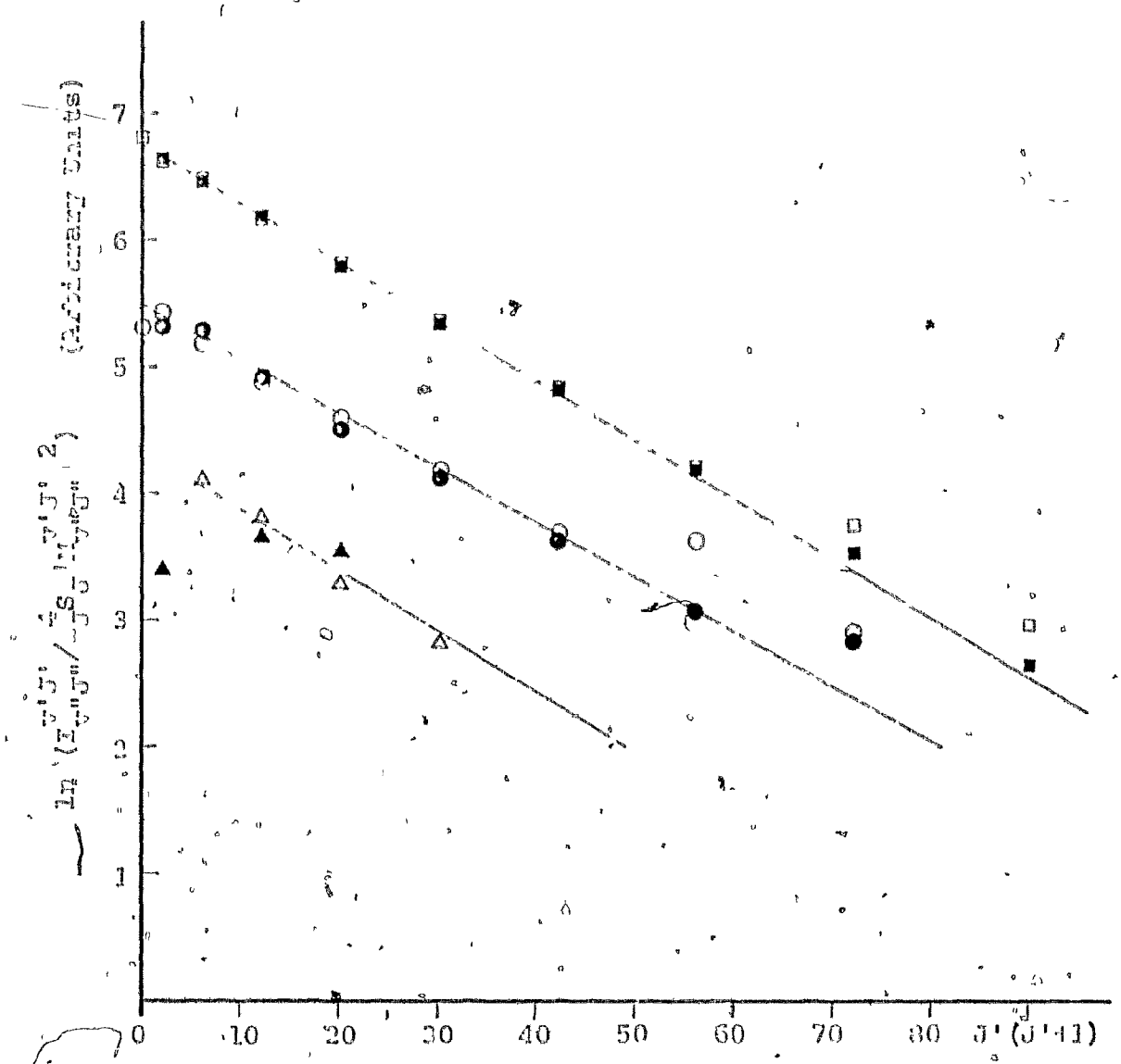

Fig. 43. Stationary-state distribution of HF among rotational states from the reaction of O atoms with C_2H_3F. □ from v(1-0), ○ from v(2-1), △ from v(3-2). Filled-in points from R branch lines, the remainder from the P branch.

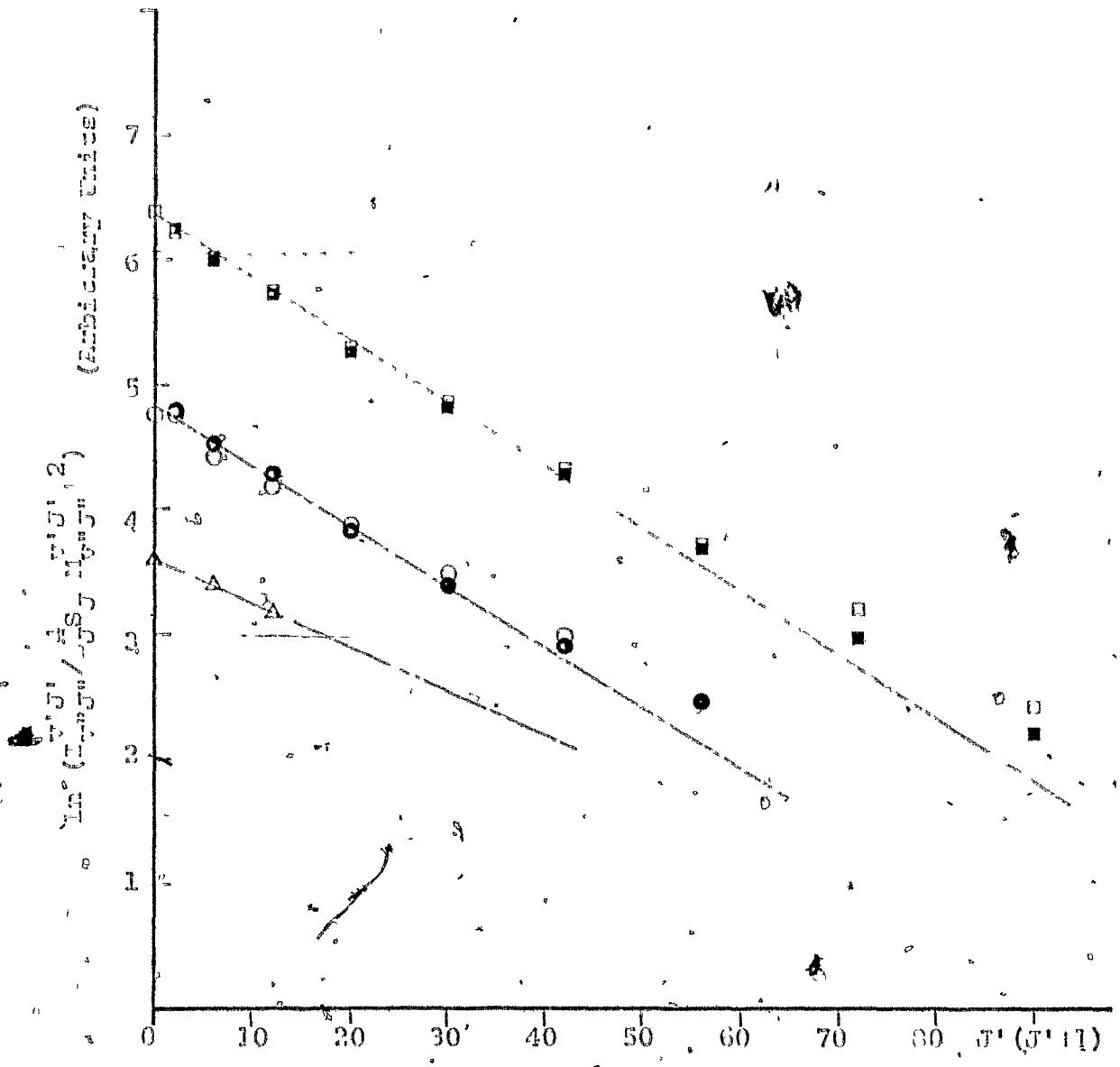

Fig. 44. Stationary-state distribution of HF' among rotational states from the reaction of O atoms with 1,1-$C_2H_2F_2$. □ from v(1,0); O from v(2-1), Δ from v(3-2). Filled-in points from R branch lines, the remainder from the P branch.

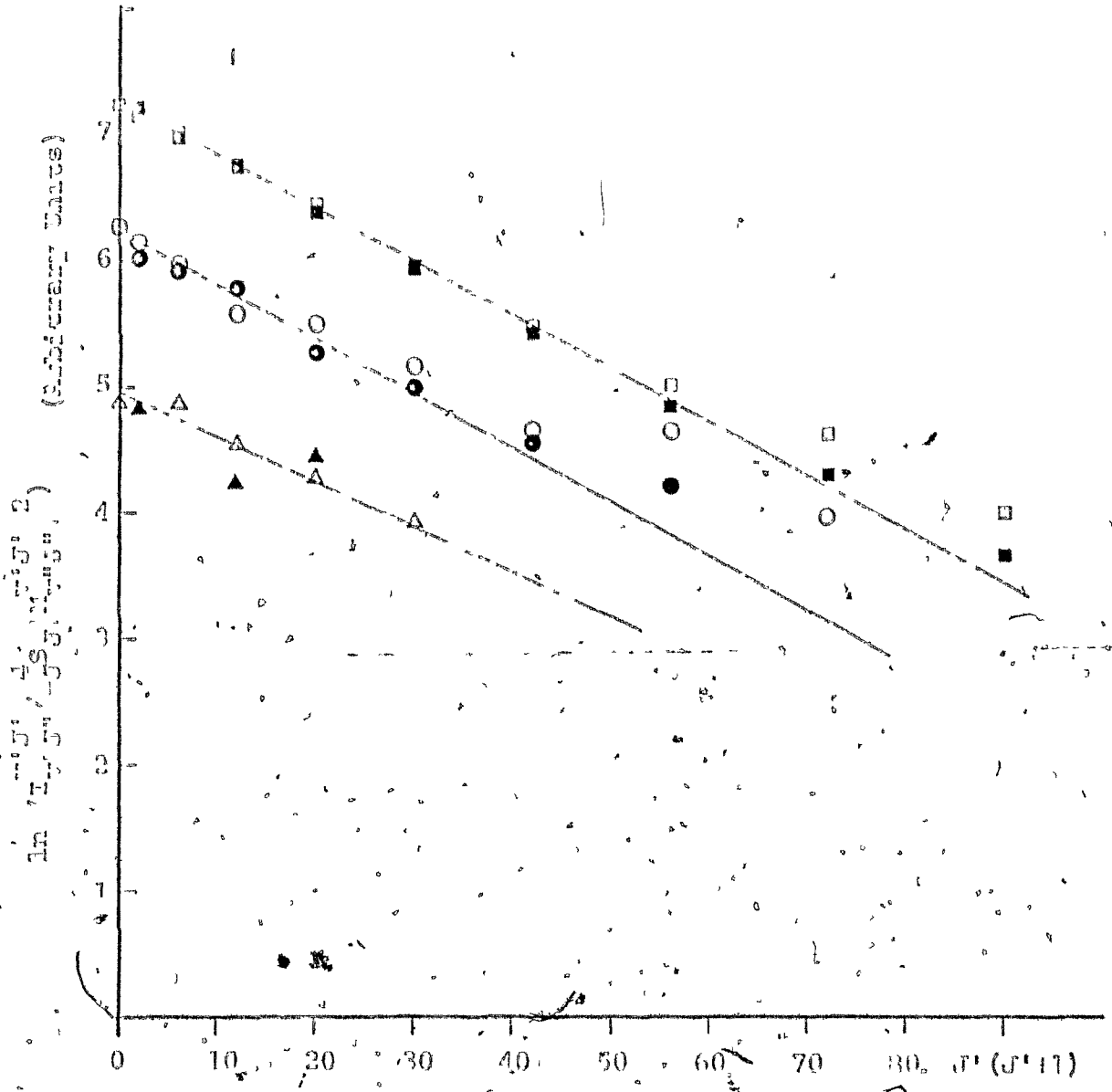

Fig. 45. Stationary-state distribution of HF' among rotational states from the reaction of O atoms with C_2HF_3. □ from v(1→0), ○ from v(2→1), △ from v(3→2). Filled-in points from R branch lines, the remainder from P branch

Table 20

Stationary-State Relative Vibrational Population for the Reaction of O atoms with Fluoroethylenes

O_2 flow rate 532 μmol/s, O flow rate 22.6 μmol/s, FE* flow rate 29.2 μmol/s

	N_1/N_1	N_2/N_1	N_3/N_1	N_4/N_1	P_2/P_1	P_3/P_1	R_4/R_1
C_2H_3F	1.	.152±.003	.027±.002		.21±.01	.057±.004	
T_{rot}	653±10	760±33	869±389				
T_{vib}		2897	2963		3541	3712	
$1,1\text{-}C_2H_2F_2$	1.	.117±.002	.027±.001	.005±.001	.15±.02	.046±.006	.012±.004
T_{rot}	639±10	639±16	734±15				
T_{vib}		2542	2954		3835	3465	
C_2HF_3	1.	.301±.005	.037±.001	.006±.001	.29±.02	.083±.009	.016±.005
T_{rot}	741±18	868±49	944±154				
T_{vib}		3400	3236		4405	4237	

* FE = Fluoroethylene

$$N_{v'} = (N/Q_v)\exp(-G_0(v)hc/kT_{vib}) \qquad [62]$$

The stationary-state vibrational populations and vibrational Boltzmann temperatures are given in Table 20.

In order to calculate the initial populations, the same relaxation model, with master equation [67], was used as in the case of atomic hydrogen. The probability of collisional deactivation of hydrogen fluoride for the v=1 level by molecular oxygen is given by Green and Hancock (131) as $P_{1,0(HF-O_2)} = 5.4\times10^{-5}$.

The calculated relative initial vibrational populations of hydrogen fluoride are given in Table 20.

2.3.3 Discussion.

Recently, Umstead, Lin and Woods observed HF laser emission from the reaction of atomic oxygen with vinyl fluoride and reported evidence that the lasing hydrogen fluoride was produced by the initial reaction (173). They also proposed that the vibrationally excited HF† is produced from the exothermic reaction

$$C_2H_3F + O \rightarrow [C_2H_3FO]^* \rightarrow CH_2CO + HF^\dagger \qquad [118]$$

It is a strong possibility that the hydrogen fluoride is a primary product of the reactions of atomic oxygen with 1,1-difluoroethylene and trifluoroethylene since, the HF' emission of these two reactions is much stronger than from the reaction with vinyl fluoride.

This is also supported by the fact that the experimental vibrational population for the v=2 vibrational level for the reactions of trifluoroethylene and 1,1-difluoroethylene, relative to the vibrational level v=2 for the reaction of vinyl fluoride, agrees with the relative total rates of the reactions calculated from products analysis (Table 21).

Table 21

Comparison of the Relative Vibrational Population for Level v=2 to the Total Rates of the Reaction of Atomic Oxygen with C_2H_3F, 1,1-$C_2H_2F_2$ and C_2HF_3 relative to C_2H_3F.

Fluoroethylene	R_2/P_1[a]		$k/k_{C_2H_3F}$	
	This work	Jones[b] et al	Huie et al[c]	Gutman[d] et al
C_2H_3F	1.	1.	1.	1.
1,1-$C_2H_2F_2$	0.71	0.52	0.83	0.76
C_2HF_3	1.38	1.39	-	2.02

[a] Corrected for radiational and collisional relaxation.
[b] ref 191. [c] ref 190. [d] ref 168.

Gutman and coworkers (168) have proposed the scheme given in Section 2.3.1 for the reactions of atomic oxygen with fluoroethylenes. Furthermore they assigned reactive routes for the reactions which are in agreement with the products they detected by using photoionization mass spectrometry. These routes and the products detected by other workers are given in Table 22.

The main route

$$O + 1,1\text{-}C_2H_2F_2 \rightarrow [C_2H_2F_2O]^* \rightarrow C_2HFO + HF \qquad [119]$$

seems to be responsible for the excited hydrogen fluoride from the reaction of 1,1-difluoroethylene with atomic oxygen ($\Delta H = -43$ Kcal/mol). The C_2HFO is formed from 1,2-elimination from the oxygen adduct.

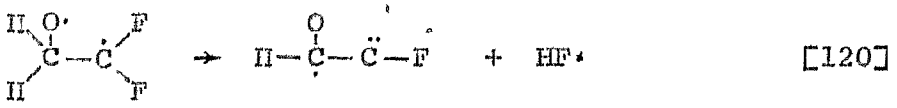

[120]

The radical 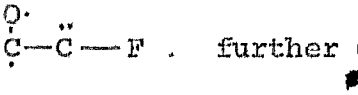 further gives 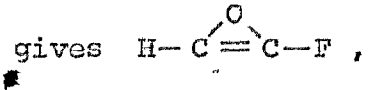 , which is assumed to be an unstable intermediate, or, ketene, which results from migration of hydrogen atom.

Gutman and coworkers (168) found CF_2 to be one of the main products of the reaction of atomic oxygen with trifluoroethylene. They suggested as the main route, the reaction [121] which is very exothermic

Table 22

Products Detected from the Reaction Routes Assigned for the Reactions of O Atoms with C_2H_3F, 1,1-$C_2H_2F_2$ and, C_2HF_3.

	Reaction Route	Products Detected by Gutman[a] et al	Other Products
C_2H_3F	CH_3+CFO (CO+F)	CH_3	
	CH_2F+CHO	CH_2F, CHO	
	C_2H_2O+HF	C_2H_2O	HF[b]
	C_2HFO+H_2	C_2H_2FO	CHFO[c], CH_2O[c], HCF[b]
1,1-$C_2H_2F_2$	CHF_2+CHO (CO+H)	CHF_2	
	C_2HFO+HF	C_2HFO	CF_2O[c], CF_2[d], CH_2O[c,d], HCF[b], HF[b]
C_2HF_3	CF_2+CHFO (CO+HF)	CF_2	CHFO[c]
	CHF+CF_2O ($CO+F_2$)	CHF	CF_2O[c]
			HCF[b], HF[b]

[a] Ref 168

[b] This work.

[c] Ref 190

[d] Ref 187

$$O + C_2HF_3 \rightarrow \begin{matrix} H & O & & F \\ & C & C & \\ F & & & F \end{matrix} \rightarrow CF_2 + CHFO \ (CO+HF) \qquad [121]$$

(ΔH= -82.3 Kcal mol) and can explain the observation of vibrationally excited hydrogen fluoride in our experiments. The fact that we did not see vibrationally excited CO is another indication that in four center eliminations the energy is trapped by the newly formed bond and is not able to perturb the already existing bond as discussed in the Introduction.

The second route (168) of this reaction (ΔH= -70 Kcal/mol) is

$$CHF=CF_2 + O \rightarrow \begin{matrix} H & O & F \\ & C-C & \\ F & & F \end{matrix} \rightarrow CHF^* + CF_2O \qquad [122]$$

Since the reaction [122] has 70 Kcal/mol exothermicity, this route can explain the observation of electronically excited CHF (60.7 Kcal/mol are needed for electronic excitation of CHF to the vibrational level 040).

Although a minor route in the reaction of atomic O with vinyl fluoride gives as product HCF, there is not

$$O + CH_2=CHF \rightarrow \begin{matrix} O \\ CH_2-CHF \end{matrix} \rightarrow CH_2O + CHF \qquad [123]$$

sufficient energy (ΔH= -29 Kcal/mol) for electronic

excitation. The situation is similar in the reaction of atomic oxygen with 1,1-difluoroethylene. One route is the decomposition of the radical product of the reaction [120] to HF and CO. The other route is the 1,2-elimination of HF from the CHF_2CHO and further decomposition of the radical. (The CHF_2CHO is an intermediate of a main route

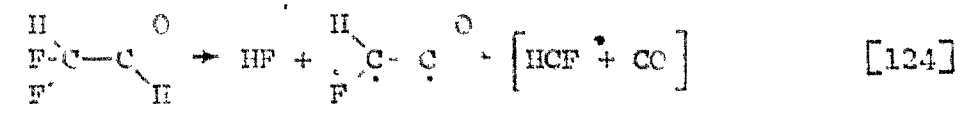

[124]

of the reaction (168)).

The exothermicity of these reactions (ΔH for [124] is -43 Kcal/mol) is not sufficient to explain the formation of electronically excited HCF.

There is no other simple route giving electronically excited HCF* as a primary product. Electronically excited HCF* can be formed as a secondary product of the reaction

$$F + CH \longrightarrow HCF^* \qquad [125]$$

(ΔH= -131 Kcal/mol).

Since, in all the reactions CH is present and the stationary state concentration of F should be larger for trifluoroethylene than for vinyl fluoride, this agrees with the observation that HCF* emission is stronger for trifluoroethylene and weaker for vinyl fluoride. The

reaction is why has HCF not been observed previously in emission since in studies of the flame inhibition (198) by halocarbons, fluorocarbons are used and CH is always a product of oxidation of hydrocarbons (198, 199).

Many reactions have been proposed for the formation of CH but not all of them are exothermic enough to give electronically excited CH (200, 201). The most probable one is the reaction [126] (H= -92 Kcal mol).

$$C_2 + OH \longrightarrow CH^* + CO \qquad [126]$$

There have been many suggestions for the formation of C_2^* but usually these reactions are very complicated since the heat of formation of C_2 is ΔH_f = 199 Kcal/mol and around 70 Kcal/mol is required for electronic excitation .

From the rotational Boltzmann plots (Fig. 44, 45), it seems that for higher J', there is an excess of rotators in the vibrational levels. This excess of rotational population may be a residue of an even larger excess present when HF was originally formed. The temperature in the reaction zone was 340-360 K measured by a thermocouple, the same as in the reaction of atomic hydrogen and nitrogen. However, from the slope of the rotational Boltzmann plots, the rotational temperature

is much higher, approximately 700±100 °K. The same has been observed for the reaction of atomic hydrogen with chlorine in the 1-2 mm pressure range and the explanation given by Polanyi was that at higher pressure, a larger amount of energy enters directly into the rotational levels (see Introduction).

The rotational excitation favors a mixed type of energy-release for the reactions of atomic oxygen with the fluoroethylenes on a repulsive surface.

3. EXPERIMENTAL

3.1 Apparatus.

3.1.1 Reaction System.

The experiments were performed in a fast flow vacuum system. A diagram of the apparatus is shown in Fig. 4b.

Hydrogen, oxygen or, nitrogen were admitted to the system through line A. Hydrogen or, nitrogen was supplied from a cylinder and passed through a Deoxo unit catalytic purifier CP and a liquid nitrogen trap NA to remove H_2O and CO_2. In the case of oxygen, the liquid nitrogen trap was replaced by a silica gel trap immersed in dry ice-acetone SA. Each gas was admitted to the reaction system through an adjustable manostat MA containing dibutyl phthalate. The level of the liquid could be varied so that the gas was always kept at constant pressure despite fluctuations in atmospheric pressure. A constant pressure was necessary in order to maintain a constant gas flow rate. The 60 cm height of the manostat could accomodate a change in atmospheric pressure of 40 mmHg. On leaving the manostat, the gas entered system FA through the stopcock S3.

This system consisted of a flask KV of volume 1108.66 cc, a manometer PA and, a micrometer needle valve VA. The

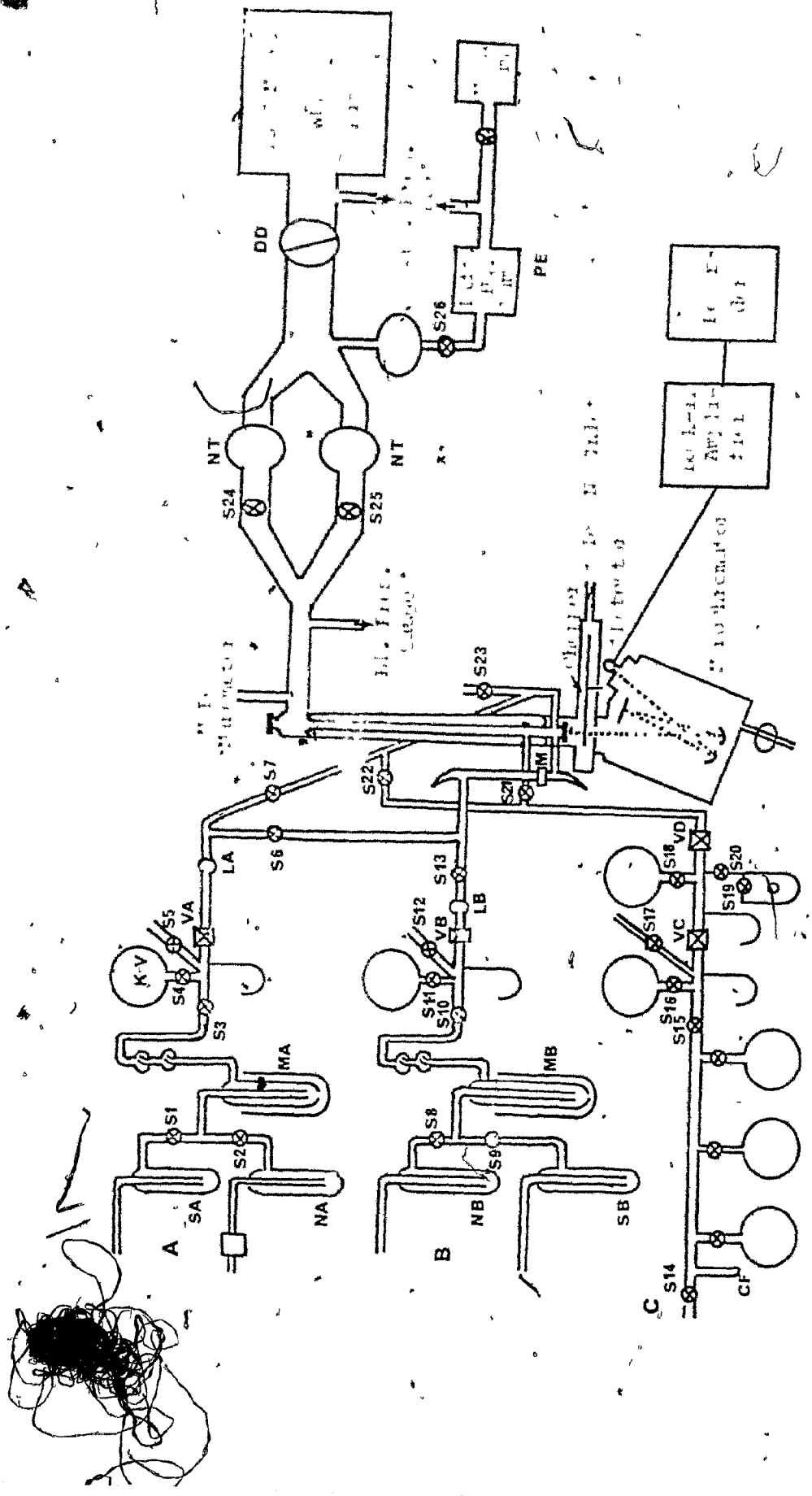

Figure 46. Gas Handling System

total volume of the portion FA was 1293 cc.

The gas flow rate, determined from the rate of evaluation of system FA, was controlled by the micrometer needle valve VA. Finally, the gas was directed through another liquid nitrogen trap LA and into the microwave discharge region M.

Flow system B, similar in all respects to system A, was used to admit an inert gas diluent. Argon or helium was used with hydrogen, while argon was used with nitrogen. Helium passed through a liquid nitrogen trap NB, while argon passed through a silica gel-molecular sieve trap SB immersed in dry ice-acetone before entering the system through the manostat MB. The volume of the system FB used for measuring the flow rate was 729.7 cc.

From the measuring system FB, the inert gas passed through a liquid nitrogen trap LB and then mixed with the reactant gas. The resulting mixture was activated in a microwave discharge M.

The microwave generator in the case of hydrogen was a Burdick Corp. Milton Model No MW/200 with power output of 200 watts. For nitrogen and oxygen a research type microwave discharge generator KIVA model with an output of 100 watts was used. Of several cavities tried, the Evanson silver plated type was found to cause the least

disturbance to the detector electronics. At first, pyrex glass was used at the region of the microwave discharge but was later replaced by quartz to avoid pinholes caused by the discharge.

The handling system for the fluoroethylenes consisted of a cold finger CF and three storage flasks each having a volume of 5 l. The fluoroethylenes entered system PC and FC similar to FA and FB. Since the pressure in the storage flasks decreased continously during a run, PC acted as a manostat connected to system FC through a micrometer needle valve VC. By manipulating valve VC, the pressure in FC was kept constant at 100 mmHg.

The flow rate of fluoroethylene was adjusted by the micrometer needle valve VD. The pressure in the system FC was determined accurately with an oil manometer O.

Another gas flow control system similar to system A but not shown in Fig. 46 was attached at S_{23}. This system was used to admit NO_2 to the reaction vessel to allow titration of the oxygen atoms. The same system was used to admit HF to the reaction cell for test reactions.

The pumping system shown in Figure 46 consisted of two parallel vacuum lines. Each line contained a 10 mm stopcock, S_{24}, S_{25} and, a large liquid nitrogen trap NT. The two lines led to a 2" diameter tube which was connec-

led through a 3" diameter inlet to a Model 1386 Welch pump (2000 l min) An auxiliary vacuum line PE parallel to the main vacuum line led to a mercury diffusion pump (90 l min) which worked continuously to maintain a vacuum in the system at all times.

3.1.2 Reaction Cell.

The reaction cell was of a Dewar type, constructed as shown in Figure 47 with calcium fluoride windows. It was prepared from pyrex tubing. The fluorocompound was introduced either through four jets situated around the reaction tube (A) or, through an inlet opposite to the hydrogen inlet B. In the former case, the discharge was about 15 cm away from the mixing region while in the latter, the discharge was about 10 cm away from the mixing region. Atoms produced in the microwave discarge entered the reaction zone through a small orifice, C, 3 mm in diameter which prevented back diffusion of the fluoroethylene to the discharge region. The walls of the cell were poisoned with concentrated phosphoric acid to prevent recombination of the atoms. A Chromel-Alumel thermocouple, D, was used for temperature measurements and the EMF produced was measured by a DANA Model 5000 digital voltmeter.

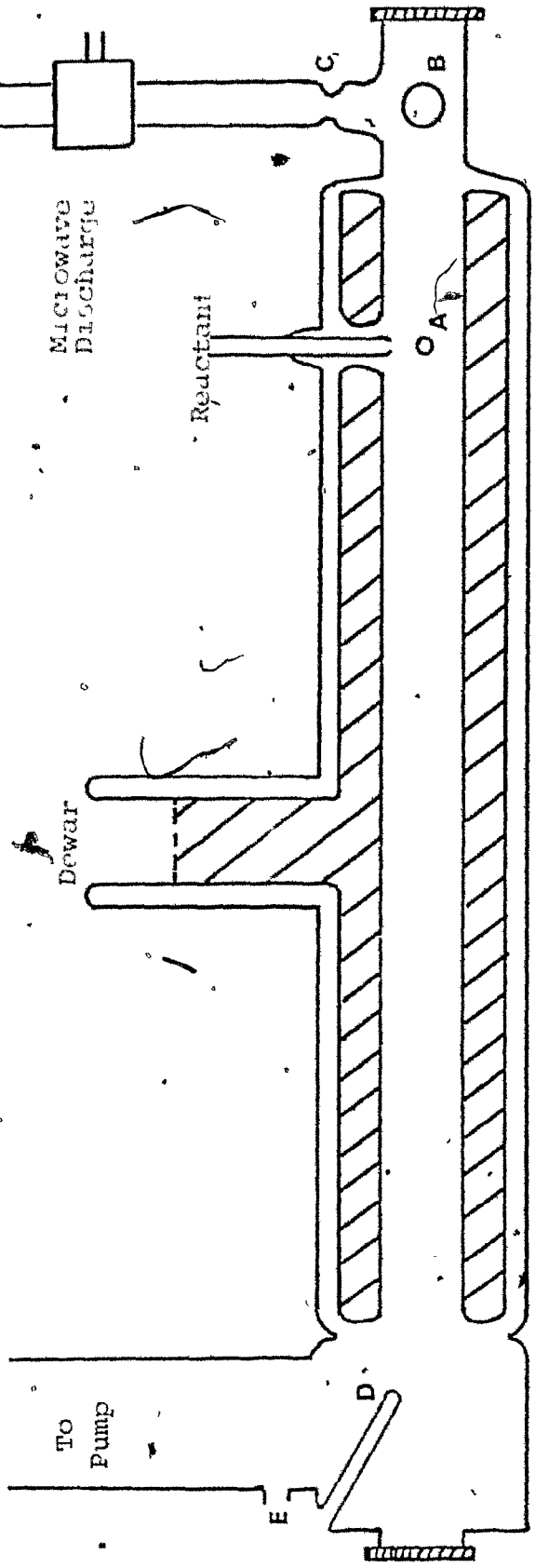

Fig. 47. Diagram of the Reaction Cell.

A McLeod gauge was used for pressure measurements at position E.

3.1.3 Detection System.

The IR emission from the reaction zone passed through a calcium fluoride window, a chopper operating at 820 Hz and into the Model 218, 0.3 m Mac-Pherson monochromator equipped with a 300 lines/mm grating blazed at 2 microns. A 0.3 mm slit was used for the reaction of H atoms with fluoroethylenes, a 0.5 mm slit for the reaction of active nitrogen and a 0.28 mm slit for the reactions of oxygen atoms. The IR emission from the exit slit of the monochromator was focused on the detector by means of the optical system shown in Figure 48. An Infrared Industries type B dewar containing the detector could be sealed in this system with O-rings. A front surface gold mirror, focal distance 9.5 cm, was employed in the system. The mirror was mounted on an Abbe optical system to allow focusing of the IR emission on the detector. The Abbe system was mounted on a translational stage C so that the emission could be made to fill the detector.

For these experiments a dry ice-acetone cooled PbS detector was used with a 0.005 cm^2 area (A). It was

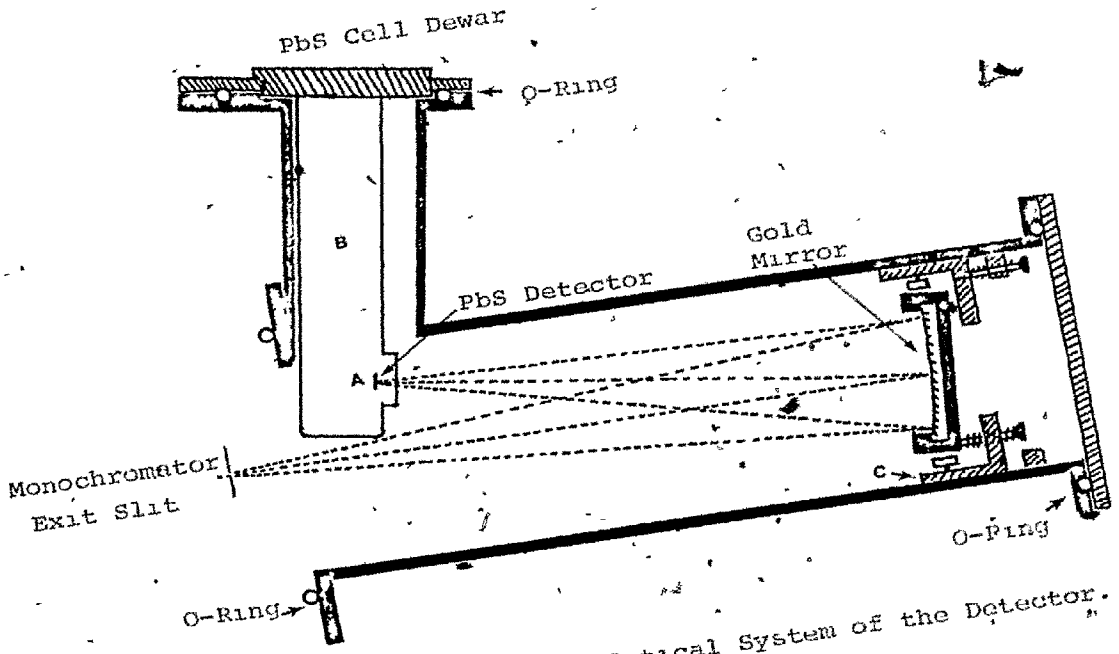

Figure 48. Optical System of the Detector.

operated with a total bias voltage of 40 V and a load resistor of 300 kΩ.

The signal from the detector was monitored by a phase sensitive PAR Model 128 lock-in amplifier and fed into a Beckmann 10" recorder.

The entire optical path was flushed with dry nitrogen purified in a molecular sieves - silica gel trap and a liquid nitrogen trap. Another liquid nitrogen trap was placed in the outlet and the outlet tube was immersed in dibutyl phthalate for preventing air from getting back into the system.

This assembly permitted spectral studies in a region of 2.0-3.2 microns. In this region, the sensitivity of the system is non linear as a result of the response of the detector and the reflectivity of grating. A black-body, described in Section 3.2, was therefore constructed for the calibration of the detection system. The relative sensitivity of the detection system with respect the $P(3)(v'=1 \rightarrow v''=0)$ transition is plotted vs the wavelength in Figure 49.

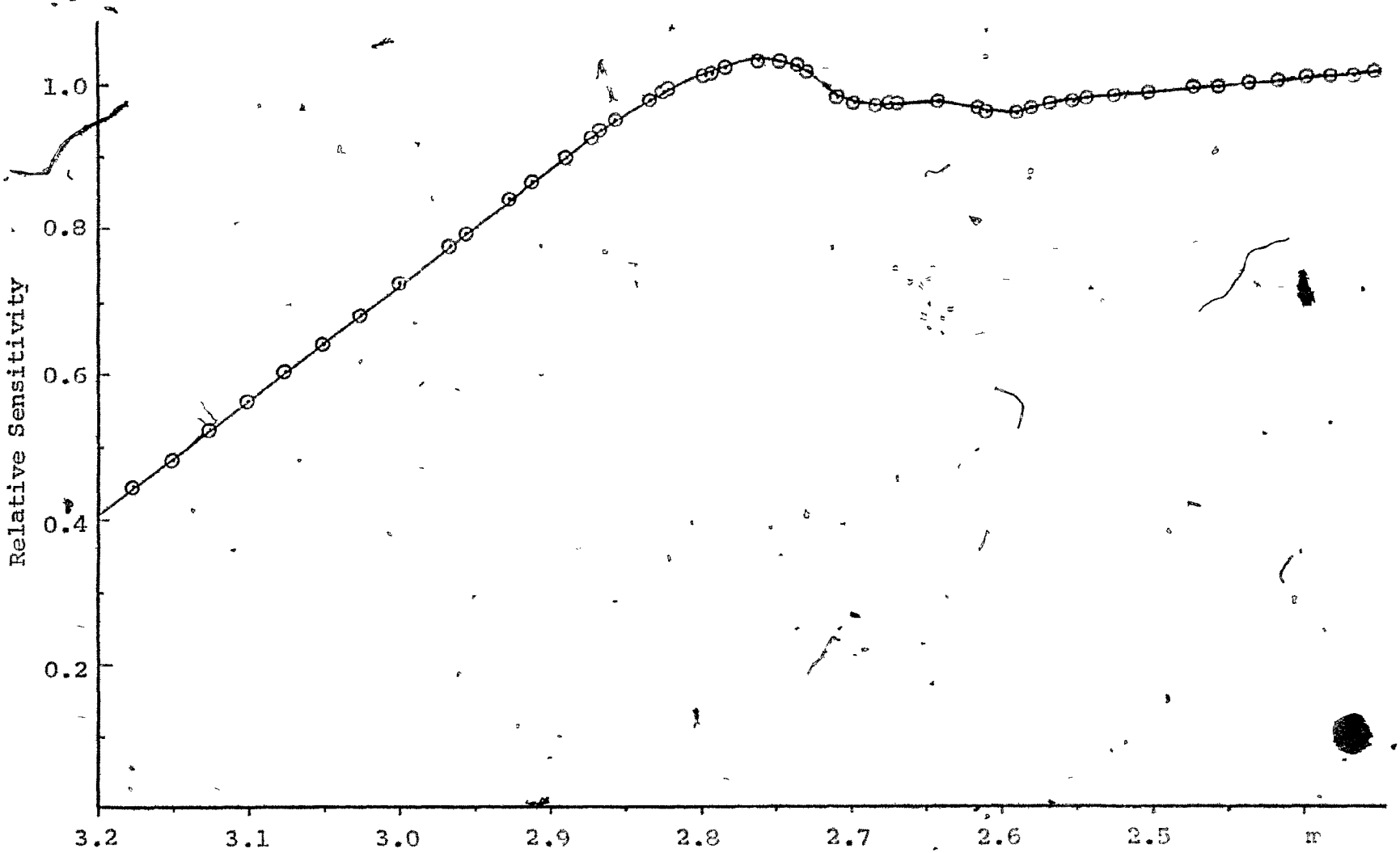

Fig. 49. Sensitivity of the Detection System Relative to the $P(3)_{v'=1\ v''=0}$ line of HF.

3.2 [illegible]

The blackbody source for calibration of the detection system was constructed on the principle given by Smith, Jones and Chasmar (S'J'C). It consisted (Fig. 50) of a cylindrical steel slug (A) 3½" long and 1" in diameter. The slug contains a conical recess (B) 2¼" deep and ½" in diameter. The angle subtended by the cone is 30 degrees. A second recess, (C) 2"deep and 0.2" in diameter in the opposite end, allows space for two thermocouples (D) one, for temperature measurements and the second for temperature regulation. The thermocouples are Chromel-Alumel, silver joined in a porcelain slug. The heating wire is coiled around the steel slug in antiparallel configuration to cancel self-induction phenomena. The wire is inside porcelaine beads (E) and covered with heat resistant porcelaine paste. In order to avoid radiation losses, it is wrapped in aluminum foil (F). A steel mirror (G) and a pyrex first surface silver mirror prevent further heat losses. In front of the recesses there are asbestos buffles (J).

A stainless steel round block (K) containing a ¼" diameter hole closes the black-body cavity and acts as

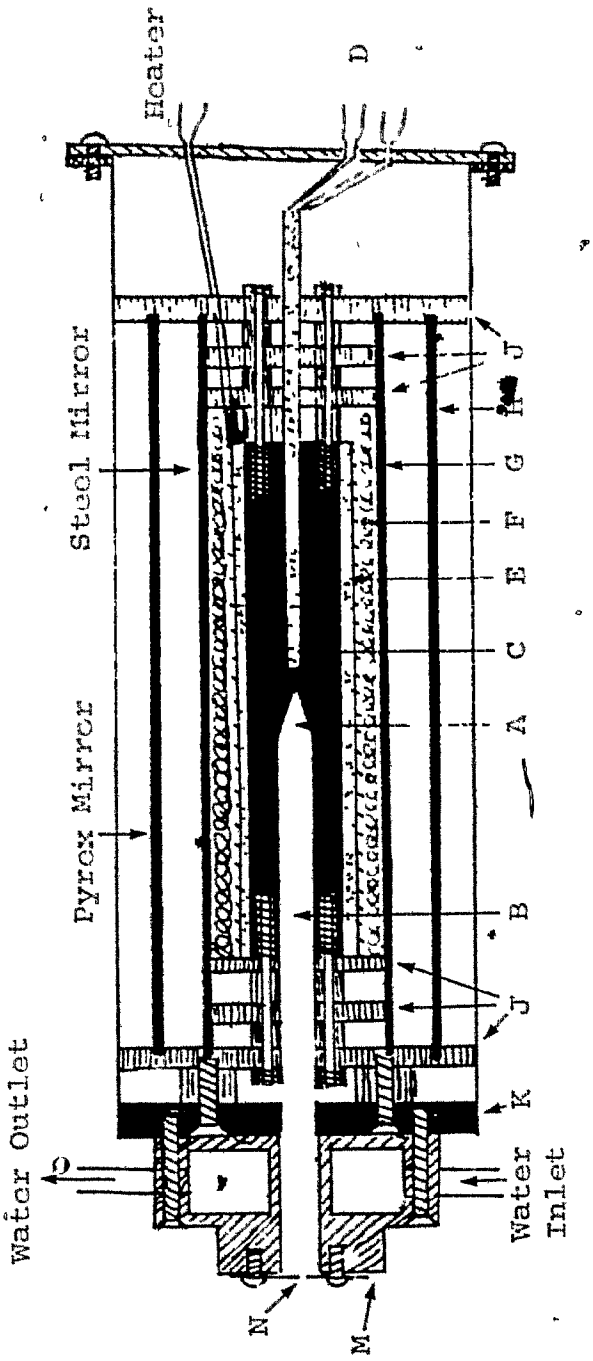

Fig. 50. Diagram of the Black-Body.

an exit for the radiation. The inside surface of the block is polished to reflect the radiation.

On the outside surface of the block there is an aluminum mantle (M) on which an aperture (N) can be attached in line with the axis of the black-body cavity. Water passes through the aluminum mantle in a closed circulation system to keep the aperture at room temperature. The mantle is constructed so as to fit exactly into the chopper in the same manner as the reaction cell and such that the exit port of the black-body lines up with the entrance slit of the monochromator. The mantle is necessary to prevent detection of radiation other than that from the cavity of the black-body.

In operation, the steel cavity becomes quickly covered with a layer of black oxide which has an emissivity better than 0.99. The temperature of the black-body can be varied from 400 to 1000 K. A block circuit diagram of the black-body controls is given in Figure 51.

A reference potential provided by RP determines the operational temperature of the black-body. The actual black body temperature is continously monitored with the thermocouple sensor. The voltage of the thermocouple is amplified through preamplifier (A1) and is fed together with the reference voltage, set by the poten-

AMPLIFIER CIRCUIT

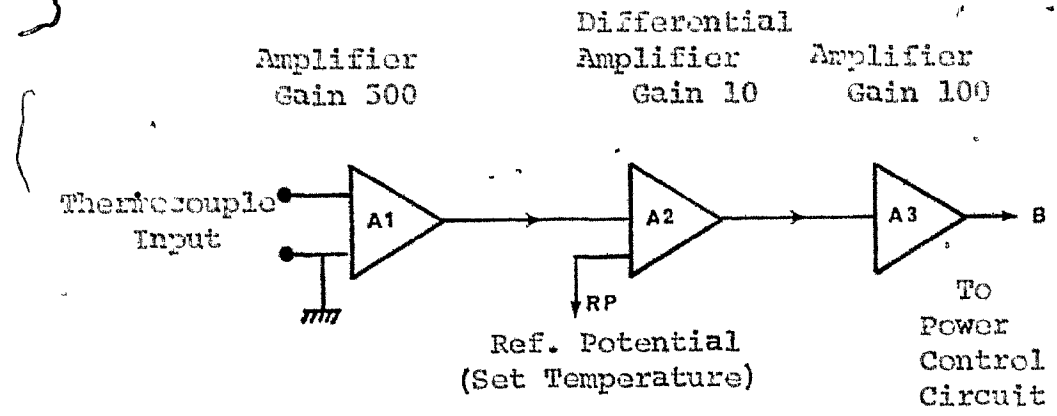

CONTROL CIRCUIT

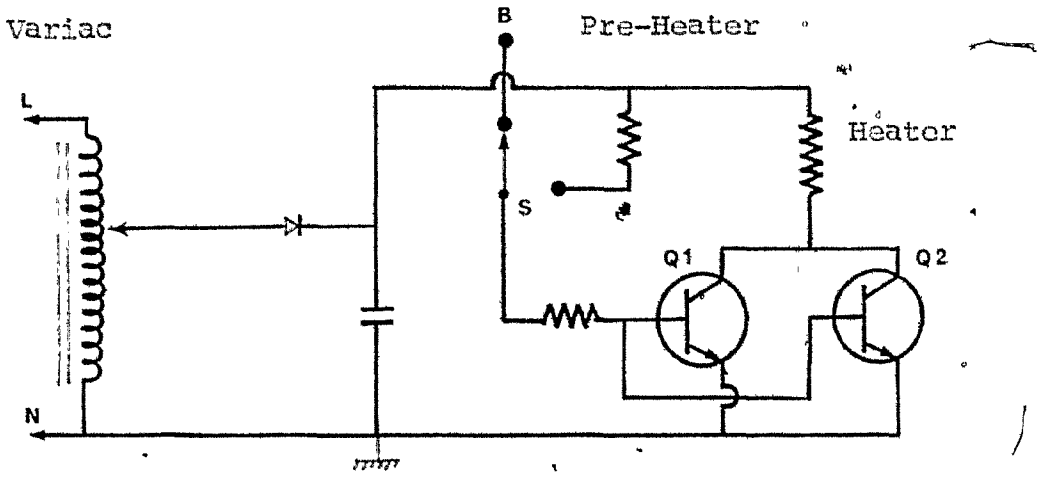

Fig. 51. Block Diagram of the Black-Body Control Circuit.

ticmeter (PP), to the differential amplifier (A2). The difference of these two voltages is amplified and fed to the bases of the power transistors Q1 and Q2 which supply the current for the heater. The EMF produced by the thermocouple in the black-body is measured by a DANA Model 5000 digital voltmeter and provided an accurate indication of the black body temperature.

3.3 - Phototransistor Device for Flow Rate Measurements.

This device was constructed to measure pressure changes in a mercury manometer as a function of time (dp/dt).

It was constructed from a block of "TUFNOL" 6x4.5x2 (cm) and could be fastened on a mercury manometer of 6 mm o.d. Figure 52a shows a cross section of the apparatus. A is the 6 mm o.d. mercury manometer which was passed through the block as shown. Seven holes (0.04" diam.) were drilled 0.5 cm apart in line with the mercury manometer and crossing it at right angles. At one side of each hole hole was a phototransistor (C) while the filament W of a tungsten lamp (D) placed at the opposite side of the block illuminated each hole. Each phototransistor was adjusted by the resistor (R) to give about 1 mV when exposed to the light. The output was connected to a 10 mV

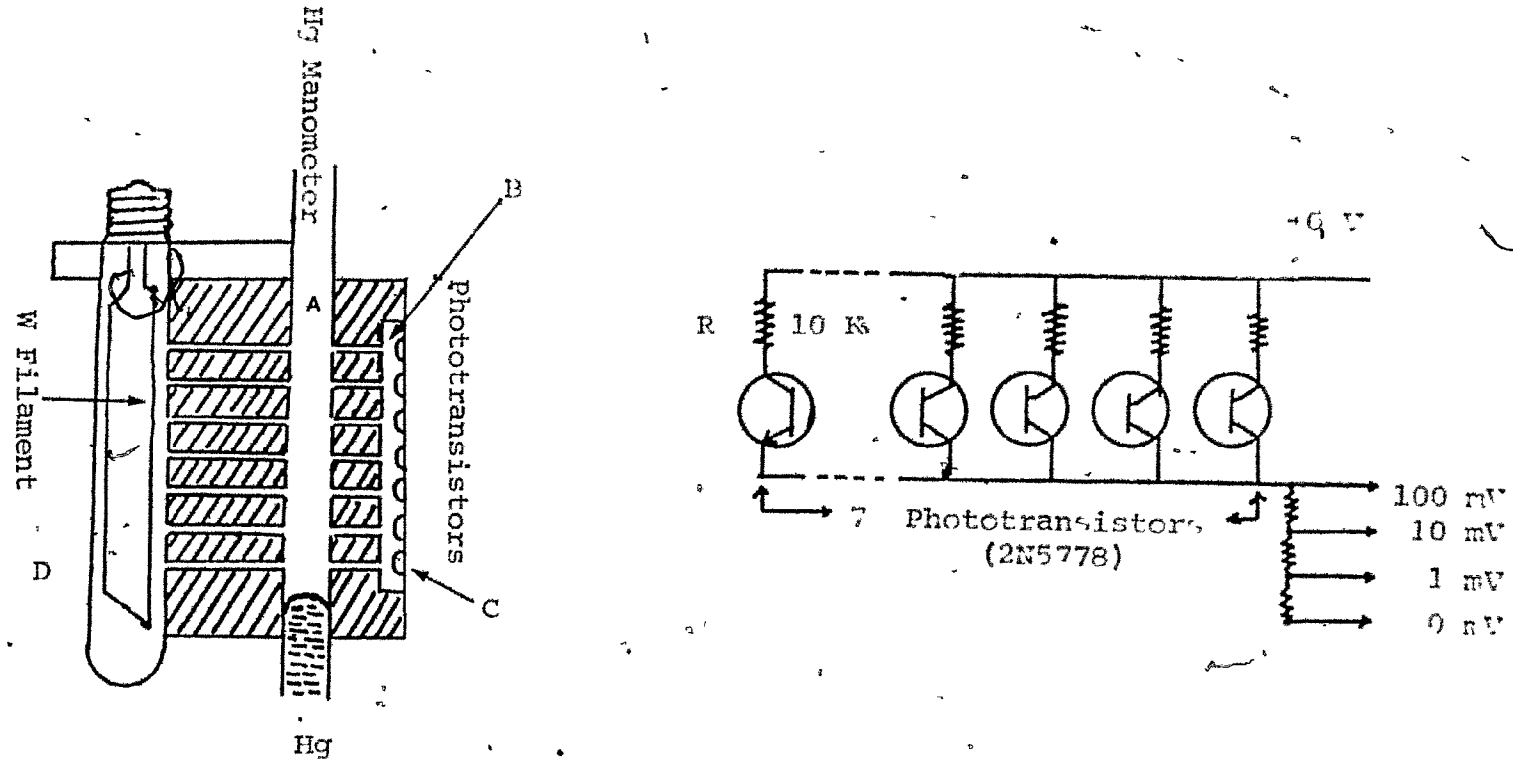

Fig . 52. Phototransistor Device for Flow Rate Measurements.

recorder. As the pressure changed, the mercury closed or opened the light path and each time this occured the signal on the recorder gave a step of 1 mV. dp/dt was thus obtained by recording these jumps on a strip chart recorder as the mercury level increased.

3.4 Chemicals.

The fluoroethylenes, obtained from the indicated sources, C_2H_3F, 1,1-$C_2H_2F_2$, C_2F_4 from Matheson Scient. Inc., C_2HF_3 from Columbia Organic Chemicals Inc., were used without further purification.

Part of the C_2F_4 was prepared by thermal decomposition of polytetrafluoroethylene. Specially prepared polytetrafluoroethylene granules under the trade name "Chemfluor" were supplied by the Chemplast Inc. The decomposition was performed in the apparatus shown in Fig. 53. It consisted of an oven (A) with a thermocouple (B), a storage bulb (C) with a cold finger (F), outlet of the gas (D), a manometer (E), a cold finger (I), a liquid nitrogen trap (LN) and the pumping system.

For the preparation of 5 l of tetrafluoroethylene under standard conditions, 50-60 g of "chemfluor" were used. The "Chemfluor" was placed in the oven (A) and the

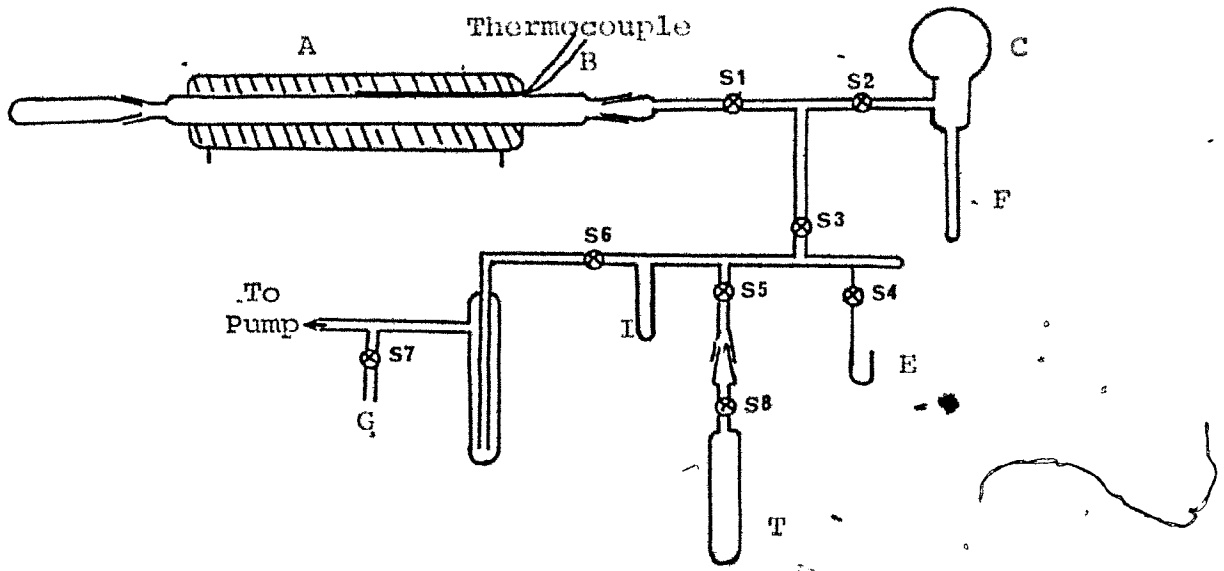

Figure 53. Apparatus for the preparation of C_2F_4.

system was pumped down for about 15 hours. After this period, the oven was switched on. A variac was used as a power supply set on a voltage to give approximately 430 °C inside the oven. When the temperature in the oven was arount 450 °C, the stopcock S_3 was closed and liquid nitrogen was used to condense the C_2F_4 in the cold finger (F) of the storage bulb (C). The decomposition takes place slowly at a temperature of 450 °C. After 12 hours, the oven was swiched off, and, the condensed C_2F_4 was pumped on until constant pressure was achieved. Then, the C_2F_4 was distilled to the cold finger (I) and transfered to the main experimental system. The last 1 cc liquid volume of C_2F_4 was discarded.

Hydrogen, helium, argon, oxygen and nitrogen were supplied by Union Carbide Ltd. Argon and oxygen were purified by passing through a gas purifier containing molecular sieves at dry ice-acetone temperature and, further by passing through a liquid nitrogen trap under low pressure. Hydrogen was purified by passing throuth a Fisher Scientific Co. Deoxo unit and a liquid nitrogen trap. Helium and nitrogen were purified by passing through a liquid nitrogen trap. Hydrogen fluoride and nitrogen dioxide were supplied by Matheson. The hydrogen fluoride was used without further purification for test reactions.

Nitrogen dioxide used for determination of O atoms flow rate was purified by bulb to bulb distillation.

3.5 Experimental Procedure.

For the reactions with hydrogen atoms, a run with the reagent 1.1-$C_2H_2F_2$ was performed under the same conditions (flow rate of 1,1-$C_2H_2F_2$ 207 μmol/s, H_2 flow rate 16 μmol/s, Ar flow rate 258 μmol/s, total pressure in the reaction cell 1.07 mmHg), before each run in order to check the apparatus and the discharge. Corrections were made to the position of microwave discharge to obtain reproducible intensities. The water absorption was checked at the same time.

The experimental procedure for a run was as follows: The optical path was flushed with nitrogen (dried by passing through a silica gel and molecular sieves trap at liquid nitrogen temperature) for about 30 hours. During this time, the system was pumped down by the mercury diffusion pump. After flushing, the large vacuum pump was switched on and after ten minutes the system was switched to the main vacuum line. At this time the pressure in the vacuum system was approximately 0.2 microns.

Hydrogen, oxygen or nitrogen and inert gas were introduced through the discharge tube by adjusting the manostats MA and MB to the proper position. The discharge was operated for about 30 minutes in order to obtain a constant production of atoms. The detector dewar was filled with dry ice - acetone and all the electrical components were switched on and allowed to warm up for 30 minutes. The micrometer needle valve (VO) was adjusted to the desired flow rate of fluoroethylene and then the micrometer needle valve (VC) was adjusted to give to system (FC) a constant pressure of 100 mmHg measured exactly with the oil manometer (O). The needle valve (VC) was adjusted continuously during the experiments in order to keep the pressure in FC constant. The detector dewar was filled with dry ice and recording of the spectrum was begun.

At the end of a run the exact flow rate of the fluoroethylene was determined experimentally. Upon completion of the run, the apparatus was pumped down, flushed a few times with the fluoroethylene to be used next and pumped down again.

After one hour of pumping the detector dewar was filled again. The needle valve (VO) was adjusted until the flow rate of the next fluoroethylene reactant was the same as that of the previous reactant and a new run

was started.

The flow rate of the gases was measured using the phototransistor device described in Section 3.3. The pressure of the gas, was adjusted to be the same as that at which the IR chemiluminescence experiment was run. The phototransistor device was placed at the lower part of the corresponding manometer in such a way that the second hole from the bottom of the device coincided with the level of the mercury. At this position the signal on the recorder was 6 mV. Then, the pressure was increased until the signal on the recorder became 7 mV at which voltage all phototransistors were activated. The proper chart velocity was chosen and the gas was allowed to flow into the reaction cell. As the gas flowed the pressure decreased and the mercury covered the holes one by one, a process which decreased the signal by 1 mV each time. Each hole corresponded to a known pressure therefore, each step of the signal gave the pressure at the corresponding time given from the chart paper speed. Thus, a plot of pressure vs time could be drawn and the slope at the 6 mV signal gave the dp/dt ratio under the experimental conditions. Assuming ideal gas behaviour, the flow rate is given by the equation

$$\text{Flow rate} = \left(\frac{\partial n}{\partial t}\right)_V = \frac{V}{RT}\left(\frac{\partial P}{\partial t}\right)_V \qquad 127$$

The volume of the system was known and constant and, the temperature (25-27°C) was measured. Thus, the flow rate of the gas could be found.

REFERENCES

1. J.J.Hood; a) Phil.Mag. 6, 371 (1878)
   b) ibid, 20, 323 (1885).

2. S.Arrhenius; Z.Phys.Chem. 4, 226 (1889).

3. W.C.McC. Lewis; J.Chem.Soc. 113, 471 (1918).

4. H.Eyring; J.Chem.Phys. 3, 107 (1935).

5. M.G.Evans,M.Polanyi; Trans.Far.Soc. 31, 875 (1935).

6. N.Basco,S.K.Dogra; Proc.Roy.Soc.(London) A323, 29 (1971).

7. I.W.M.Smith; Disc.Far.Soc. 44, 194 (1967).

8. M.Karplus,R.N.Porter,R.D.Sharma; J.Chem.Phys. 43, 3259 (1965).

9. M.Karplus,K.T.Tong; Disc.Far.Soc. 44, 56 (1967).

10. G.S.Schatz,J.M.Bowman,A.Kuppermann; J.Chem.Phys. 63, 685 (1975).

11. P.J.Kuntz,E.M.Nemeth,J.C.Polanyi,S.D.Rosner,C.E.Young; J.Chem.Phys. 44, 1168 (1966).

12. Y.A.Shreider; "Monte Carlo Methods" Chap.1 and 7, (Pergamon,Oxford) (1966).

13. J.M.Hammersley,D.C,Handscomb; "Monte Carlo Methods" Chap.5, (Wiley,New York)(1964).

14. H.C.Blais,D.L.Bunker; J.Chem.Phys. 37, 2713 (1962).

15. K.J.Laidler; "Theories of Chemical Reaction Rates" (McGraw-Hill,New York) (1969).

16. J.C.Polanyi; Disc.Far.Soc. 55, 389 (1973).

17. M.Polanyi; "Atomic Reactions" (Williams and Norgate,London) (1932).

19. J.C.Polanyi; J.Chem.Phys. 31, 1338 (1959).

19. J.D.McKinley,D.Carrin,M.Boudart;
J.Chem.Phys. 23, 784 (1955).

20. F.S.Lipscomb,F.G.W.Norrish,B.A.Thrush;
Proc.Roy.Soc. A233, 455 (1956).

21. W.D.McGrath,F.G.W.Norrish;
a) Proc.Roy.Soc. A242, 265 (1957)
b) Nature (London) 182, 235 (1958)
c) Proc.Roy.Soc. A254, 317 (1960).

22. J.K.Cashion,J.C.Polanyi; J.Chem.Phys. 29, 455 (1958).

23. J.K.Cashion,J.C.Polanyi; J.Chem.Phys. 30,1097(1959).

24. J.K.Cashion,J.C.Polanyi;
Proc.Roy.Soc. A258, 529, 564, 570 (1960).

25. P.E.Charters,J.C.Polanyi; Can.J.Chem. 38,1743(1960).

26. P.E.Charters,J.C.Polanyi; Disc.Far.Soc. 33, 107
(1962).

27. P.N.Clough,J.C.Polanyi,R.T.Taguchi;
Can.J.Chem. 48, 2919 (1970).

28. E.H.Taylor,S.Datz; J.Chem.Phys. 23, 1711 (1955).

29. S.Datz,D.R.Herschbach,E.H.Taylor;
J.Chem.Phys. 35, 1549 (1961).

30. P.E.Charters,B.N.Khare,J.C.Polanyi;
Nature 193, 367 (1962).

31. F.D.Findlay,J.C.Polanyi; Can.J.Chem. 42, 2176(1964).

32. J.R.Airey,F.D.Findlay,J.C.Polanyi;
Can.J.Chem. 42, 2193 (1964).

33. J.C.Polanyi; J.Appl.Optics,Suppl. 2, 109 (1965).

34. D.R.Herschbach,G.H.Kwei,J.A.Norris;
Disc.Far.Soc. 33, 149 (1962).

35. J.P.Airey,E.R.Getty,J.C.Polanyi,D.R.Snelling;
J.Chem.Phys. 41, 3255 (1964).

36. F.C.Anlauf,P.J.Kuntz,D.H.Maylotte,P.D.Pacey,
J.C.Polanyi; Disc.Far.Soc. 44, 183 (1967).

37. P.D.Pacey,J.C.Polanyi; Appl.Optics 10, 1725 (1971).

38. a) N.Jonathan,C.M.Melliar-Smith,D.H.Slater;
Mol.Phys. 20, 93 (1971)
b) N.Jonathan,C.M.Melliar-Smith,S.Okuda,D.H.Slater
and D.Timlin; Mol.Phys. 22, 561 (1971).

39. N.Jonathan,S.Okuda,D.Timlin;
Mol.Phys. 24, 1143 (1972).

40. P.E.Charters,R.G.Macdonald,J.C.Polanyi;
Appl.Optics 10, 1747 (1971).

41. H.W.Chang,D.W.Setser; J.Chem.Phys. 58, 2298 (1973).

42. W.H.Duewar,D.W.Setser; J.Chem.Phys. 58, 2310 (1973).

43. P.J.Kuntz,M.H.Mok,J.C.Polanyi;
J.Chem.Phys. 50, 4623 (1969).

44. P.J.Kuntz,E.M.Nemeth,J.C.Polanyi;
J.Chem.Phys. 50, 4607 (1969).

45. J.C.Polanyi; Disc.Far.Soc. 44, 293 (1967).

46. J.C.Polanyi,W.H.Wong; J.Chem.Phys. 51, 1439 (1969).

47. M.H.Mok,J.C.Polanyi; J.Chem.Phys. 51, 1451 (1969).

48. G.S.Hammond; J.Amer.Chem.Soc. 77, 334 (1955).

49. C.A.Parr,J.C.Polanyi,W.H.Wong;
J.Chem.Phys. 58, 5 (1973).

50. L.J.Kirsch,J.C.Polanyi; J.Chem.Phys. 57, 4498(1972).

51. N.H.Hijazi,J.C.Polanyi; J.Chem.Phys. 63, 2249(1975).

52. J.C.Polanyi,J.J.Sloan; J.Chem.Phys. 57, 4988 (1972).

53. P.E.Charters,B.N.Khare,J.C.Polanyi;
Disc.Far.Soc. 33, 107 (1962).

54. J.C.Polanyi; Acc.Chem.Res. 5, 161 (1972).

55. D.S.Perry,J.C.Polanyi; Can.J.Chem. 50, 3916 (1972).

56. M.J.Berry; J.Chem.Phys. 61, 3114 (1974).

57. D.J.Bogan,D.W.Setser; J.Chem.Phys. 64, 586 (1976).

58. R.L.Johnson,K.C.Kim,D.W.Setser;
J.Phys.Chem. 77, 2499 (1973).

59. K.C.Kim,D.W.Setser,C.M.Bogan;
J.Chem.Phys. 60, 1837 (1974).

60. P.N.Clough,B.A.Thrush;
a) Proc.Roy.Soc. A309, 419 (1969)
b) Trans.Far.Soc. 65, 23 (1969).

61. a) P.N.Clough,S.E.Schwartz,B.A.Thrush;
Proc.Roy.Soc. A317, 575 (1970).
b) D.M.Creek,C.M.Melliar-Smith,N.Jonathan;
J.Chem.Soc.A, 646 (1970).

62. S.J.Arnold,G.H.Kimbell; Can.J.Chem. 51, 451 (1973).

63. J.C.Polanyi; J.Chem.Phys. 34, 347 (1961).

64. S.V.V.Kasper,G.C.Pimentel; Appl.Phys.Lett. 5, 231
(1964).

65. K.L.Kompa,J.H.Parker,G.C.Pimentel;
J.Chem.Phys. 49, 4257 (1968).

66. M.J.Berry,G.C.Pimentel; J.Chem.Phys. 49, 4190 (1968).

67. C.K.N.Patel; Phys. Rev. 136, A 1187 (1964).

68. W.H.Green,M.C.Lin; J.Chem.Phys. 54, 3222 (1971).

69. M.C.Lin; J.Phys.Chem. 76, 811 (1972).

70. M.C.Lin; J.Phys.Chem. 76, 1425 (1972).

71. J.H.Parker,G.C.Pimentel; J.Chem.Phys. 51, 91 (1969).

72. M.J.Berry,G.C.Pimentel; J.Chem.Phys. 53, 3153 (1970).

73. F.M.S.Tablas,G.C.Pimentel;
IEEE J.Quant.Electr. QE-6, 176 (1970).

74. M.J.Molina,G.C.Pimentel;
J.Chem.Phys. 56, 3988 (1972).

75. M.J.Molina,G.C.Pimentel;
IEEE J.Quant.Electr. QE-9, 64 (1973).

76. P.R.Poole,G.C.Pimentel; J.Chem.Phys. 63, 1950(1975).

77. T.M.Hard; Appl.Optics 9, 1825 (1970).

78. D.H.Maylotte,J.C.Polanyi,K.B.Woodall;
J.Chem.Phys. 57, 1547 (1972).

79. J.G.Pruett,R.N.Zare; J.Chem.Phys. 64, 1774 (1976).

80. F.Menard-Bourcin,J.Menard,L.Henry;
J.Chem.Phys. 63, 1479 (1975).

81. H.W.Cruse,P.J.Dagdigian,R.N.Zare;
Disc.Far.Soc. 55, 277 (1973).

82. K.E.Holdy,L.C.Klotz,K.R.Wilson;
J.Chem.Phys. 52, 4588 (1970).

83. M.Shapiro,R.D.Levine; Chem.Phys.Lett. 5, 499 (1970).

84. C.E.Caplan,M.S.Child; Mol.Phys. 23, 249 (1972).

85. R.C.Mitchell,J.P.Simons;
Disc.Far.Soc. 44, 208 (1967).

86. J.P.Simons,P.W.Tasker; Mol.Phys. 26, 1267 (1973).

87. R.G.Gilbert,I.G.Ross; Austr.J.Chem. 24, 145 (1971).

88. a) A.J.Blake,J.K.Bahr,J.H.Carver,V.Kumar;
Phil.Trans.Roy.Soc. 268A, 159 (1970).
b) M.E.Wacks; J.Res.Nat.Bur.Stand.(U.S.) 68A, 631 (1964).
c) D.Villarejo; J.Chem.Phys. 49, 2523 (1968).

89. M.J.Berry; Chem.Phys.Lett. 27, 73 (1974).

90. M.J.Berry; Chem.Phys.Lett. 29, 329 (1974).

91. a) I.Procaccia,R.D.Levine;
J.Chem.Phys. 63, 4261 (1975).
b) J.S.Rowlinson; Nature 225, 1196 (1970).

92. G.S.Schatz,J.M.Bowman,A.Kuppermann;
J.Chem.Phys. 63, 674 (1975).

93. C.F.Bender,S.V.O'Neil,P.K.Pearson,H.F.Schaefer III;
Science 176, 1412 (1972).

94. D.G.Truhlar; J.Amer.Chem.Soc. 94, 7584 (1972).

95. A.A.Zavitsas,A.A.Melikain;
J.Amer.Chem.Soc. 97, 2757 (1975).

96. G.E.Whitten,B.S.Rabinovitch;
J.Chem.Phys. 41, 1883 (1964).

97. M.C.Lin,R.G.Shortridge,M.E.Unstead;
Chem.Phys.Lett. 37, 279 (1976).

98. R.B.Bernstein,R.D.Levine;
J.Chem.Phys. 57, 434 (1972).

99. R.D.Levine,R.B.Bernstein;
Accts.Chem.Res. 7, 393 (1974).

100. M.Rubinson,J.I.Steinfeld; Chem.Phys. 4, 467 (1974).

101. A.Ben-Shaul,R.D.Levine,R.B.Bernstein;
Chem.Phys.Lett. 57, 5427 (1972).

102. a) C.E.Shannon,W.Weaver;
"Mathematical Theory of Communication"
University of Illinois Press, Urbana Ill., (1949)
b) A.Hobson,B.Cheng;
J.Statistical Phys. 7, 301 (1973).

103. R.D.Levine,R.B.Bernstein; Chem.Phys.Lett. 22, 217 (1973).

104. D.S.Perry,J.C.Polanyi; Chem.Phys. 12, 37 (1976).

105. R.D.Levine,R.B.Bernstein,P.Kahana,I.Procaccia,
E.T.Upchurch; J.Chem.Phys. 64, 796 (1976).

106. H.M.Markel',T.Titani; J.Amer.Chem.Soc. 55, 1363 (1933).

107. J.R.Dacey,J.W.Hodgins; Can.J.Res.B, 28, 173 (1933).

108. D.T.Clark,J.M.Tedder; Trans.Far.Soc. 62, 393 (1966).

109. D.T.Clark,J.M.Tedder; Trans.Far.Soc. 62, 399 (1966).

110. D.T.Clark,J.M.Tedder; Trans.Far.Soc. 62, 405 (1966).

111. P.M.Scott,P.P.Jennings; J.Phys.Chem. 73, 1521(1969).

112. P.E.M.Allen,H.M.Melville,J.C.Pobb; Proc.Roy.Soc. A218, 311 (1953).

113. R.D.Penzhorn,H.L.Sandoval; J.Phys.Chem. 74, 2065 (1970).

114. L.Teng,W.E.Jones; Can.J.Chem. 47, 1696 (1969).

115. P.Cadman, et. al.; Chem. Comm. 1970, 203.

116. L.Teng,W.E.Jones; Far.Trans.I, 68, 1267 (1972).

117. L.Teng,W.E.Jones; Far.Trans.I, 69, 189 (1973).

118. J.C.Polanyi,J.L.Schreiber,J.J.Sloan; Chem.Phys. 9, 403 (1975).

119. R.L.Wilkins; a) J.Chem.Phys. 58, 2326 (1973).
b) J.Chem.Phys. 58, 3038 (1973).

120. J.P.Airey; Int.J.Chem.Kinetics 2, 65 (1970).

121. M.J.Perona; J.Chem.Phys. 54, 4024 (1971).

122. O.D.Krogh,G.C.Pimentel; J.Chem.Phys. 56, 969 (1972).

123. R.F.Heidner III,J.V.V.Kasper; Chem.Phys.Lett. 15, 179 (1972).

124. D.E.Monn,B.A.Thrush,D.R.Lide Jr.,J.J.Ball,N.Acquista; J.Chem.Phys. 34, 420 (1961).

125. G.A.Kuipers; J.Mol.Spectr. 2, 75 (1958).

126. R.Herman,R.F.Wallis; J.Chem.Phys. 23, 637 (1955).

127. H.S.Heaps,G.Herzberg; Zeitschrift fur Phys. 133, 48 (1952).

128. J.F.Cashion; Aeronautical Research Lab.Tech.Report, ARL 62-412 August 1962.

129. G.Herzberg; "Molecular Spectra and Molecular Structure. I. Spectra of Diatomic Molecules."

130. V.L.Landau,E.Teller; Physik.Zeitschrift der Sowjetunion 10, 34 (1936).

131. W.H.Green,J.F.Hancock; IEEE J.Quantum Electr. QE-9, 50 (1973).

132. J.O.Hirschfelder,C.F.Curtis,R.B.Bird; "Molecular Theory of Gases and Liquids" John Wiley and Sons Inc., New York,London.

133. G.P.Quigley,G.J.Wolga; Chem.Phys.Lett. 27, 276 (1974).

134. M.Rujimethabhas; Thesis.

135. K.C.Kirk,D.W.Setser,B.E.Holmes; J.Phys.Chem. 77, 725 (1973).

136. W.B.Miller,S.A.Satron,D.R.Herschbach; Disc.Far.Soc. 44, 108 (1967).

137. M.J.Berry; J.Chem.Phys. 59, 6229 (1973).

138. H.J.Johnston; "Gas Phase Reaction Rate Theory" Ronald Press (1966).

139. R.M.Jordan,F.Kaufman; J.Chem.Phys. 63, 1691 (1975).

140. Simone Bourcier; "Selected Constants Spectroscopic Data Relative to Diatomic Molecules" Pergamon Press Ltd,1970.

141. P.M.Morse; Phys.Rev. 34, 57 (1929).

142. Eugen Merzbacher; "Quantum Mechanics" John Lively and Sons p.470 (1962).

143. I.N.Levine; 'Quantum Chemistry" Vol.II (Sect.3.2,3.3) Allyn and Bacon Inc. (1970).

144. K.Denbigh; 'The Principles of Chemical Equilibrium' (Sect. 12.10) CUP (1966).

145. J.L.Carlos Jr.,R.R.Karl Jr.,S.H.Bauer; J.Chem.Soc.Faraday Trans.II 70, 177 (1974).

146. S.W.Benson; "Foundation of Chemical Kinetics" McGraw-Hill Inc. (1960).

147. J.C.Hassler,D.W.Setser; J.Chem.Phys. 45, 3246(1966).

148. R.Dees,D.W.Setser; J.Chem.Phys. 49, 1193 (1968).

149. H.W.Chang,D.W.Setser; J.Amer.Chem.Soc. 91, 7648 (1969).

150. P.J.Strutt; Proc.Roy.Soc. A85, 219 (1911).

151. H.G.Evans,G.R.Freeman,G.A.Winkler; Can.J.Chem. 34, 1971 (1956).

152. V.H.Kiess,H.P.Broida; 5th Int.Combustion,Symp. (Oxford,1958).

153. D.R.Safrany; Progr.Reaction Kinetics 6, 1 (1971).

154. D.R.Safrany,W.Jaster; J.Phys.Chem. 72, 3305 (1968).

155. G.J.Verbeke,C.A.Winkler; J.Phys.Chem. 64, 319(1960).

156. W.Forst,H.G.Evans,C.A.Winkler; J.Phys.Chem. 61, 320 (1957).

157. D.R.Safrany,P.Harteck,R.R.Reeves; J.Chem.Phys. 39, 1161 (1964).

158. G.B.Kistiakowsky,G.G.Volpi; J.Chem.Phys. 27, 1141 (1957).

159. K.R.Jennings,J.W.Linnet; Trans.Far.Soc. 56, 1737 (1960).

160. S.E.Sobering,C.A.Winkler; Can.J.Chem.36, 1223(1958).

161. B.Dunford,H.C.Evans,C.A.Winkler;
Can.J.Chem. 34, 1074 (1956).

162. W.M.Jones,M.Rugimethabhas;
Can.J.Chem. 51, 3680 (1973).

163. S.E.Johnson,A.Fontijn; Chem.Phys.Lett. 23,252(1973).

164. N.Madhavan,W.E.Jones; Can.J.Chem. 46, 3483 (1968).

165. M.Rugimethabhas,W.E.Jones;
Can.J.Chem. 50, 346 (1972).

166. S.Takahashi;
Men of the Def. Academy, Japan XII, 237 (1972).

167. E.Tschuikow-Roux,K.R.Maltman;
Int.J.Chem.Kinetics 7, 363 (1975).

168. J.R.Gilbert,I.R.Slagle,R.E.Graham,D.Gutman;
J.Phys.Chem. 80, 14 (1976).

169. H.E.Radford,H.P.Broida; J.Chem.Phys. 38, 644 (1963).

170. a) W.H.Duewer,J.A.Coxon,D.W.Setser;
J.Chem.Phys. 56, 4355 (1972)
b) J.A.Coxon,D.W.Setser,W.H.Duewer;
J.Chem.Phys. 58, 2244 (1973).

171. a) T.Iway,M.I.Savadatti,H.P.Broida;
J.Chem.Phys. 47, 3861 (1967)
b) K.M.Evenson,H.P.Broida;
J.Chem.Phys. 44, 1637 (1966).

172. R.G.Bennett,F.W.Dalby; J.Chem.Phys. 36, 399 (1962).

173. M.E.Umstead,M.G.Lin,F.J.Woods;
Paper No.123 presented at the 169th American
Chemical Society National Meeting,Philadelphia,Pa.
April, 1975.

174. R.J.Cvetanovic; Adv.Photochem. 1, 115 (1963).

175. R.J.Cvetanovic; Can.J.Chem. 36, 623 (1958).

176. R.J.Cvetanovic; J.Chem.Phys. 23, 1375 (1955).

177. A.N.Ponomarev; Kinetika i Kataliz 1, 237 (1964).

178. R.Klein,M.D.Scheer; a) J.Phys.Chem. 72, 616 (1968)
b) J.Phys.Chem. 74, 613 (1970).

179. M.D.Scheer,R.J.Klein; a) J.Phys. Chem. 74, 2732(1970)
b) Science , 1214 (1966).

180. A.N.Hughes,M.D.Scheer,R.J.Klein;
J.Phys.Chem. 70, 798 (1966).

181. S.Sato,R.J.Cvetanovic; Can.J.Chem.a) 36, 970 (1958)
b) 36,1668 (1958).

182. J.M.S.Jarvie,R.J.Cvetanovic;
Can.J.Chem. 37, 529 (1959).

183. R.J.Cvetanovic; J.Phys.Chem. 74, 2730 (1970).

184. M.D.Scheer,R.J.Klein; J.Phys.Chem. 73, 597 (1969).

185. a) J.Heicklen,V.Knight,S.A.Greene;
J.Chem.Phys. 42, 221 (1965).
b) J.Heicklen,V.Knight; J.Chem.Phys.70, 3893 (1966).

186. D.Saunders,J.Heicklen;
a) J.Amer.Chem.Soc. 87, 2088 (1965).
b) J.Chem.Phys. 70, 1950 (1966).

187. R.C.Mitchell,J.P.Simons; J.Chem.Soc.B 1005 (1968).

188. W.J.R.Tyerman; Trans. Far. Soc. 65, 163 (1969).

189. S.J.Moss; Trans. Far. Soc. 67, 3503 (1971)

190. R.E.Huie, J.T.Herron, D.D.Davis;
Int. J. Chem. Kinetics iv, 521 (1972).

191. D.S.Jones, S.J.Moss;
Int. J. Chem. Kinetics vi, 443 (1974).

192. R.E.Huie, J.T.Herron;
"Progress in Reaction Kinetics" Vol 8.

193. J.R.Kanofsky, D.Lucas, D.Gutman;
"14th Symposium of Combustion" (1973) Page 285.

194. B.Rosen; "Spectroscopic Data Relative to Diatomic Molecules", Pergamon Press, Oxford (1970).

195. A.J.Meyer,D.N.Travis; Can.J.Phys. 44, 1541 (1966).

196. S.J.Arnold,G.H.Kimbell,D.R.Snelling; Can.J.Chem. 52, 2608 (1974).

197. V.Ya.Shlyapintokh et al.; "Chemiluminescence Techniques in Chemical Reactions", Consultants Bureau, N.Y.(1968).

198. J.C.Biordi,C.P.Lazzara,J.F.Papp; 14th Symposium on Combustion p.367 (1973).

199. T.Kinbara,K.Noda; 14th Symposium on Combustion p.321 (1973).

200. D.Boothman,J.Lawton,S.J.Melinek,F.Weinberg; 12th Symposium on Combustion p.969 (1969).

201. J.Peeters,C.Vinckier; 15th Symposium on Combustion p.969 (1975).

202. R.A.Smith,F.E.Jones,R.P.Chasmar; "The Detection and Measurement of Infra-Red Radiation" 2nd Edition, Oxford at the Clarendon Press p.29 (1968).

APPENDIX A

Physical and Spectroscopical Constants

and, Heats of Formation.

Table A1

Physical and Spectroscopic Constants.

k	Boltzmann Const.	1.38×10^{-16} erg/molecule	
h	Planck's "	6.625×10^{-27} erg s	
R	Gas "	8.3143×10^{7} erg mol^{-1} K^{-1}	
N	Avogadro's Number	6.0225×10^{23} gram mol	
c	Speed of Light	2.998×10^{10} cm/s	
M_1	First Derivative of Dipole Moment of HF.	1.6×10^{-10} esu	(125)
θ	for HF	1.18	"
B_e	" "	20.9560 cm^{-1}	(124)
ω_e	" "	4139.04 "	"
α_e	" "	0.7958 "	"
$B_{v=1}$	" "	19.788 "	"
$B_{v=2}$	" "	19.035 "	"
$B_{v=3}$	" "	18.299 "	"
$\omega_e x_e$	" "	90.05 "	"
$\omega_e y_e$	" "	0.932 "	"
r_e	Internuclear Distance	9.168×10^{-9} cm	"

TABLE A2

Heat of Formation of Some Molecules and Radicals.

Compound	ΔH_f^*	Ref	Compound	ΔH_f^*	Ref
C_2H_3F	-28.	A1	H	52.092	A1
1,1-$C_2H_2F_2$	-78.6	"	O (^3P)	59.55	"
C_2HF_3	-111.9	"	N (^4S)	112.97	"
C_2F_4	-155.5	"	HF	64.8	"
C_2H_5F	-60.05	"	CHO	-2.9	A3
1,1-$C_2H_4F_2$	-114.3	"	CHF	30.	"
1,1,2-$C_2H_3F_3$	-154.1	A2	CFO	-41.	"
1,1,1-$C_2H_3F_3$	-176.	A1	CHF_2	-70.2	"
1,1,2,2-$C_2H_2F_4$	-204.6	A2	CH_2F	-6.6	"
CH_3COF	-104.9	A1	CH_3	34.8	"
CH_3CHO	-39.72	"	CF_3	112.4	"
$CH_3C{=}O$	-4.5	"	CH_2	92.07	"
$CH_2{=}C{=}O$	-14.6	"	CF_2	-43.5	"
CHFO	-90.	A3	CH	142.	"
COF_2	-152.7	"	CF	61.	"
CH_2O	-27.7	"	CO	-26.42	"

A1. J.L.Franklin et al; N.S.R.D.S-NBS 26(1969).

A2. S.W.Benson; "Thermochemical Kinetics". John Wiley & Sons Inc., (1968).

A3. D.R.Stull and H.Prophet; "JANAF Thermochemical Tables" 2nd Edition N.S.R.D.S-NBS 37.

* in Kcal/mol at 25 °C.

APPENDIX B

Summary of the Experimental Data.

TABLE L1

Areas Representing Intensities of Rotational Lines for the Reaction of H + Fluoroethylene. (Pressure 1.07 mmHg).
Flow Rates: H_2 16 μmol/s; Ar 250 μmol/s; FE 207 μmol/s

Rot. Line		C_2H_3F	$C_2H_2F_2$	C_2HF_3	C_2F_4	% Error
P(1)	(1→0)*	1510	1608	2048	1677	4
P(2)	(1 0)	2630	2512	3243	2565	2
P(3)	(1 0)	2952	2852	3677	2577	2
P(4)	(1 0)	2446	2509	3243	2171	3
P(5)	(1 0)	1419	1551	2104	1607	4
P(6)	(1 0)	824	895	1129	781	4
P(7)	(1 0)	373	397	635	345	3
P(8)	(1 0)	117	171	183	141	5
R(0)	(1 0)	1300	1300	1775	1335	5
R(1)	(1 0)	1836	1705	2265	1733	4
R(2)	(1 0)	1619	1773	1796	1417	4
R(3)	(1 0)	1232	1456	1411	1110	2
R(4)	(1 0)	699	883	876	614	3
R(5)	(1 0)	325	443	431	302	3
R(6)	(1 0)	126	195	157	124	5
R(7)	(1 0)	42	54	45	39	7
P(1)	(2→1)	279	320	493	297	5
P(2)	(2 1)	585	584	917	491	4
P(3)	(2 1)	695	615	1032	527	3
P(4)	(2 1)	569	539	866	433	4
P(5)	(2 1)	356	366	591	324	3
P(6)	(2 1)	211	210	301	143	4
P(7)	(2 1)	93	90	129	67	6
P(8)	(2 1)	38	-	-	-	8
R(1)	(2 1)	391	438	606	335	7
R(2)	(2 1)	368	391	582	277	7
R(3)	(2 1)	235	300	361	238	8
R(4)	(2 1)	205	175	200	109	8
P(2)	(3→2)	127	138	182	85	5
P(3)	(3 2)	116	104	143	64	5
P(4)	(3 2)	87	93	108	60	6
P(5)	(3 2)	65	64	68	43	6
P(6)	(3 2)	26	30	34	-	8
R(2)	(3 2)	81	80	92	45	8

* Vibrational Transition (v'→v").

TABLE F2

Areas Representing Intensities of Rotational Lines for the Reaction of H + Fluoroethylene. (Pressure .83 mmHg).
Flow Rates: H_2 16 μmol/s; Ar 258 μmol/s; FE 207 μmol/s

Rot. Line		C_2H_3F	$C_2H_2F_2$	C_2HF_3	C_2F_4	% Error
P(1)	(1→0)*	1202	1307	1228	1062	4
P(2)		2097	2153	2127	1775	2
P(3)		2262	2430	2338	1773	2
P(4)		1957	1945	1740	1396	3
P(5)		1179	1277	1146	713	4
P(6)		687	683	616	463	4
P(7)		293	268	222	188	3
P(8)		113	114	94	82	5
R(0)		1037	1116	1004	832	5
R(1)		1412	1425	1314	1058	4
R(2)		1197	1207	1188	937	4
R(3)		788	809	819	713	2
R(4)		449	468	366	356	3
R(5)		187	213	159	146	3
R(6)		72	85	49	53	5
R(7)		23	25	-	22	7
P(1)	(2→1)	344	342	452	239	5
P(2)		578	610	838	445	4
P(3)		618	657	842	445	3
P(4)		517	547	621	387	4
P(5)		354	376	453	269	3
P(6)		194	195	203	136	4
P(7)		88	87	85	51	6
P(8)		-	-	-	11	8
R(1)		380	387	501	291	7
R(2)		310	366	482	263	7
R(3)		231	252	298	142	8
R(4)		135	172	161	79	8
P(1)	(3→2)	-	-	-	-	-
P(2)		-	118	107	58	5
P(3)		105	108	109	57	5
P(4)		87	84	82	46	6
P(5)		59	54	55	30	6
P(6)		31	28	29	-	8
R(2)		68	68	84	32	8

* Vibrational Transition (v'→ v").

TABLE B2

Areas Representing Intensities of Rotational Lines for the Reaction of H + Fluoroethylene. (Pressure .65 mmHg).
Flow Rates: H2 16 mol/s; Ar 29 mol's; FE 207 mol's

Rot. Line		C_2H_3F	$C_2H_2F_2$	C_2HF_3	C_2F_4	% Error
P(1)	(1→0)	1179	1274	1064	1421	4
P(2)		2020	2325	1880	2760	2
P(3)		2242	2521	2125	3242	2
P(4)		1844	2051	1677	2261	3
P(5)		1165	1154	922	1411	4
P(6)		672	698	495	925	4
P(7)		284	308	202	416	3
P(8)		110	119	-	131	5
R(0)		958	1135	929	1239	5
R(1)		1316	1514	1239	1662	4
R(2)		1160	1387	1033	1402	4
R(3)		810	931	689	986	2
R(4)		466	502	347	530	3
R(5)		191	228	153	255	3
R(6)		107	75	58	100	5
R(7)		-	29	14	33	7
P(1)	(2→1)	-	317	350	302	5
P(2)		608	730	622	757	4
P(3)		664	716	654	717	3
P(4)		466	677	519	682	4
P(5)		370	454	343	448	3
P(6)		182	242	185	220	4
P(7)		93	102	93	105	6
P(8)		-	-	-	34	8
R(0)		226	197	-	283	8
R(1)		370	-	405	465	7
R(2)		343	432	360	384	7
R(3)		205	230	225	256	8
R(4)		129	159	130	157	8
R(5)		54	-	68	56	8
R(6)		25	-	-	34	8
P(1)	(3→2)	37	45	39	-	8
P(2)		-	-	-	76	5
P(3)		87	106	76	60	5
P(4)		77	80	57	42	6
P(5)		55	63	-	-	6
R(0)		42	49	24	-	8
R(1)		-	-	-	39	8
R(2)		84	80	52	-	8
R(3)		53	53	-	55	8

TABLE 34

Areas Representing Intensities of Rotational Lines for the Reaction of H + Fluoroethylene. (Pressure .63 mmHg).
Flow Rates: H² 16 μmol/s; Ar 29 μmol/s; FE 207 μmol/s

Pot.	Line	C_2H_3F	$C_2H_3F_2$	C_2HF_3	C_2F_4	% Error
P(1)	(1→0)	778	1017	1141	779	4
P(2)		1313	1749	1916	1243	2
P(3)		1539	1933	2190	1314	2
P(4)		1265	1622	1716	1026	3
P(5)		785	1001	1063	643	4
P(6)		450	580	596	313	4
P(7)		205	248	249	123	3
P(8)		75	88	87	33	5
R(0)		664	865	970	644	5
R(1)		999	1164	1244	848	4
R(2)		763	1004	1060	719	4
R(3)		557	699	734	285	2
R(4)		227	347	397	205	3
R(5)		139	157	165	101	3
R(6)		-	64	69	32	5
R(7)		-	-	22	-	7
P(1)	(2→1)	218	320	346	198	5
P(2)		407	572	730	360	4
P(3)		449	629	769	352	3
P(4)		381	545	601	274	4
P(5)		252	340	404	160	3
P(6)		127	199	225	72	4
P(7)		54	90	100	-	6
P(8)		-	-	37	-	8
R(0)		-	-	-	-	-
R(1)		256	372	481	247	8
R(2)		245	352	412	229	7
R(3)		396	231	271	142	7
R(4)		109	151	161	80	8
R(5)		-	-	52	23	8
P(1)	(3→2)	-	-	35	13	8
P(2)		-	-	-	-	-
P(3)		62	85	87	23	5
P(4)		61	76	59	-	6
P(5)		26	52	38	-	6
R(0)		36	-	37	14	8
R(2)		56	67	64	33	8
R(3)		-	-	43	29	8

TABLE B1

Areas Representing Intensities of Rotational Lines for the Reaction of H + Fluoroethylene. (Pressure .150 mmHg).
Flow Rates: H 13 mol/s; Ar 17 mol/s; FE 20 mol/s

Rot. Line		C_2H_2F	$C_2H_2F_2$	C_2HF_3	C_2F_4	% Error
P(1)	(1→0)	218	492	371	371	4
P(2)		390	875	602	672	2
P(3)		412	979	684	756	2
P(4)		362	810	549	665	3
P(5)		203	490	313	388	4
P(6)		115	279	174	247	4
P(7)		62	124	74	116	3
P(8)		16	44	-	48	5
R(0)		201	378	307	304	5
R(1)		253	491	415	401	4
R(2)		216	365	337	356	4
R(3)		160	258	240	227	2
R(4)		73	131	106	152	3
R(5)		33	55	37	48	3
R(6)		19	17	18	14	5
P(1)	(2→1)	44	115	89	75	5
P(2)		129	241	129	138	4
P(3)		132	277	221	221	3
P(4)		120	226	164	186	4
P(5)		76	147	112	123	3
P(6)		33	79	56	63	4
P(7)		9	-	24	-	6
R(0)		39	-	-	-	8
R(1)		82	169	131	102	7
R(2)		76	147	124	90	7
R(3)		43	85	68	50	8
R(4)		30	59	48	44	8
R(5)		10	22	17	-	8
P(1)	(3→2)	13	22	27	-	8
P(2)		-	-	-	-	-
P(3)		29	42	33	40	5
P(4)		20	21	18	32	6
P(5)		-	-	13	22	6
R(0)		-	-	-	-	-
R(1)		-	-	-	-	-
R(2)		21	33	30	23	8
R(3)		-	24	25	-	8

TABLE B6

Areas Representing Intensities of Rotational Lines for the Reaction of H + Fluoroethylene. (Pressure .62 mmHg).
Flow Rates: H2 16 μmol/s; He 29 μmol/s; FE 281 μmol/s

Rot. Line		C_2H_3F	$C_2H_2F_2$	C_2HF_3	C_2F_4	% Error
P(1)	(1→0)	372	450	523	350	4
P(2)		623	763	875	606	2
P(3)		1065	815	1425	619	2
P(4)		875	695	876	500	3
P(5)		542	410	501	288	4
P(6)		196	272	280	143	4
P(7)		74	87	104	50	3
P(8)		38	80	49	24	5
R(0)		303	379	436	158	5
R(1)		420	481	568	384	4
R(2)		371	424	464	275	4
R(3)		245	276	304	204	2
R(4)		123	152	151	107	3
R(5)		64	62	60	50	3
R(6)		20	-	23	-	5
P(1)	(2→1)	143	168	202	82	5
P(2)		311	302	418	158	4
P(3)		252	437	420	164	3
P(4)		188	342	351	143	4
P(5)		138	222	226	80	3
P(6)		64	43	118	40	4
P(7)		-	26	37	25	6
R(0)		81	61	104	54	8
R(1)		142	187	355	118	7
R(2)		139	158	212	94	7
R(3)		87	104	139	66	8
R(4)		54	61	73	36	8
R(5)		-	18	20	-	8
P(1)	(3→2)	18	28	26	11	8
P(2)		-	-	-	-	-
P(3)		47	53	50	32	5
P(4)		49	33	38	27	6
P(5)		19	-	17	-	6
R(0)		21	22	26	-	8
R(1)		-	-	-	-	-
R(2)		43	44	27	-	8
R(3)		-	-	32	-	8

TABLE B7

Areas representing Intensities of Rotational Lines for the Reaction of N + Fluoroethylene. (Pressure 4.47 mmHg).
Flow Rates: N2 510 mol/s; Ar 640 mol/s; FE 45 umol/s

Pol. Line		C_2H_3F	$C_2H_2F_2$	C_2HF_3	% Error
P(1)	(1→0)*	405	434	610	4
P(2)		617	753	1064	2
P(3)		729	858	1228	2
P(4)		593	677	976	3
P(5)		386	457	653	4
P(6)		212	257	384	4
P(7)		77	107	216	3
P(8)		-	-	79	5
R(0)		337	341	544	5
R(1)		455	477	740	4
R(2)		420	461	649	4
R(3)		303	328	490	2
R(4)		167	185	257	3
R(5)		68	113	121	3
P(1)	(2→1)	-	-	93	5
P(2)		121	169	252	4
P(3)		137	209	327	3
P(4)		120	180	298	4
P(5)		83	112	191	3
P(6)		-	-	116	4
R(0)		-	-	53	8
R(1)		116	129	145	7
P(2)		95	113	153	7
R(3)		-	-	110	8
R(4)		24	-	57	8

* Vibrational Transition (v'→v").

TABLE B8

Areas Representing Intensities of Rotational Lines for the Reaction of O + Fluoroethylene. (Pressure 1.08 mmHg).
Flow Rates: O_2 532 μmol/s; O 22.6 mol/s; FE 29.2 μmol/s

Pot. Line	C_2H_3F	$C_2H_2F_2$	C_2HF_3	% Error
P(1) (1→0)	1019	670	1573	4
P(2)	1695	1117	2877	2
P(3)	2179	1359	3666	2
P(4)	2131	1398	3840	3
P(5)	1876	1110	3471	4
P(6)	1421	860	2558	4
P(7)	1019	610	1913	3
P(8)	608	369	1340	5
P(9)	412	236	985	6
P(10)	193	111	542	8
R(0)	859	567	1539	5
R(1)	1436	899	2351	4
R(2)	1611	1016	2811	4
R(3)	1436	830	260	2
R(4)	1131	664	2008	3
R(5)	801	463	1451	3
R(6)	487	295	935	5
R(7)	278	159	605	7
R(8)	126	81	349	8
P(1) (2→1)	189	109	501	5
P(2)	424	223	883	4
P(3)	519	246	1144	3
P(4)	529	261	1047	4
P(5)	481	230	1167	3
P(6)	364	178	962	4
P(7)	243	119	629	6
P(8)	239	-	655	8
P(9)	117	-	337	9
R(0)	185	110	375	8
R(1)	359	168	679	7
R(2)	369	196	872	7
R(3)	323	167	686	8
R(4)	280	135	672	8
R(5)	199	100	504	9
R(6)	128	70	407	9

cont.

TABLE B8 (cont.)

Pot.	Line	C_2H_3F	$C_2H_2F_2$	C_2HF_3	% Error
P(1)	(3→2)	-	30	107	5
P(3)		138	68	297	6
P(4)		130	68	266	6
P(5)		90	-	237	8
P(6)		61	-	184	9
P(0)		24	-	100	9
R(2)		88	-	155	9
R(3)		103	-	250	9
P(3)	(4→3)	-	21	46	10
P(4)		-	23	50	10
P(5)		-	-	50	10
P(6)		-	-	43	10

APPENDIX C

Calculation of the Residence Time in the Reaction Cell.

The residence time was calculated from the equation

$$\tau = b/v \qquad [128]$$

where, v = linear velocity of the gases in the reaction cell

b = the calculated length of flame.

The linear velocity was found assuming ideal behaviour of the gases. That is,

$$pV = nRT \qquad [129]$$

or, since

$$dV/dt = s(d\ell/dt) \qquad [130]$$

where, s is the cross section of the reaction cell and, ℓ the length,

$$d\ell/dt = (dn/dt)\ \frac{RT}{ps} \qquad [131]$$

and,

$$v = \left(\frac{d\ell}{dt}\right)_p = \left(\frac{\partial n}{\partial t}\right)_p \frac{RT}{sp} \qquad [132]$$

$(\partial n/\partial t)_p$ is the flow rate at constant pressure.

The length of the flame b was found from the inverse square law of photometry. The reaction cell has two inlets (A and B of Fig.4) for the reactant fluoroethylenes. Assuming that the flame is approximately of the same intensity and shape when the fluoroethylene is introduced from either inlet, a cylindrical light source with length b and measured diameter a=1.8 cm is produced. The detector is on the axis of the cylinder at a distance c (7.6 cm from the front window). The illuminance E of the detector is given by the equation

$$E = \frac{I}{(c + b)^2} \qquad [133]$$

which is the inverse square law for such a source with $c + b >> a$.(Cl,C2). In [133], I is the intensity of the source. Thus, if the distance between the two inlets A and B is known, d=4.3 cm, Then

$$E_B/E_A = (c+d+b)^2/(c+b)^2 \qquad [134]$$

where, E_A, E_B are the intensities measured by the detector when the inlets A, B respectivily are used.

Setting $E_B/E_A = p$ equation [134] becomes

$$p(7.6+b)^2 = (11.9+b)^2 \qquad [135]$$

or,

$$(p-1)b^2 + 2(7.6p-11.9)b + (7.6^2p-11.9^2) = 0 \quad [136]$$

Since the parameter $p=E_B/E_A$ can be determined experimentally the flame length, b, can be calculated from equacion [136].

The flame lengths were found to be between 14-16 cm for the reactions of fluoroethylenes with hydrogen atoms, 14-17 cm with oxygen atoms and, 15-17 cm with active nitrogen.

C1. J.Valasek; "Introduction to Theoretical and Experimental Optics", John Wiley and Sons, Inc., N.Y. (1949).

C2. H.P.Greenspan, D.J. Benney; "Calculus an Introduction to Applied Mathematics'. McGraw-Hill, Inc., N.Y. (1973).

APPENDIX D

Errors Calculation.

The errors of the areas are given in Appendix B and they were calculated from the accuracy of the readings of the areas.

The random error of the points of the rotational lines plots was calculated from the error propagation applied to the quantity ln Y

where,

$$Y = I^{v'J'}_{v''J''}/\omega_J^4 S_J F_J \qquad [137]$$

The error of the $I^{v'J'}_{v''J''}$ is the error of the measured area, i.e. 3-8%, S_J is an integer, the error of the frequency, ω_J, is negligible and the error of F_J is less than 1% (F_J is the rotation-vibration interaction).

The error of lnY is $\lambda(\ln Y)$

$$\lambda(\ln Y) = (\partial \ln Y/\partial Y)\, dY = \lambda(Y)/Y \qquad [138]$$

where

$$\lambda(Y) = Y\sqrt{(\lambda(I)/I)^2+(\lambda(F_J)/F_J)^2} \qquad [139]$$

therefore , from [138] and [139]

$$\lambda(\ln Y) = \sqrt{(\lambda(I)/I)^2+(\lambda(F_J)/F_J)^2} \qquad [140]$$

This error was found to be small and is given

approximately from the size of the points on the graphs. Since the rotational temperature is affected from the bath temperature therefore, there is a random error due to changes of the reaction bath temperature during a run for which the equation [137] cannot account.

Thus, the error of the slope from the linear least squares fit is more suitable to give the error of the rotational temperature.

The intercept and the slope of the linear least squares method are given by (D1)

$$\text{int} = \text{Intercept} = \frac{\Sigma Y_i \Sigma x_i^2 - \Sigma x_i \Sigma x_i Y_i}{n\Sigma x_i^2 - (\Sigma x_i)^2} \qquad [141]$$

$$b = \text{slope} = \frac{n\Sigma x_i Y_i - \Sigma x_i \Sigma Y_i}{n\Sigma x_i^2 - (\Sigma x_i)^2} \qquad [142]$$

The standard error of the intercept and slope is calculated using the formula

$$SE(\text{int}) = \sqrt{\frac{\Sigma x_i^2 \; \Sigma(y_i - bx_i - \text{int})^2}{(n-2)(n\Sigma x_i^2 - (\Sigma x_i)^2)}} \qquad [143]$$

and

$$SE(b) = \sqrt{\frac{n\Sigma(y_i - bx_i - \text{int})^2}{(n-2)(n\Sigma x_i^2 - (\Sigma x_i)^2)}}$$

The error of the rotational population is

$$\lambda(N_{v',J'}) = N_{v',J'}\sqrt{(SE(int)/int)^2+(SE(b)/b)^2} \quad [144]$$

Therefore, the error of the vibrational population is

$$(N_{v'}) = \sqrt{\Sigma(\lambda(N_{v',J'}))^2} \quad [146]$$

Since only radiation relaxation and the physical removal of the excited hydrogen fluoride affect the initial populations under these experimental conditions, the errors of the initial populations, $\lambda(R_1)$, $\lambda(R_2)$ and $\lambda(R_3)$, were calculated from the equations:

$$\lambda(R_v) =$$

$$= \sqrt{\left\{A_{v,u}N_v\sqrt{\bar{A}^2_{v,u}+\bar{N}^2_v}\right\}^2+\left\{(N_v/\tau)\sqrt{\tau^2+\bar{N}^2_v}\right\}^2+\left\{A_{w,v}N_w\sqrt{\bar{A}^2_{w,v}+\bar{N}^2_w}\right\}^2} \quad [147]$$

where, $w-1 = v = u+1$ and $\bar{x} = \lambda(x)/x$

The error of $A_{1,0}$ was found from the error propagation of the equation [68]

$$\lambda(A_{1,0}) = A_{1,0}\,2\lambda(R_{1,0}) \quad [148]$$

and for the $A_{v',v''}$ from

$$\lambda(A_{v',v''}) = A_{v',v''}\sqrt{(\bar{A}^2_{v',v''(rel)}+\bar{A}^2_{1,0}}$$

The error of $R_{1,0}$ is 1%.

The error of the residence time in the reaction cell, ', was 7%, calculated from error propagation. It was, however, taken as 10% to account for the non-linear gas flow in the reaction cell.

Dl. J.W.Mellor; "Higher Mathematics for Students of Chemistry and Physics", Dover Publications,Inc. 4th Edition.

APPENDIX E

Results Obtained Using Einstein Coefficients Given by Meredith and Smith and, Accounting for Collisional Deactivation by Fluoroethylenes.

Recently, more accurate values for the Einstein coefficients of HF have been reported (ref E1) (Table E1) which differ significantly from the values derived by Cashion (128) (Table 11) used in the body of the thesis.

Accordingly, we calculated the values of population ratios using the more recent values. The population ratios so derived (Table E2) agree with the values previously derived for the reactions with hydrogen atoms (Table 4-9) within experimental error except for the values R_4/R_1 and R_3/R_1 for the reactions of O atoms with trifluoroethylene and 1,1-difluoroethylene (Table E3). Using these values we found a population inversion between the vibrational levels v=3 and 4 in the latter two reactions. Otherwise the discussion and conclusions in the body of the thesis are unaltered by the new Einstein coefficients. For consistency the new Einstein coefficients are used throughout the Tables E2 and E3.

Table E1

Einstein Coefficients of HF Given in Ref E1.

v' \ v''	0	1	2	3
1	209.2			
2	22.93	322.5		
3	1.223	65.44	406.1	
4	0.06159	4.913	134.1	446.3

Up to this point the collisional deactivation of HF by fluoroethylenes has been neglected. Qualitatively it was observed, in the manner described on page 92 for comparing deactivation by hydrogen and fluoroethylene, that the deactivation due to fluoroethylenes is about the same as argon.

In Table E2 population ratios derived by using deactivation probability of HF by fluoroethylenes equal to that of Ar are recorded. These results are equal to the results neglecting deactivation by fluoroethylene within experimental error. Therefore it appears that neglect of collisional deactivation by the fluoroethylenes does not effect the results. If, however, the probability of deactivation by fluoroethylenes is taken to be equal to

the experimental deactivation probability by ethylene (ref 32) the population ratios are increased significantly although the same trends are observed. However there is an independent reason for believing that these populations are unrealistically high. The vibrational populations of HF produced by elimination from 1,1,1-trifluoroethylene (27) are similar to the values derived neglecting the deactivation of HF by fluoroethylenes.

E1. R.E.Meredith and F.G.Smith;

J. Quant. Spectrosc. Radiat. Transfer. 13, 89, (1973).

E2. K.G.Anlauf, P.H.Dawson and J.A.Herman;

J. Chem. Phys. 58, 5354 (1973).

Table E2

Calculated Vibrational Populations for the Reactions of H Atoms with Fluoroethylenes Using Einstein Coefficients Given by Meredith and Smith.

P number			a		b		c	
			R_2/R_1	R_3/R_1	R_2/R_1	R_3/R_1	R_2/R_1	R_3/R_1
C_2H_3F	1.07	Ar	.19	.041	.19	.041	.47	.067
	.83	"	.24	.047	.24	.048	.54	.077
	.65	"	.25	.053	.25	.054	.73	.100
	.63	"	.30	.051	.31	.053	.90	.101
	.15	"	.25	.087	.25	.087	.33	.097
	.62	He	.33	.071	.33	.072	1.08	.158
$1,1\text{-}C_2H_2F_2$	1.07	Ar	.19	.039	.19	.040	.45	.063
	.83	"	.25	.045	.25	.045	.56	.075
	.65	"	.27	.052	.27	.053	.79	.099
	.63	"	.32	.058	.32	.059	.97	.118
	.15	"	.29	.059	.29	.059	.38	.067
	.62	He	.39	.071	.39	.072	1.44	.179

continued

a Deactivation by fluoroethylene (FE) is neglected.

b Assumed deactivation probability by FE 1×10^{-5}.

c " " " " " 1.8×10^{-3}.

Cont.

Table F3

Calculated Vibrational Populations for the Reactions of H Atoms with Fluoroethylenes Using Einstein Coefficients given by Meredith and Smith.

	P mmHg		a		b		c	
			2 - 1	3 - 1	2 - 1	3 - 1	2 - 1	3 - 1
C_2HF_3	1.07	Ar	.24	.040	.24	.040	.61	.069
	.83	"	.35	.054	.35	.054	.91	.100
	.65	"	.33	.049	.33	.050	1.08	.103
	.63	"	.36	.046	.36	.047	1.20	.101
	.15	"	.30	.067	.30	.067	.40	.077
	.62	He	.43	.057	.44	.058	1.82	.160
C_2F_4	1.07	Ar	.17	.026	.17	.026	.39	.041
	.83	"	.23	.031	.23	.031	.51	.050
	.65	"	.25	.031	.25	.032	.68	.055
	.63	"	.28	.037	.28	.038	.79	.070
	.15	"	.24	.068	.24	.068	.32	.078
	.62	He	.25	.034	.26	.035	.73	.066

a Deactivation by fluoroethylene (FE) is neglected.

b Assumed deactivation probability by FE 1×10^{-5}.

c " " " " " 1.8×10^{-3}.

Table E3

Calculated Vibrational Populations for the Reactions of O Atoms and Active Nitrogen Using Einstein Coefficients Given by Meredith and Smith.

		P mmHg		a			b			c		
				R'_2	R'_3	R'_4	R'_2	R'_3	R'_4	R'_2	R'_3	R'_4
Active N	C_2H_3F	4.47	Ar	.21			.21			.35		
	$1,1\text{-}C_2H_2F_2$	"	"	.27			.27			.47		
	C_2HF_3	"	"	.23			.23			.40		
O atoms	C_2H_3F	1.08	Ar	.21	.050		.21	.050		.26	.057	
	$1,1\text{-}C_2H_2F_2$	"	"	.14	.015	.07	.14	.015	.06	.18	.012	.07
	C_2HF_3	"	"	.28	.031	.11	.28	.030	.89	.36	.026	.10

a, b, c as in Table E2.

$R'_v = R_v/R_1$